Design and Implementation of

Robotic Devices for

Physical Therapy of Distal Upper Extremity

by

İsmail Hakan Ertaş

Submitted to the Graduate School of Sabancı University
in partial fulfillment of the requirements for the degree of
Master of Science

Sabancı University

August, 2010

Design and Implementation of Robotic Devices for

Physical Therapy of Distal Upper Extremity

APPROVED BY:

Assist. Prof. Dr. Volkan Patoğlu
(Thesis Advisor)   ....

Assoc. Prof. Dr. Mahmut F. Aksit   ....

Assoc. Prof. Dr. Erhan Budak   ....

Assoc. Prof. Dr. Kemalettin Erbatur   ....

Assist. Prof. Dr. Gürdal Ertek   ....

DATE OF APPROVAL: ....

Design and Implementation of Robotic Devices for Physical Therapy of Distal Upper Extremity

İsmail Hakan Ertaş

ME, Master's Thesis, 2010

Thesis Supervisor: Assist. Prof. Volkan Patoğlu

Abstract

According to statistics of World Health Organization, hand injuries count for 1/3 of all injuries with more than one million emergency cases annually. Physical rehabilitation accounts for most of the recovery experienced by patients suffering from hand injury. Robotic devices decrease the cost of therapy while providing repetitive exercises with quantitative measurements. In this study, we present the design and implementation of two robotic devices for hand therapy. After kinematic type selection ensuring safety, ergonomics and adjustability; both of the devices are optimally dimensioned to achieve best kinematic and dynamic performance.

The primary use for the first device is to assist flexion/extension motions of a finger within its full range, in a natural and coordinated manner, while keeping the tendon tension within acceptable limits to avoid rupture of the suture.

The second device is designed for forearm/wrist and grasp therapy of a neurologically injured human arm and hand. Emphasizing the importance of coordinated movements of the wrist and the hand while performing activities of daily living (ADL) tasks, the device possesses 3 degrees of freedom and is designed to assist abduction/adduction and palmar/dorsal flexion of the wrist or pronation/supination of the forearm, concurrently with the grasping and releasing movements of the hand. Thanks to its modular, interchangeable end effectors, the device supports ADL exercises.

Both devices are built and experimentally characterized. Human subject experiments and usability tests have been conducted for the devices and the efficacy of devices to deliver desired wrist and hand therapies have been demonstrated.

Uzak Üst Uzuvların Fizyoterapisi Amaçlı Robot Tasarımı ve Uygulaması

İsmail Hakan Ertaş

ME, Master Tezi, 2010

Tez Danışmanı: Yar. Doç. Dr. Volkan Patoğlu

Özet

Dünya Sağlık Örgütünün istatistiklerine göre, günlük hayatta karşılaşılan tüm yaralanmaların 1/3'ü el bölgesinde meydana gelmekte olup bu yaralanma vakaları yılda bir milyondan fazla olmaktadır. Fizyoterapi el yaralanmalarının tedavisinde uygulanan en yaygın yöntemdir. Robot destekli rehabilitasyon bu tedavi sürecinin masraflarını azaltmakla birlikte tekrarlı egzersizler ve niceliksel ölçüm imkanı sunmaktadır. Bu çalışmada, el terapisinde kullanılmak üzere iki adet robot tasarımı ve uygulaması sunulmaktadır.

İlk robot tendon ameliyatı sonrası, tendon gerilimini belli limitler arasında tutarak ve yaralı bölgede dikişin kopmasını engelleyerek, parmağın fleksiyon/extansiyon egzersizlerine yardımcı olmak için tasarlanmıştır. Bu robot aynı zamanda hareket genişliği sağlama ve güçlendirme çalışmalarında da kullanılabilecek şekilde tasarlanmıştır.

İkinci robot nörolojik yaralanmalar sonrası önkol/bilek ve kavrama terapisi için tasarlanmıştır. Gündelik yaşam aktiviteleri genellikle bilek ve elin ortak hareketlerini içermektedir. İkinci robot bu aktiviteleri destekleyecek şekilde bileğin abdüksiyon/addüksiyon, extansiyon/fleksiyon ve önkolun pronasyon/supinasyon hareketleri ile elin kavrama hareketini aynı anda hastaya yükleyebilmektedir. Kolaylıkla değiştirilebilen modüler sonlandırıcıları sayesinde robot farklı gündelik aktiviteleri uygulayabilmektedir. Ayrıca robot bilek ve önkolun izometrik gücünü ve hareket sınırlarını ölçmek için kullanılabilir.

Her iki robot da inşa edilip, performansları deneysel olarak nitelendirilmiştir. Ayrıca, insanlı deneyler ve kullanılabilirlik testleri düzenlenmiş olup, robotların el ve bilek tedavisinde kullanılabilirliği ve yararlılığı gösterilmiştir.

Acknowledgements

It is a great pleasure to extend my gratitude to my thesis advisor Assist. Prof. Dr. Volkan Patoğlu for his precious guidance and support. I am greatly indebted to him for his supervision and excellent advises throughout my Master study. I would gratefully thank Assoc. Prof. Dr. Mahmut F. Akşit, Assoc. Prof. Dr. Erhan Budak, Assoc. Prof. Kemalettin Erbatur and Assist. Prof. Dr. Gürdal Ertek for their feedbacks and spending their valuable time to serve as my jurors.

I would like to acknowledge the stipend support provided by TÜBİTAK under the BİDEB scholarship and Sabanci University for waiving the tuition throughout my master study.

I would sincerely like to thank to Elif Hocaoğlu for her pleasant teamwork during my experiments, Ahmetcan Erdoğan and Aykut Cihan Satici for their incessant help and all HMI members. Thanks to Mr. Mehmet Güler and Süleyman Tutkun for their support throughout my research and for sharing their experience and technical knowledge.

Many thanks to my lifelong friend Mert Abka who has important role in my way to haptics, Utku Seven, Serhat Dikyar, Melda Sener, Metin Yılmaz and all mechatronics laboratory members I wish I had the space to acknowledge in person, for their great friendship throughout my Master study.

I would like to thank my family for all their love and support throughout my life. Finally, I wish to express my deepest gratitude to Özlem Çoban for providing me the necessary motivation and being my source of strength and happiness in the hardest/most stressful times.

Contents

List of Figures

List of Tables

Chapter I

1   Introduction

In this chapter the injuries of distal upper extremity which consists hand, wrist, forearm and fingers, drawbacks and therapy methods used for treatment of these injuries are introduced. This chapter may include some unusual medical or biological terms and reader is kindly suggested to refer Appendix A for terminology.

1.1   Motivation

The human hand is vital for performing most of the activities of daily living (ADL) tasks. Hand injuries are common results of accidents and permanent impairments are regular consequences of these injuries. More than one million people in all over the world receive treatment in emergency departments annually due to acute hand and finger injuries [1]. These injuries include paralysis, cuts, lacerations, fractures, sprains, burns or broken bones. Tendon injuries and stroke are the most frequently encountered ones among the mentioned injuries [2] which result in the loss of hand function.

Hand injuries are difficult to impair because of complexity of the hand. After an injury, the hand may not function as it did before due to loss of

motion, dexterity, grip and ability to complete even simple tasks. The loss of hand function results in severe consequences like: disability to perform ADL, decrease in labor force or alienation from economic and social life [3]. The loss of hand function does not only affect patients' personal life but also is a cruel burden for society economic growth. According to Bureau of Labor Statistics(BLS), 27 % of total injuries which requires to rest away work are related to hand function [4]. Furthermore, Occupational Safety and Health Administration(OSHA) Fact Sheet 93-03 declares annual cost of hand injuries as about $ 300 million just in US for medical costs, workers' compensation and loss in production time [5].

1.2 Types of Injury

Hand injuries can be loosely classified into two main categories: Neurological injuries like stroke and physical injuries like tendon breaks.

1.2.1 Neurological Injuries

Stroke is the major neurological injury where blood supply into an area of brain is blocked by a blood clot or ruptured blood vessel. This interruption causes brain damage or death due to lack of oxygen and glucose flow to the brain which results in movement, speech problems or even death.

There are two main types of stroke: ischemic stroke (Figure 1.1-a) and hemorrhagic stroke (Figure 1.1-b). Ischemic stroke is the most common type of all stroke cases and occurs when the bloodstream to the brain is interrupted by a blood clot or thrombus. On the other hand, hemorrhagic stroke occurs

when a blood vessel in the brain breaks and fills the surrounding tissue with blood. Both result in a lack of blood flow to the brain and a buildup of blood that puts too much pressure on the brain.
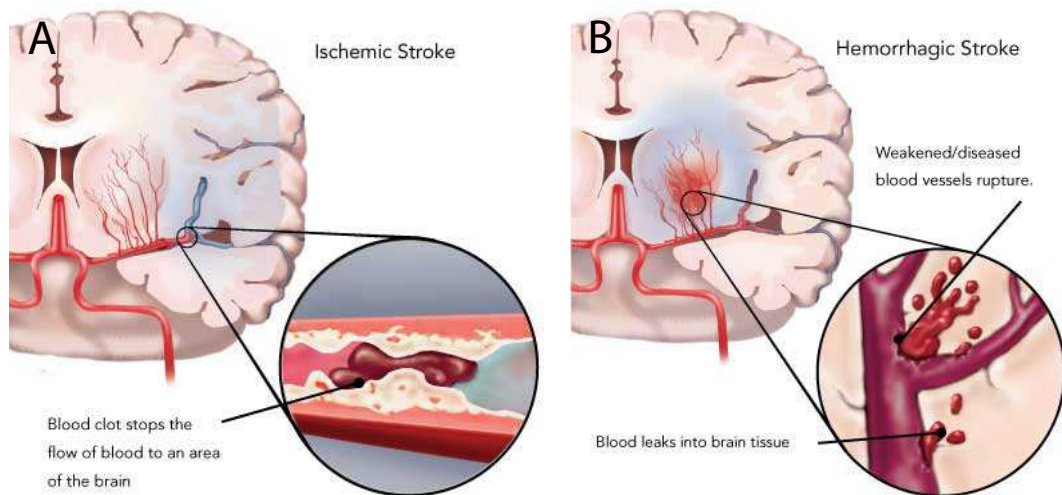
Figure 1.1: Types of stroke: (a)Ischemic, (b)Hemorrhagic

The consequences of stroke depends on the area of the brain where stroke occurs. If the right part of the brain is damaged, problems in judging distances, impaired behavior or short-term memory loss can be observed. Else if the left part of the brain is damaged, speech and language problems, slow behavior or memory problems may occur. A stroke in the cerebellum can cause balance problems, nausea, dizziness, vomiting or disordered reflexes of upper extremity.

Additionally, extent of the brain injury is affects the result of stroke. In particular slight strokes may cause weakness in an arm or leg while acute strokes may lead to paralysis or death.

1.2.2 Physical Injuries

The most frequent physical injuries of hand are tendon rupture (Figure 1.2). Flexor tendons connect muscles of the forearm to the bones of the thumb and the fingers, while extensor tendons are responsible to straighten the fingers by connecting the muscles of the forearm and hand to the bones in the fingers and the thumb. The most common and disturbing problem that patients experience after a tendon injury is finger stiffness, that is, inability to either fully bend (flexor tendon injury) or straighten the finger (extensor tendon injury). Avoiding finger stiffness requires complete recovery of tendon excursion so that the full range of motion (RoM) of the finger is regained.

Figure 1.2: A sample tendon injury

Most tendon injuries require surgical repair of damaged tendons with the goal of restoring the normal function of joints or their surrounding tissue. After a tendon repair surgery, healing may take couple of weeks, during which the injured finger is immobilized in a splint. Unfortunately, healing of scar tissue causes adhesion of the tendons, tendon sheath, and the surrounding tissue, limiting the motion of the finger after the repair. Adhesion of the

tendon can be avoided if an appropriate early hand rehabilitation protocol is followed to enforce gliding of the tendon [6]. Hence, while treating tendon injuries, it is of utmost importance to ensure the right balance between postoperative immobilization of the finger to allow for healing and early mobilization of the finger to avoid adhesion formation and to improve strength of the repair site [7, 8]. Interim period finger rehabilitation exercises include pinching to promote isolated tendon gliding [9, 10], while late period patients are asked to perform resistance exercises to ensure strength [11, 12].

For individuals recovering from such conditions, vigilant, appropriate and effective therapy of the hands can significantly improve the outcome of the healing process and the restoration of hand function [13].

1.3   Traditional Therapy Methods

Regaining the function of hand after an injury is a highly difficult but essential work which is mostly performed by an occupational or physical therapist. Occupational therapy methods like splinting, ADL exercises, scar management and physical therapy methods like stretching, joint mobilization, ultrasound are combined in hand therapies.

In traditional hand therapy, physical methods such as exercise, splinting and wound care are commonly used. Combined and coordinated movements of wrist and hand are excessively exercised in these physical methods. Hand therapies also include exercises for other upper limbs that affect hand function.

Hand therapy has a crucial role in the recovery from injury of the hand or wrist, and in the recovery from hand surgical operations.

1.3.1 Stroke Therapy

Conventional rehabilitation programs for stroke therapy include various methods such as functional electrical stimulation (FES), bilateral exercises or impairment-oriented training of the arm. All of the conventional rehabilitation methods require a lot of intense work for both the patient and the therapist.

In FES technique (Figure 1.3-a), muscles are contracted by applying electrical pulses to the peripheral nerves of the damaged part of body. The efficacy of FES has been demonstrated in reducing spasticity and improving muscle activation level of the disabled limb in [14].

Figure 1.3: Stroke therapy methods: (a)FES, (b)Mirror, (c)Physical

Mirror therapy treatment is a bilateral method used in stroke therapy (Figure 1.3-b). A mirror is used to hide the disabled limb and only show the remaining functional limb. This method was successfully used for the aim of decreasing the pain in amputee cases. It was proposed that this treatment would work for repairing the damaged parts of brain which has loss of connections due to stroke. Although using this method for stroke rehabilitation results in dexterity progress in patients disabled side, it is still time consuming and costly [15].

Physical therapy is the most widely used method which aims to relearn simple motor activities through training sessions with physical manipulation of the stroke patient's body with the intent of restoring movement, balance, and coordination (Figure 1.3-c). On the other hand, occupational therapy aims the patient to become independent through exercising everyday activities such as eating, drinking, writing, brushing, knob using, dressing or cooking. These exercises require coordinated motion of hand with wrist as most of the ADL and yields better results in regaining the hand function.

1.3.2   Tendon Therapy

In many references [8, 16, 17], efficacy of early mobilization of the finger, starting within a few days of repair, is advocated. In particular, early mobilization techniques are claimed not only to inhibit adhesion formation but also to promote intrinsic healing, producing a stronger repair site than with possible immobilization [6]. The major challenge during implementation of early mobilization techniques is to ensure that an appropriate amount of stress is induced to overcome internal resistance to initiate tendon gliding but not to cause gap formation or breaking of the suture.

Early mobilization can be exercised when the injured finger is active or passive. There exists two commonly used early mobilization techniques for rehabilitation of hand function due to a tendon injury, namely, the modified Duran technique and the Kleinert method.

In the modified Duran technique (Figure 1.4-a), a therapist enforces coordinated motions to the injured finger within closely controlled joint limits while the patient stays passive throughout the therapy [16]. Due to excessive

involvement of the therapist in the modified Duran technique, this therapy has relatively high treatment costs. Moreover, therapist induced trajectories lack repeatability and quantitative measurements of patient progress.
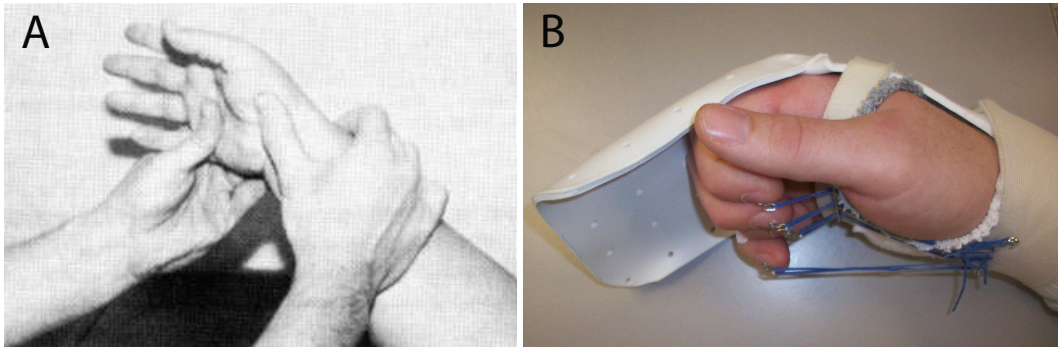
Figure 1.4: Tendon therapy methods: (a)modified Duran technique (b)Kleinert technique

The Kleinert method (Figure 1.4-b) utilizes a dynamic splint that attaches the proximal phalanx of the finger to the wrist with a rubber band and constrains the wrist movements. For flexor (extensor) tendon injuries, the rubber band applies forces to aid flexion (extension) of the finger. The Kleinert method combines active and passive movements of the finger such that the patient stay passive while flexing (extending) the injured finger, while the patient is active during extension (flexion) of the finger [9, 10, 18]. Unfortunately, the Kleinert method cannot provide coordinated motion to the injured finger due to the simple structure of the dynamic splint.

Early active mobilization techniques require patients to perform active movements of flexion and extension exercises. Active motion protocols are risky, since inappropriate amount of stress induced on the tendon by the voluntary muscle contractions may cause gap formation or rupture of the repair site [19]. In the early literature, it has been proposed that the extension

of the injured finger against resistance, provided by a rubber band as utilized in the Kleinert technique, may result in synergetic relaxation of the flexor tendons; thus, lower the stress transmitted along flexor tendon. Such rubber bands also aid flexion by reducing the force required to bend the finger.

1.4   Robot Assitance In Hand Therapy

From the explained conventional therapy methods, one can realize that physical rehabilitation protocol accounts for most of the recovery after a hand injury. These methods share the common problems like high-cost, time required protocols and needs repetitive exercises. Robotic devices reduces cost of therapies, while increasing the willingness of patient to attend the treatment sessions due to virtual reality integration. Moreover, robotic rehabilitation provides quantitative measurements of patient progress with repetitive therapeutic exercises.

1.4.1   Devices Used In Stroke Therapy

Many robotic devices have been proposed in the literature to assist rehabilitation exercises of wrist and hand after neurological injuries. These rehabilitation robots can be loosely categorized as exoskeleton type and end effector type devices. The exoskeleton type rehabilitation devices are advantageous in that, they can precisely impose/measure individual joint movements. The upper extremity exoskeletons [20, 21, 22, 23, 24, 25, 26, 27, 28] are capable of assisting all forearm wrist joint rotations, while [29, 30, 31] can assist forearm pronation/supination and wrist flexion/extention motions.

9

HWARD [32](Figure 1.5-a) and PERCRO [33] (Figure 1.5-b) are two exoskeleton type systems that can assist both grasping and wrist motions. All exoskeleton type devices share the common disadvantage of being relatively complex and too expensive to be employed as home based therapy devices.
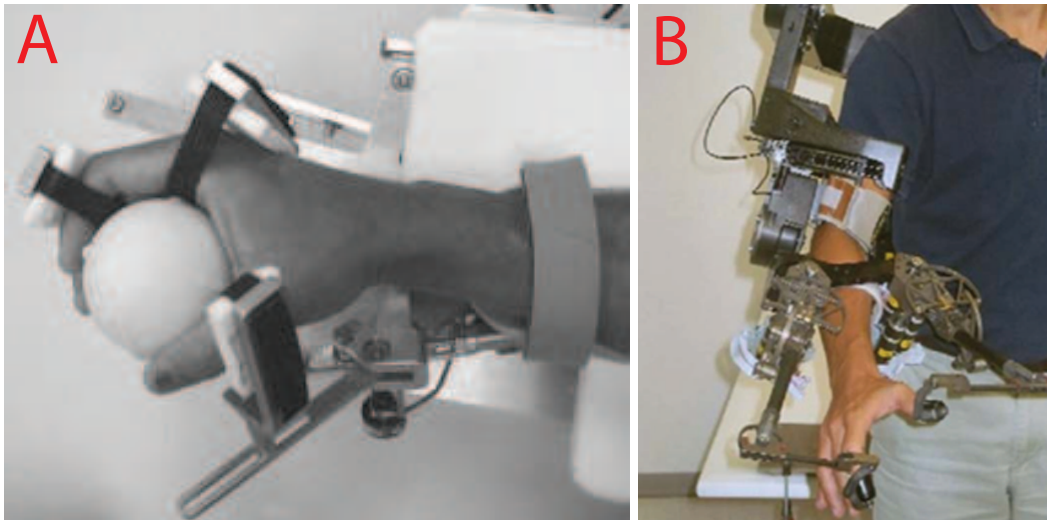
Figure 1.5: Sample exoskeleton type robots: (a)HWARD (b)PERCRO

Task space rehabilitation devices, on the other hand, are generally more practical, since they are simpler to implement with lower costs. For instance, the wrist module of the MIT Manus system [34] comprises of an actuated cardan joint coupled to a curved slider, and allows for assistance and measurement of 3 DoF forearm/wrist movements [35]. Another wrist module, which is proposed as a part of the Robotherapist upper extremity rehabilitation support system [36], can control all forearm/wrist rotations [37]. Even though these systems are simple and practical, they lack in supporting the vital grasp functionality for the hand. 9 DoF Gentle/G [38] and 18 DoF GiHapIn [39] are other examples of task space based neuro-rehabilitation systems. Both of these systems can deliver full arm therapy including fore-

arm/wrist and grasp exercises. Unfortunately, both of these devices are very complex and high cost. Dovat et.al. has proposed another task-space rehabilitation device, the Haptic Knob (Figure 1.6-a), that specifically targets combined wrist/grasp therapy exercises [40]. In particular, Haptic Knob is a 2 DoF back drivable mechanism, with one rotation assigned for the wrist movements [41] and the other for grasping actions. This simple yet elegant device is effective in delivering combined wrist and grasp therapies, but is limited to single wrist rotations at a time, due to its low-DoF kinematic structure. HandCARE (Figure 1.6-b) is another end effector type device developed by the same group which has 1 dof and suffers uncoordinated motion of hand since it applies forces to fingertips only.
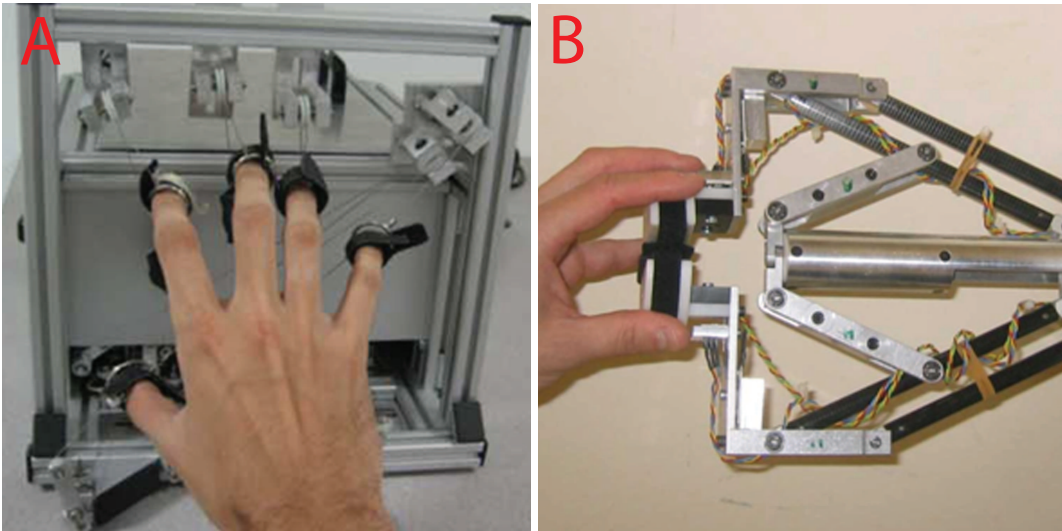
Figure 1.6: Sample end effector type robots: (a)HandCARE (b)Haptic Knob

Emphasizing the importance of coordinated movement of wrist and hand grasp while performing ADL tasks, we propose a novel task space oriented physical rehabilitation device for forearm/wrist and grasp therapy. The device possesses 3 DoF, allows for individual and coupled abduction/adduction

and palmar/dorsal flexion of the wrist or pronation/supination of the forearm, concurrently with functional grasping and releasing movements of the hand. With the help of its modular interchangeable end effectors, the device can be used to exercise ADL tasks, such as brushing and door opening. It can also be used as a practical measurement device, to characterize the range of motion and the isometric strength of the injured forearm/wrist and the hand throughout a therapy programme.

1.4.2 Devices Used In Tendon Therapy

The most basic type of devices that are used in the treatment to aid in the recovery of joints immediately after trauma or surgery are non-actuated devices like Thera-Band [42], Digiflex [43] and Power-Web [44] as illustrated in Figure 1.7. These non-actuated devices help opening and closing of hand or extension/flexion motion of fingers.
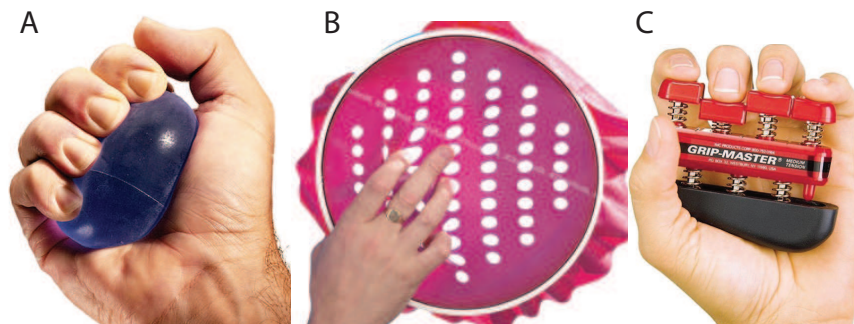
Figure 1.7: Non-actuated devices for hand therapy: (a)Theraband (b)PowerWeb (c)Digi-Flex

Continuous passive motion (CPM) is another frequent therapy method to assist motion of hand. CPM devices like Hand 8091 [45] or Amedeo system [46] constantly move the joint through a controlled range of motion,

the exact range is dependent upon the joint, but in most cases the range of motion is increased over time. Effect of CPM on reducing edema in the treatment of tendon injuries are illustrated in [47, 48, 49]. However, in order to have positive effects with CPM, it is required to exercise 8 hours a day [48].

Figure 1.8: CPM type devices for hand therapy: (a)Hand 8091 (b)Amedeo (c)Maestra

In addition to these simple devices, various finger/hand exoskeleton devices have been developed for rehabilitation of finger/hand function [50, 51, 52, 53, 54, 55]. However, most of these devices target treatment of stroke patients. Devices proposed for stroke therapy are not appropriate for administration of tendon therapy exercises, since these devices are designed for high torque outputs and lack the desired level of back-driveability required for tendon therapy. Furthermore, some of these devices are based on restricting joint motions [56, 57], while some others can only exert forces in one direction [58].

Hence, the design of finger exoskeleton and administration of tendon therapy need be handled carefully, as the challenges involved in robotic assisted tendon therapy exercises are significantly different than other robot assisted therapies. There exits several devices that are designed for tendon therapies [59, 60, 61, 62]. In particular, in [60] (Figure 1.9-b), an end effector type device is proposed for hand injuries. This device can exert forces only

13
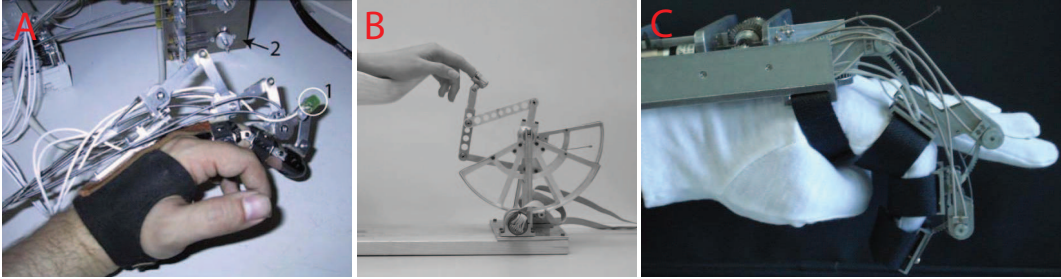
Figure 1.9: Finger exoskeletons for hand therapy: (a)Wege et al. (b)Mali et al. (c)Fu et al.

at the finger tip and may not ensure coordinated motion of the fingers as required for the tendon therapies. The devices proposed in [59](Figure 1.9-a) and [61, 62] (Figure 1.9-c) are fully actuated, tendon based devices. These designs require many actuators to be employed; hence, they are complex, expensive and hard to control.

We propose an underactuated finger rehabilitation system that is specifically designed for the tendon repair therapy exercises. The system can provide quantitative measurements of finger movements, interaction forces, and muscle activities; assist the finger motion within its full range in a natural and coordinated manner; and keep the tendon tension within acceptable limits to avoid gap formation or rupture of the suture.

1.5 Contributions of This Thesis

- Two novel rehabilitation robots are designed for hand (grasp), wrist and finger tharapy:

    - An end effector type robot is designed for stroke therapy, enabling coordinated motions of wrist and functional grasp of hand.
    - A linkage based, underactuated exoskeleton type robot is designed for tendon repair therapy exercises.

- Kinematics and dynamics of both devices are solved analytically and multicriteria optimal dimentional synthesis is performed.

- Both of the systems are implemented and experimentally characterized:

    - Modular end effectors are designed to exercise ADL with VR integration.
    - A multidisciplinary research is conducted for decision analysis of best mounting structure of a finger exoskeleton.

- Both of the rehabilitation systems are bilaterally controlled with virtual reality integration.

- Human subject experiments and user studies are conducted:

    - Usability tests are performed with various end effectors and measurement accuracy of the stroke device is characterized.
    - sEMG signals are used for estimation of tendon tension and efficacy of the exoskeleton in reducing muscle activation levels are demonstrated.

1.6 Outline of the Thesis

The thesis is organized as follows:

Importance of hand injuries is presented in this chapter, followed by the injury types and the current therapy methods applied for stroke and tendon breaks. Also robotic devices in literature which are used in rehabilitation, are reviewed is this chapter.

In Chapter 2, design of two rehabilitation systems which we propose for tendon break and stroke therapy are introduced. Before introducing the devices, design requirements of a rehabilitation robots are discussed. Then kinematic selection and analysis of the introduced robots are presented. This chapter is concluded with optimal dimensional synthesis of the robots.

Implementation details of the proposed systems are presented in Chapter 3. Working modes of the devices, use of different end effectors, integration of virtual reality and other details in order to operate the systems are given in this section.

Controllers used in the devices are explained in Chapter 4. In particular, implementation of disturbance observer based position controller and impedance controller are discussed.

The experiments for testing the usability and performance of the devices are presented in Chapter 5. A human subject experiment and characterization are done for tendon device while a comparison and functionality test and characterization are performed for the stroke device. Results of these tests are also discussed in this chapter.

Thesis is concluded with the summary of contributions and future work in Chapter 6.

Chapter II

2   Design of the Rehabilitation Robots

2.1   Design Requirements

Although using robots in a rehabilitation therapy may be very advantageous, it may also result in harmful effects in the case of a wrong usage. Therefore, there are some standards which a rehabilitation robot must ensure. For a hand rehabilitation device, anatomy of not only the hand but also the wrist must be taken into consideration. The requirements of a rehabilitation device can be analyzed within two major categories: Anatomical (functional) requirements and design requirements.

2.1.1   Functional Requirements of Distal Upper Extremity

Hand, wrist, forearm and finger can be considered as distal upper extremity of human. The movements of human wrist and forearm are directly related to each other. Human wrist is capable of lateral and palmar flexion motions around the radiocarpal and midcarpal joints axes, as well as abduction and adduction motions about an axis that passes through the capitate.

Table 2.1: Workspace and torque limits of human forearm and wrist

Joint	Human Isometric Strength	Human Joint Workspace Limits
Forearm Supination/Pronation	9.1 Nm	Supination: 86° Pronation: 71°
Wrist Palmar/Dorsal Flexion	19.8 Nm	Palmar Flexion: 73° Dorsiflexion: 71°
Wrist Abduction/Adduction	20.8 Nm	Adduction: 33° Abduction: 19°

Furthermore, forearm appends one more degrees of freedom to wrist with the motion of pronation/supination. Thus, simplified kinematics of the human forearm and wrist can be modeled as a 3 DoF kinematic chain that allows supination/pronation of the forearm and flexion/extension and abduction/adduction of the wrist joint (see Figure 2.1). Workspace and torque limits of human forearm and wrist are listed in Table 2.1.
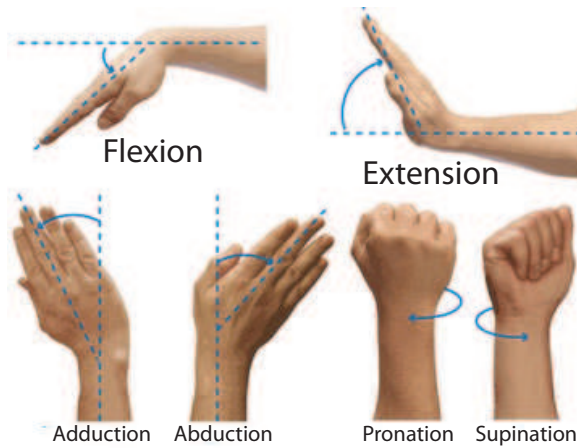
Figure 2.1: Wrist movements

Human hand is very dexterous and possesses high DoF. However, for patients recovering from neurological injuries, being able to perform several

major grasps is of highest importance for them to perform ADL tasks. In that respect, hand therapies after neurological injuries mostly focus on the grasp and release movements of the hand, rather than its fine movements. However, human hand and forearm/wrist almost always work in coordination while performing ADL tasks. For instance, successful competition of the simple task of door opening requires a coordinated motion of the wrist and hand grasp. Along these lines, medical experts advocate for the rehabilitation procedures that contain ADL tasks necessitating coordinated motion of the forearm/wrist and the hand grasp. Some examples of such coordinated motions, commonly employed in traditional therapies, are demonstrated in Figure 2.2. Particularly, in Figure 2.2-a hand is kept in its closed position during palmar/dorsal flexion of the wrist. In Figure 2.2-b hand is opened concurrently with the palmar/dorsal flexion of wrist. In Figure 2.2-c hand is kept in its closed position during the abduction/adduction of wrist. In Figure 2.2-d hand is opened concurrently with the abduction/adduction of the wrist.

Figure 2.2: Coordinated forearm/wrist and hand motions

Human hand has a wide range of grasp ability and can stably grasp many objects. There are many researchers who have classified grasp types such as Iberal, Cutkosky, Cooney and Chao, Jocobson and Sperling, Kamakura, Griffiths and Kapandji, Naiper, Brunnstrom and so on. Among these researchers, Brunnstrom defined eight grasp types as illustrated in Figure 2.3 which are mostly used for stroke therapy [63].
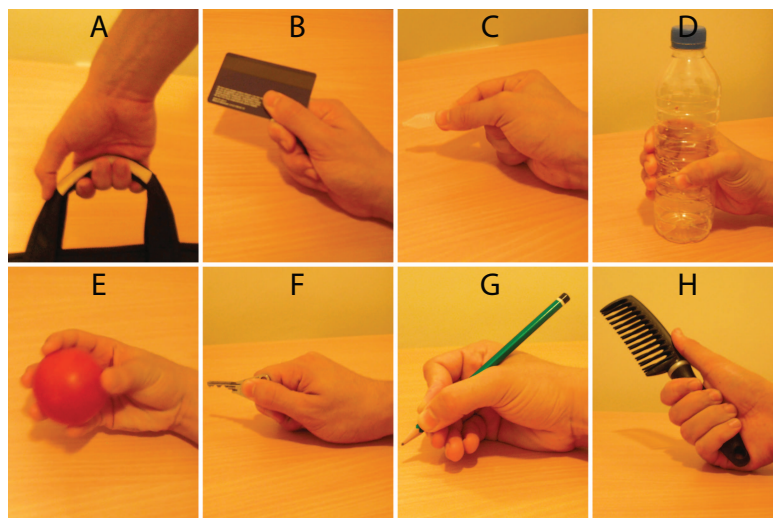
Figure 2.3: Grasp types used in Brunnstrom's therapy

Hook Grasp This type of grasp is used for tasks like holding a handle which consists flexion of all the fingers at once (Figure 2.3-a).

Lateral Prehension This type of grip is used to pick up tiny objects like card between the thumb and index finger (Figure 2.3-b).

Palmar Prehension This type of grip is used to hold an item such as pencil between the thumb and the first one or two fingers (Figure 2.3-c).

Cylindrical Grasp This type of grasp is used to hold medium sized cylindrical objects in the palm by the fingers and the thumb (Figure 2.3-d).

Spherical Grasp This type of grasp is used to pick up round objects, such as a ball, in the palm (Figure 2.3-e).

Key Pinch This type of pinch is used to pick up a key. Thumb is pressed to the side of index finger as the finger is in flexion (Figure 2.3-f).

Chuck Grip This grip is similar to palmar prehension using the thumb and two fingers to hold a cylindrical item as in a drill chuck (Figure 2.3-g).

Power Grasp This grasp consists flexion of fingers around the object while the thumb stands along the object for stabilization (Figure 2.3-h).
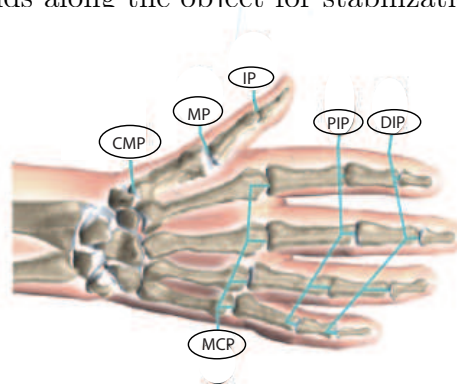
Figure 2.4: Finger joints

On the other hand, biomechanics literature suggest that the human finger (except the thumb) can be modeled as a serial URR manipulator, which has four degrees of freedom (DoF). From the distal end, the joints are named as distal interphalangeal (DIP), proximal interphalangeal (PIP), and metacarpophalangeal (MCP), respectively (see Figure 2.4). The DIP and PIP joints have flexion/extension DoF, while the MCP joint has both flexion/extension and abduction/adduction DoF. Conforming with the ergonomics of the human finger is an imperative requirement that is satisfied thanks to the kinematic design of the finger exoskeleton.

Table 2.2: Anthropomorphic data for human finger lengths

Finger	$L_{proximal}$(mm)	L_{middle}(mm)	L_{distal}(mm)
Index	45.48	25.96	22.99
Middle	41.95	30.87	25.85
Ring	44.5	30.3	20.02
Pinky	35.2	25.2	18.8

Motion of a finger is performed in a coordinated path. Through the path, rotation axes of the human finger have to be aligned with the joint axes of the exoskeleton which means length of finger knuckles are important for a device to impose a healthy motion. Distance between these joints depends on person's gender, age and other characteristics. Therefore the exoskeleton device is designed with nominal link lengths of human hand size of anthropomorphic data for finger knuckle lengths as given in Table 2.2 [64, 65] and can be increased and decreased in a small range to fit every subject finger comfortably.

Table 2.3: Means and standard deviations (in brackets) of finger ROM

Finger	PIP (deg)	MCP (deg)	DIP (deg)
Index	70.83 (11.09)	103.87 (7.79)	61.17 (12.71)
Middle	85.30 (9.87)	103.98 (8.98)	73.64 (16.30)
Ring	85.09 (14.46)	107.15 (13.49)	66.96 (15.77)
Pinky	85.58 (18.09)	98.95 (11.20)	70.79 (15.84)

A finger exoskeleton that is appropriate for treatment of tendon injuries is required to cover the natural range of motion of the flexion/extension motion of each joint of the finger which is given in Table 2.3 [66]. Hence, the mechanism must at least attain three DoF. Ergonomics not only necessitates

22

Table 2.4: Required joint torques

	Thumb(Nm)	Fingers(Nm)
PIP abd/add	0.33	0.17
PIP flex/ext	0.29	0.29
MCP flex/ext	0.26	0.29
DIP flex/ext	0.25	0.20

the collocation of finger and device joint axis concentrically but also requires that the kinematics of the exoskeleton support for natural finger motions without any interference through whole motion range.

Moreover, the amount of torque generated by the robot at each joint of the hand is required to overcome the tone and spasticity at patient's digits. The minimum torque that is transmitted to the joints must satisfy minimum required activation torque of a joint. In order to gain the required torque with a small actuator, linkage based design would be more appropriate instead of cable driven design. The torque transmitted through the joints should be calculated by kinematics of the robot and ensured that supplied torque overcomes the required actuation torque for each joint given in Table 2.4 [67].

2.1.2 Design Requirements for Rehabilitation Devices

In addition to anatomical and physiological requirements of human distal upper extremity, there are also some phycological and mechanical requirements that a rehabilitation hand robot must meet.

Ensuring the safety and complying with the ergonomic needs of the human are two imperative design requirements every rehabilitation device must satisfy [68]. For a rehabilitation device, the most important requirement is

that the robot must be safe. This requirement includes the need for the robot to be back drivable, as well as the inclusion of software limits in the robot controls and mechanical limits to prevent any possible injury. Also ergonomics necessitate that the movements imposed by the robot must be compatible with the natural movement of human.

The performance requirements for the rehabilitation device can be considered as the span of the singularity-free workspace, the force/torque limits that can be provided at end effector and a uniform feel of the device. Since these requirements are related with the dimensions and kinematics, they are considered while performing of optimal dimensional synthesis.

Primary requirements include: comfort, adjustability and aesthetics. Robot must be comfortable for the patient, not cause any physical or phycological pain to the patient since many patients might also be dealing with the discomfort of injury in their hands. Being able to fit different patients and being easy to get on and off can be considered a necessity for comfort. Furthermore the robot must be aesthetically pleasing since it will interact with the patient who might ever not been interacted with a robot. Device should also actuate both grasp and release function and include a passive mechanism in order to compensate for hypertonia.

Compactness, portability and manufacturing costs of the device are secondary design requirements ensured by appropriate material and design choice. Also actuation and transmission selection should be performed which satisfies high motion resolution and low parasitic dynamics (friction and backlash), so that the device can be effectively employed as a measurement tool.

2.2 Kinematic Type Selection

After deciding on the requirements like degrees of freedom, range of motion, safety and functionality of device, appropriate kinematic selection is performed for both devices.

2.2.1 Stroke Device

The kinematics of the stroke device is selected to allow rotations of the wrist/forearm, concurrently with the hand grasp/release action within the natural workspace of these joints. In particular, a planar parallel $3 - \underline{R}RP$ robot is selected as the main kinematic structure of the rehabilitation system (see Figure 2.5). Here "R" refers to revolute joint and "P" refers to prismatic joint while underlined joint is the actuated one.
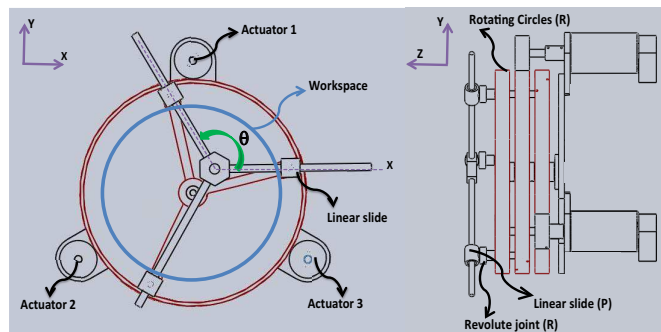
Figure 2.5: Kinematics of the 3-RRP mechanism

The $3 - \underline{R}RP$ mechanism has 3 DoF on the plane: two translations and one rotation of its end effector. The mechanism is constructed and dimensioned such that its end effector can span a circular workspace of 130 mm diameter. More importantly, the device end effector can rotate more

than 360 degrees at any point within the workspace of the device. The kinematics of $3 - \underline{R}RP$ mechanism allows for concurrent rotations of the wrist joint through its translations, while the rotation of the device end effector can accommodate, either the forearm rotations, or the grasp/release actions of the hand, thanks to specially designed modular end effectors. The workspace of the device is set large enough to fit various hand sizes and set to be symmetric to allow for both right-handed or left-handed use.

2.2.2 Tendon Device

In order to span the whole natural flexion/extension range of motion of the human finger and to do so robustly for various operators with different finger dimensions, a parallel mechanism based kinematic structure is adapted for the finger exoskeleton, for which the kinematics of the human finger is an integral part of the device kinematics. The device is only operational when worn by a human operator. When coupled to the human operator, the parallel kinematic structure of exoskeleton supports three independent DoF, dictated by the kinematics of the human finger. Hence, not only can the device cover the whole RoM of any operator, but it can do so in a completely ergonomic manner. Moreover, the linkage based kinematic structure of the parallel mechanism is advantageous over cable driven transmission mechanisms, since linkages allow for direct and efficient transfer of forces form the grounded actuators to each phalanx of the finger.

Having three DoF, up to three independent actuators can be utilized to control the mechanism. However, for physical therapy exercises following tendon injuries, independent motion of each phalanx of the finger is hardly

26

necessary as long as a wide range of coordinated finger motions can be supported and the whole RoM of the finger is covered. Hence, an underactuated mechanism is selected for the kinematic structure of the finger exoskeleton. The choice of an underactuated mechanism is also advantageous as it embodies further ergonomy and safety into the design. In particular, the uncontrolled degree of freedom of the device can passively compensate for the alignments errors between the joint axes of the finger and the exoskeleton. In addition to the utilization of adjustable linkages and connectors to ensure that the center of rotation of the human joints are aligned with the device axis, the inherent passive compensation adds further robustness into the device. Furthermore, underactuation enables size, weight, and cost reduction for the exoskeleton, since the actuators are the largest, heaviest, and most expensive parts of the device.
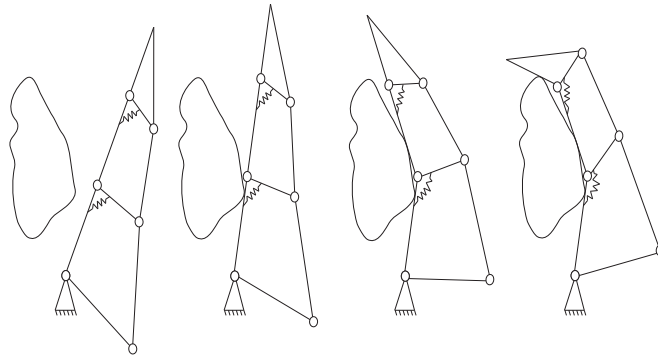
Figure 2.6: Schematic representation of the motion of the underactuated parallel kinematic chain against an obstacle

Figure 2.6 depicts a schematic representation of the kinematic structure used for the exoskeleton and presents motion of the device against an obstacle. The kinematics of the exoskeleton is similar to the underactuated fingers introduced by Gosselin et al. [69] and is effectively equivalent to the kine-

matics of a series of four/six-bar mechanisms that are coupled to each other with compliant springs and constrained by mechanical joint limits. Compliant springs are used for the mechanism to ensure a coordinated motion of the phalanxes. In particular, the springs maintain the second and third phalanxes of the finger in fully extended configurations until the first phalanx comes in contact with an obstacle or reaches a mechanical limit. When the mechanism is free of contacts and within joint limits, it behaves like a single rigid body. But when the motion of a phalanx is resisted, the torque generated by the motor overcomes the spring pre-load and the adjacent phalanx initiates motion. The motion continues sequentially until motion of all phalanxes are resisted due to either contact with the object or a joint limit is encountered. Hence, the mechanism is capable of reproducing many of the natural finger trajectories and the actuator forces are distributed over all phalanxes. The spring pre-load at each joints can be customized to accommodate patients with different finger stiffness levels.

During therapy, the motion of the underactuated mechanism complies with the natural grasping motions of the finger and motion can easily be modulated to target different exercises through the introduction of custom joint limits, spring pre-loads, or obstacles. Hence, the exoskeleton is appropriate to target RoM and strengthening exercises. During flexion, the motion starts around the MCP joint until the first phalanx encounters an obstacle or the MCP joint limit is achieved. When the motion around the MCP joint is resisted, the force threshold dictated by the compliant spring between first and second phalanx is overcome and motion around the PIP joint initiates. Once again if the motion around the PIP joint is resisted due to an obstacle or joint limit, then the force threshold of the second compliant spring is

achieved and the third phalanx moves about the DIP joint. During extension movements takes place in the reverse order until joint limits of DIP, PIP, and MCP are reached, sequentially.

2.3 Kinematic Analysis

The performance of a machine is analyzed by calculating the position, velocity and acceleration of points on the different parts of the mechanisms and tracing the trajectory they follow.

2.3.1 Stroke Device

Configuration and motion level kinematics of the stroke device are analytically calculated in order to see the performance of the device before dimensional synthesis.

System Description

The planar kinematic model of the stroke device is depicted in Figure 2.7. The mechanism consists of five rigid bodies, N, S, T, V , and the symmetric body E. Body N is the fixed link, the links S, T, V have simple rotations about the fixed link around point O, and the symmetric end effector link E is attached to the links S, T, V through prismatic and revolute joints concurrently located at points $P, Q,$ and $R,$ respectively. Point O is fixed in N, point P is fixed in T, point Q is fixed in S, point R is fixed in V , and point Z is fixed in E. The common out of the plane unit vector is denoted

by $\overrightarrow{k}$ and basis vectors of each body are indicated in Figure 2.7.
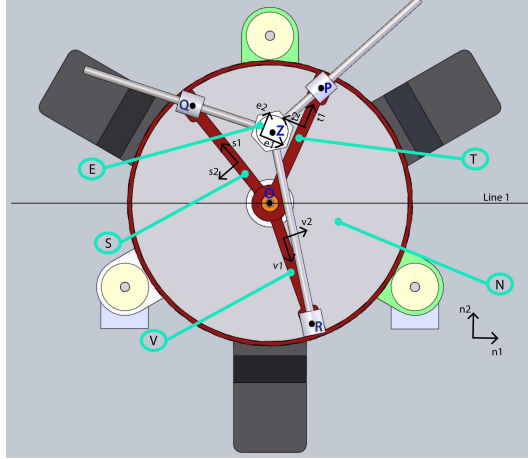
Figure 2.7: The 3-RRP planar robot

Dimensions of the mechanism are to be taken as follows: The fixed distance OP is defined as l_1, the fixed distance OQ is defined as l_2, and the fixed distance OR is defined as l_3, while the distance ZP is defined a s_1, the distance ZQ is defined a s_2, and the distance ZR is defined a s_3. The angle between the line l and $\overrightarrow{t_1}$ vector is $\widehat{q_1}$, the angle between the line l and $\overrightarrow{s_1}$ vector is $\widehat{q_2}$, and the angle between the line l and $\overrightarrow{v_1}$ vector is $\widehat{q_3}$. All angles are measured counter clockwise.

The inputs to the system are the angles q_1, q_2, q_3 (i.e. links S, T, and V are actuated) and their time derivatives. At the initial configuration, $\overrightarrow{e_1}$ is parallel to $\overrightarrow{n_1}$. The output of the system is the position of the end effector point Z, when measured from point O, and the orientation of body E, with respect to body N. Scalar variables for outputs are defined as $x = r^{OZ}\overrightarrow{n_1}$, $y = r^{OZ}\overrightarrow{n_2}$, and the angle $\theta = atan2\left(\frac{\overrightarrow{e_2}\cdot\overrightarrow{n_2}}{\overrightarrow{e_2}\cdot\overrightarrow{n_2}}\right)$ where r^{OZ} is the distance between point O and point Z.

Configuration Level Kinematics

In order to have a clear system of calculations, three auxiliary reference frames (K,L,M) are defined as: $\overrightarrow{k_1}$ extends from Z to P, $\overrightarrow{l_1}$ extends from Z to S, $\overrightarrow{m_1}$ extends from Z to R while $\overrightarrow{k_3} = \overrightarrow{l_3} = \overrightarrow{m_3} = \overrightarrow{n_3}$

Using the defined auxiliary reference frames 3 loop equations are defined:

$$x \cdot \overrightarrow{n_1} + y \cdot \overrightarrow{n_2} + s_1 \cdot \overrightarrow{k_1} - l_1 \cdot \overrightarrow{t_1} = \overrightarrow{0} \tag{1}$$

$$x \cdot \overrightarrow{n_1} + y \cdot \overrightarrow{n_2} + s_2 \cdot \overrightarrow{l_1} - l_2 \cdot \overrightarrow{s_1} = \overrightarrow{0} \tag{2}$$

$$x \cdot \overrightarrow{n_1} + y \cdot \overrightarrow{n_2} + s_3 \cdot \overrightarrow{m_1} - l_3 \cdot \overrightarrow{v_1} = \overrightarrow{0} \tag{3}$$

Vector loop equations can be defined in one generalized frame (frame N) through rotation matrices.

$$x \cdot \overrightarrow{n_1} + y \cdot \overrightarrow{n_2} + s_1 \cdot [\cos(\theta + \frac{\pi}{3})\overrightarrow{n_1} + \sin(\theta + \frac{\pi}{3})\overrightarrow{n_2}]$$
$$- l_1 \cdot [\cos(q_1)\overrightarrow{n_1} + \sin(q_1)\overrightarrow{n_2}] = \overrightarrow{0}$$

$$x \cdot \overrightarrow{n_1} + y \cdot \overrightarrow{n_2} + s_2 \cdot [\cos(\theta + \pi)\overrightarrow{n_1} + \sin(\theta + \pi)\overrightarrow{n_2}]$$
$$- l_2 \cdot [\cos(q_2)\overrightarrow{n_1} + \sin(q_2)\overrightarrow{n_2}] = \overrightarrow{0}$$

$$x \cdot \overrightarrow{n_1} + y \cdot \overrightarrow{n_2} + s_3 \cdot [\cos(\theta - \frac{\pi}{3})\overrightarrow{n_1} + \sin(\theta - \frac{\pi}{3})\overrightarrow{n_2}]$$
$$- l_3 \cdot [\cos(q_3)\overrightarrow{n_1} + \sin(q_3)\overrightarrow{n_2}] = \overrightarrow{0}$$

The obtained vector equations yield 6 independent scalar equations which will form the base for solution of configuration level kinematics.

Configuration Level Forward Kinematics: For a configuration level forward kinematics problem actuated angle q_1, q_2, q_3 are given and it is expected to solve for end effector positions x, y, θ (and optionally s_1, s_2, s_3). In the previous section we have derived three vector equations corresponding to six nonlinear scalar equations and six unknowns are called for solution. The forward kinematics problem is solved analytically by eliminating passive variables from the six equations (derivation can be found from Appendix B).

$$x = -\frac{M}{\sqrt{(3)(K^2 + L^2)}}$$

$$y = c_{22} - \frac{K}{L}c_{21} - \frac{KM}{\sqrt{(3)L(K^2 + L^2)}}$$

$$\theta = tan^{-1}(\frac{K}{L})$$

where

$$K = c_{12} + c_{32} + \sqrt{3}c_{31} - 2c_{22} - \sqrt{3}c_{11}$$

$$L = c_{11} + c_{31} + \sqrt{3}c_{12} - 2c_{21} - \sqrt{3}c_{32}$$

$$M = L(L - \sqrt{(3)}K)c_{12} - L(K + \sqrt{(3)}L)c_{11} - (L - \sqrt{(3)}K)(Lc_{22} - Kc_{21})$$

$$c_{11} = l_1 cos(q_1)$$

$$c_{12} = l_1 sin(q_1)$$

$$c_{21} = l_2 cos(q_2)$$

$$c_{22} = l_2 sin(q_2)$$

$$c_{31} = l_3 cos(q_3)$$

$$c_{32} = l_3 sin(q_3)$$

Configuration Level Inverse Kinematics: For inverse kinematics end effector positions x, y, θ are given and it is expected to solve for actuator positions q_1, q_2, q_3(and optionally s_1, s_2, s_3). Inverse kinematics problem includes 3 coupled triangle equations and solved analytically by using the vector cross product method suggested by Chace. Derivation can be found from Appendix B.

$$q_1 = tan^{-1}(\frac{M_1}{L_1})$$

$$q_2 = tan^{-1}(\frac{M_2}{L_2})$$

$$q_3 = tan^{-1}(\frac{M_3}{L_3})$$

where

$$M_1 = K_1 cos(\theta + \frac{\pi}{3}) - \sqrt{(l_1^2 - K_1^2)} sin(\theta + \frac{\pi}{3})$$

$$L_1 = -K_1 sin(\theta + \frac{\pi}{3}) - \sqrt{(l_1^2 - K_1^2)} cos(\theta + \frac{\pi}{3})$$

$$M_2 = K_2 cos(\theta + \pi) - \sqrt{(l_2^2 - K_2^2)} sin(\theta + \pi)$$

$$L_2 = -K_2 sin(\theta + \pi) - \sqrt{(l_2^2 - K_2^2)} cos(\theta + \pi)$$

$$M_3 = K_3 cos(\theta - \frac{\pi}{3}) - \sqrt{(l_3^2 - K_3^2)} sin(\theta - \frac{\pi}{3})$$

$$L_3 = -K_3 sin(\theta - \frac{\pi}{3}) - \sqrt{(l_3^2 - K_3^2)} cos(\theta - \frac{\pi}{3})$$

$$K_1 = x \sin(\theta + \frac{\pi}{3}) - y \cos(\theta + \frac{\pi}{3})$$

$$K_2 = x\sin(\theta + \pi) - y\cos(\theta + \pi)$$

$$K_3 = x\sin(\theta - \frac{\pi}{3}) - y\cos(\theta - \frac{\pi}{3})$$

Motion Level Kinematics

Motion level kinematic equations are derived by taking the time derivative of the 3 vector equations for configuration level kinematics. After taking derivative of the equations 3 vector equations are obtained as:

$$\dot{x}\overrightarrow{n_1} + \dot{y}\overrightarrow{n_2} + \dot{s_1}[\cos(\theta + \frac{\pi}{3})\overrightarrow{n_1} + \sin(\theta + \frac{\pi}{3})\overrightarrow{n_2}] + s_1\dot{\theta}[-\sin(\theta + \frac{\pi}{3})\overrightarrow{n_1}$$
$$+ \cos(\theta + \frac{\pi}{3})\overrightarrow{n_2}] - l_1\dot{q_1}[-\sin(q_1)\overrightarrow{n_1} + \cos(q_1)\overrightarrow{n_2}] = \overrightarrow{0}$$

$$\dot{x}\overrightarrow{n_1} + \dot{y}\overrightarrow{n_2} + \dot{s_2}[\cos(\theta + \pi)\overrightarrow{n_1} + \sin(\theta + \pi)\overrightarrow{n_2}] + s_2\dot{\theta}[-\sin(\theta + \pi)\overrightarrow{n_1}$$
$$+ \cos(\theta + \pi)\overrightarrow{n_2}] - l_2\dot{q_2}[-\sin(q_2)\overrightarrow{n_1} + \cos(q_2)\overrightarrow{n_2}] = \overrightarrow{0}$$

$$\dot{x}\overrightarrow{n_1} + \dot{y}\overrightarrow{n_2} + \dot{s_3}[\cos(\theta - \frac{\pi}{3})\overrightarrow{n_1} + \sin(\theta - \frac{\pi}{3})\overrightarrow{n_2}] + s_3\dot{\theta}[-\sin(\theta - \frac{\pi}{3})\overrightarrow{n_1}$$
$$+ \cos(\theta - \frac{\pi}{3})\overrightarrow{n_2}] - l_3\dot{q_3}[-\sin(q_3)\overrightarrow{n_1} + \cos(q_3)\overrightarrow{n_2}] = \overrightarrow{0}$$

Six scalar equations can be obtained by considering the $\overrightarrow{n_1}$ and $\overrightarrow{n_2}$ directions of each vector equation separately.

Motion Level Forward Kinematics: For the motion level forward kinematics problem actuator velocities $\dot{q_1}, \dot{q_2}, \dot{q_3}$ are given and it is expected to solve for end effector velocities $\dot{x}$, $\dot{y}$, $\dot{\theta}$ (and optionally $\dot{s_1}, \dot{s_2}, \dot{s_3}$). In the previous section we have derived three vector equations corresponding to six linear equations and six unknowns are called for solution. Problem is solved

by a matrix calculation.

$$A_1 \dot{X}_1 = B_1$$

$$\dot{X}_1 = A_1^{-1} B_1$$

where

$$A_1 = \begin{pmatrix} 1 & 0 & -s_1 \sin(\theta + \frac{\pi}{3}) & \cos(\theta + \frac{\pi}{3}) & 0 & 0 \\ 0 & 1 & s_1 \cos(\theta + \frac{\pi}{3}) & \sin(\theta + \frac{\pi}{3}) & 0 & 0 \\ 1 & 0 & -s_2 \sin(\theta + \pi) & 0 & \cos(\theta + \pi) & 0 \\ 0 & 1 & s_2 \cos(\theta + \pi) & 0 & \sin(\theta + \pi) & 0 \\ 1 & 0 & -s_3 \sin(\theta - \frac{\pi}{3}) & 0 & 0 & \cos(\theta - \frac{\pi}{3}) \\ 0 & 1 & \varnothing s_3 \cos(\theta - \frac{\pi}{3}) & 0 & 0 & \sin(\theta - \frac{\pi}{3}) \end{pmatrix}$$

$$\dot{X}_1 = \begin{pmatrix} \dot{x} \\ \dot{y} \\ \dot{\theta} \\ \dot{s}_1 \\ \dot{s}_2 \\ \dot{s}_3 \end{pmatrix} \qquad B_1 = \begin{pmatrix} -l_1 \dot{q}_1 \sin(q_1) \\ l_1 \dot{q}_1 \cos(q_1) \\ -l_2 \dot{q}_2 \sin(q_2) \\ l_2 \dot{q}_2 \cos(q_2) \\ -l_3 \dot{q}_3 \sin(q_3) \\ l_3 \dot{q}_3 \cos(q_3) \end{pmatrix}.$$

Motion Level Inverse Kinematics: For a motion level inverse kinematics problem end-effector velocities $\dot{x}$, $\dot{y}$, $\dot{\theta}$ are given and it is expected to solve for actuator velocities $\dot{q}_1, \dot{q}_2, \dot{q}_3$ (and optionally $\dot{s}_1, \dot{s}_2, \dot{s}_3$). Again using the derived six linear equations six unknowns are called for solution. Similarly problem is solved by a matrix calculation:

$$A_2 \dot{X}_2 = B_2$$

$$\dot{X}_2 = A_2^{-1} B_2$$

where

$$A_2 = \begin{pmatrix} l_1 \sin(q_1) & 0 & 0 & \cos(\theta + \frac{\pi}{3}) & 0 & 0 \\ -l_1 \cos(q_1) & 0 & 0 & \sin(\theta + \frac{\pi}{3}) & 0 & 0 \\ 0 & l_2 \sin(q_2) & 0 & 0 & \cos(\theta + \pi) & 0 \\ 0 & -l_2 \cos(q_2) & 0 & 0 & \sin(\theta + \pi) & 0 \\ 0 & 0 & l_3 \sin(q_3) & 0 & 0 & \cos(\theta - \frac{\pi}{3}) \\ 0 & 0 & -l_3 \cos(q_3) & 0 & 0 & \sin(\theta - \frac{\pi}{3}) \end{pmatrix}$$

$$X_2 = \begin{pmatrix} \dot{q}_1 \\ \dot{q}_2 \\ \dot{q}_3 \\ \dot{s}_1 \\ \dot{s}_2 \\ \dot{s}_3 \end{pmatrix} \qquad B_2 = \begin{pmatrix} -\dot{x} + s_1 \dot{\theta} \sin(\theta + \frac{\pi}{3}) \\ -\dot{y} - s_1 \dot{\theta} \cos(\theta + \frac{\pi}{3}) \\ -\dot{x} + s_2 \dot{\theta} \sin(\theta + \pi) \\ -\dot{y} - s_2 \dot{\theta} \cos(\theta + \pi) \\ -\dot{x} + s_3 \dot{\theta} \sin(\theta - \frac{\pi}{3}) \\ -\dot{y} - s_3 \dot{\theta} \cos(\theta - \frac{\pi}{3}) \end{pmatrix}$$

2.3.2 Tendon Device

Before making a decision on the optimum link lengths, configuration and motion level kinematics of the tendon robot are analytically calculated in order to estimate the performance of the device.

System Description

As previously mentioned, tendon device has a linkage based planar kinematic structure which is formed by a series of four-bar structures. Motion of each joint is ensured through different four-bars. MCP joint can cover its range of motion satisfying the vector loop equation

$$\vec{r0} + \vec{r1} + \vec{r2} + \vec{r3} = \vec{0}$$

shown in Figure 2.8-a. When first knuckle completes its motion second knuckle rotates around PIP joint in all its motion range under constraint of the vector loop equation

$$\vec{r1} + \vec{r2} + \vec{r4} + \vec{r5} = \vec{0}$$
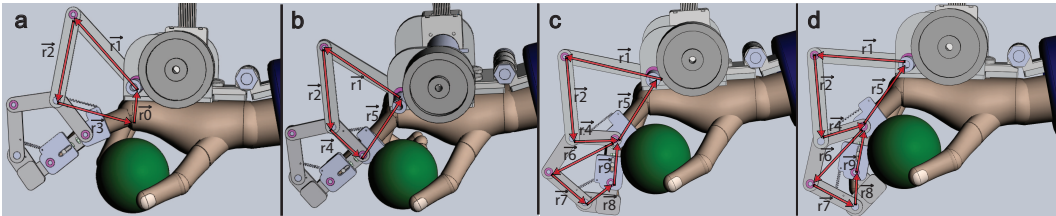
Figure 2.8: Kinematic constraint loops for joint motion of: (a)MCP (b)PIP (c)DIP

shown in Figure 2.8-b. Finally the third knuckle turns around DIP joint with the kinematic constraint

$$\overrightarrow{r1} + \overrightarrow{r2} + \overrightarrow{r4} + \overrightarrow{r5} = \overrightarrow{0}$$

coupled with

$$\overrightarrow{r6} + \overrightarrow{r7} + \overrightarrow{r8} + \overrightarrow{r9} = \overrightarrow{0}$$

indicated as in Figure 2.8-c.

Configuration Level Kinematics

Although kinematic calculations of an underactuated mechanism seem complex, it basically refers to kinematics of different four-bar structures for each actuated finger joint. Position level kinematics of a four-bar structure is applied to all loops for the tendon device. The derivation of configuration level kinematics solution for a four-bar structure is attached to Appendix B. This solution is applied to corresponding four-bars for MCP, PIP and DIP actuation.

Motion Level Kinematics

Motion level kinematic problem of the four-bar mechanism is easy to solve. Differentiating configuration level loop equation gives us a set of linear equations.

$$r_1 sin(\theta_1)\omega_1 + r_2 sin(\theta_2)\omega_2 + r_3 sin(\theta_3)\omega_3 = 0$$

$$r_1 cos(\theta_1)\omega_1 + r_2 cos(\theta_2)\omega_2 + r_3 cos(\theta_3)\omega_3 = 0$$

where ω_i corresponds to the angular velocity of ith linkage.

Motion Level Forward Kinematics: In the motion level forward problem ω_1 is given and it is expected to solve for end effector velocities which are ω_3, ω_4 and ω_8 for MCP, PIP and DIP joints respectively. The motion level loop equations can be written in matrix form as:

$$A_1 X_1 = B_1$$

$$X_1 = A_1^{-1} B_1$$

when MCP joint is actuated:

$$A_1 = \begin{pmatrix} r_2 \sin(\theta_2) & r_3 \sin(\theta_3) \\ r_2 \cos(\theta_2) & r_3 \cos(\theta_3) \end{pmatrix}$$

$$X_1 = \begin{pmatrix} \omega_2 \\ \omega_3 \end{pmatrix} \qquad B_1 = \begin{pmatrix} -r_1 \sin(\theta_1)\omega_1 \\ -r_1 \cos(\theta_1)\omega_1 \end{pmatrix}.$$

when PIP joint is actuated:

$$A_1 = \begin{pmatrix} r_2 \sin(\theta_2) & r_4 \sin(\theta_4) \\ r_2 \cos(\theta_2) & r_4 \cos(\theta_4) \end{pmatrix}$$

$$X_1 = \begin{pmatrix} \omega_2 \\ \omega_4 \end{pmatrix} \qquad B_1 = \begin{pmatrix} -r_1 \sin(\theta_1)\omega_1 \\ -r_1 \cos(\theta_1)\omega_1 \end{pmatrix}.$$

when DIP joint is actuated:

$$A_1 = \begin{pmatrix} r_7 \sin(\theta_7) & r_8 \sin(\theta_8) \\ r_7 \cos(\theta_7) & r_8 \cos(\theta_8) \end{pmatrix}$$

$$X_1 = \begin{pmatrix} \omega_7 \\ \omega_8 \end{pmatrix} \qquad B_1 = \begin{pmatrix} -r_6 \sin(\theta_6)\omega_6 \\ -r_6 \cos(\theta_6)\omega_6 \end{pmatrix}.$$

where $\omega_6 = \omega_4$ and ω_4 can be solved as done for PIP joint.

Motion Level Inverse Kinematics: For the motion level inverse problem end effector velocities ω_3, ω_4 and ω_8 for MCP, PIP and DIP joints respectively are given and it is expected to solve for actuator velociy ω_1. The motion level loop equations can be written in matrix form as:

$$A_2 X_2 = B_2$$

$$X_2 = A_2^{-1} B_2$$

when MCP joint is actuated:

$$A_1 = \begin{pmatrix} r_1 \sin(\theta_1) & r_2 \sin(\theta_2) \\ r_1 \cos(\theta_1) & r_2 \cos(\theta_2) \end{pmatrix}$$

$$X_1 = \begin{pmatrix} \omega_1 \\ \omega_2 \end{pmatrix} \qquad B_1 = \begin{pmatrix} -r_3 \sin(\theta_3)\omega_3 \\ -r_3 \cos(\theta_3)\omega_3 \end{pmatrix}.$$

when PIP joint is actuated:

$$A_1 = \begin{pmatrix} r_1 \sin(\theta_1) & r_2 \sin(\theta_2) \\ r_1 \cos(\theta_1) & r_2 \cos(\theta_2) \end{pmatrix}$$

$$X_1 = \begin{pmatrix} \omega_1 \\ \omega_2 \end{pmatrix} \qquad B_1 = \begin{pmatrix} -r_4 \sin(\theta_4)\omega_4 \\ -r_4 \cos(\theta_4)\omega_4 \end{pmatrix}.$$

when DIP joint is actuated:

$$A_1 = \begin{pmatrix} r_6 \sin(\theta_6) & r_7 \sin(\theta_7) \\ r_6 \cos(\theta_6) & r_7 \cos(\theta_7) \end{pmatrix}$$

$$X_1 = \begin{pmatrix} \omega_6 \\ \omega_7 \end{pmatrix} \qquad B_1 = \begin{pmatrix} -r_8 \sin(\theta_8)\omega_8 \\ -r_8 \cos(\theta_8)\omega_8 \end{pmatrix}.$$

after solving ω_6 the equations of PIP joint can be used to find ω_1 since $\omega_4 = \omega_6$.

2.4 Optimal Dimensional Synthesis

Preliminary designs and experiments brought out that performance of the mechanism is highly sensitive to its dimensions and optimization studies are absolutely necessary for design of the mechanism. The performance requirements to be optimized are highly dependent on the final use of the device. For a rehabilitation device, kinematic/dynamic isotropy and torque transmission efficiency of the device should be maximized while effective moving mass should be minimized to achieve high torque transmission and a uniform feel for the device.

2.4.1 Stroke Device

Parallel manipulators have several advantages over serial manipulators, including high stiffness, low inertia, and good dynamic characteristics. However they also have disadvantages like limited workspace, difficulties in their analysis, synthesis, control and trajectory planning while their direct or forward kinematics are also typically challenging [70]. One of the primary challenges of a parallel manipulator is the appearance of singularities in the workspace and consequently small workspace areas. Therefore various optimization studies are performed in literature to increase efficiency of parallel mechanism. In [71],unreachable areas of a parallel robot is minimized using a geometric approach. A parallel manipulator is optimized in terms of kinematic isotropy and force balancing in [72]. In [73] singularities for different kinematic structures including 3-RRP are categorized. In [74], singularities in the workspace of a 3-PRR device are minimized. An RPR device is also opti-

mized by architectural parameters in [75] to achieve optimal singularity-free workspace. Circular singularity-free zones within the workspace of an RPR manipulator are solved in [76], indicating the difficulty of having large singularity free workspace with large rotational motion range. Similar to most of the studies in literature, for our device we have performed an optimization study to achieve the required singularity-free workspace with minimum device size.

Problem Definition

After deciding the kinematic structure of the robot to be $3 - \underline{R}RP$ a parallel mechanism, optimal lengths of the links which ensure the required motion with a uniform feel is to be determined since the performance of parallel mechanisms are highly dependent upon to its link lengths.

Table 2.5: Anthropomorphic data for human hand size

Hand	NASA(inch)	Airforce (inch)	Buchholz (inch)
Breadth (male)	3.44	3.47	3.48
Breadth (female)	2.99	-	3.22
Length (male)	7.59	7.68	7.42
Length (female)	7.25	-	6.76
Palm Length (male)	4.3	-	-
Palm Length (female)	3.78	-	-
Wrist Breadth (male)	-	-	2.59
Wrist Breadth (female)	-	-	2.4

The required workspace is defined as a circular area which covers the whole motion range of hand and wrist while forearm is stabilized. Using the anthropomorphic hand dimensions given in Table 2.5 and range of motion

43

of wrist given in Table 2.1, the workspace is defined as an arc with angle of 160° and radius of 110 mm. Also in order to impose all wrist and forearm movements to human by alternating the configuration of device, another criteria is appended that the end effector must rotate at least 360° in all over the defined workspace.

In order to obtain the desired workspace with minimum device size two assumptions are done:

- The decrease in the workspace due to mechanical components, assembly features and manufacturing errors are neglected.

- The mechanism is totally symmetric that distance between actuators and lengths of the links are exactly same.

To sum up, the optimization problem can be defined as

Decision variables: link lengths (l_1, l_2, l_3 in Figure 2.7)

Objective Function: minimize the device size (or minimize l_1, l_2, l_3)

Constraints: End effector must reach every point in an arc with angle of 160° and radius of 110 mm. Also the end effector must rotate at least 360° at each point in the workspace.

With the symmetry assumption, since objective function and decision variables are same, the objective function can be defined as:

$$F(x) = x,$$

While constraints are nonlinear functions of the inverse kinematic problem.

Solution Methods

As defined in the previous section, we have a single objective linear minimization problem with nonlinear constraints. A line search algorithm is used for parameter-space search and a brute-force algorithm is used for workspace search.

The algorithm can be summarized as:

1. Define upper and lower bound for the link length: x_{ub} and x_{lb} respectively. Also set $e =$ a sufficiently large number and $\epsilon =$ a sufficiently small number

2. Define the initial choice: x_i

3. Check whether $e \leq \epsilon$ or $e > \epsilon$

   - if $e \leq \epsilon$, Go to Step 5;

   - if $e > \epsilon$, Go to Step 4.

4. Check whether x_i holds the constraints or not

   - if holds

     – Define new decision as $x_{i+1} = (x_i + x_{ub}) * r$

     – Change the lower bound as $x_{lb} = x_i$

     – Change the value of epsilon as $\epsilon = x_{i+1} - x_i$

     – Return to step 3.

   - if does not hold

     – Define new decision as $x_{i+1} = (x_i + x_{lb}) * r$

45

- Change the upper bound as $x_{ub} = x_i$

- Change the value of epsilon as $\epsilon = x_i - x_{i+1}$

- Return to step 3.

5. Halt the program

Since the objective function is linear and unimodal, this algorithm guarantees the global optimum. The coefficient r is selected as r=0.5 to achieve best timing performance. Also the constraint check is performed by a brute-force search throughout the workspace over inverse kinematics of the system.

Results

The problem is coded and ran through MATLAB and optimum solution is calculated. To check the feasibility of the solution, an animation code is also ran which constructs a video of the device end effector moving in the required workspace with the determined lengths.

The minimum value of l_1, l_2, l_3 which satisfy the required workspace is found as 80 mm.

2.4.2 Tendon Device

In literature, several optimal performance of finger devices are calculated. Cabas optimized a robotic hand which has three underactuated fingers to increase manipulate capability [77]. Nacy et al. optimized grasp stability of a three phalanx prosthesis underactuated finger by particle swarm optimization method [78]. Wu et al. performed an optimization study for efficiency

of object adaptation for a finger with 1 active degrees of freedom [79]. In [80] a multiobjective optimization is done an underactuated finger to maximize transmission efficiency and grasp stability. Birglen and Gosselin optimized a two phalanx underactuated finger to have force isotropy and grasp stability [81]. As discussed, most of the optimization studies for fingers are performed for prosthetics in order to obtain force isotropy and grasp stability by varying mostly knuckle lengths. Yet exoskeleton type finger devices can not be optimized in such a way since knuckle lengths are not configurable. Therefore we have performed an optimal dimensional synthesis of exoskeleton type devices through study of several design matrices, including kinematic Jacobian and mass matrix considering global performance measures and characterizing the performance of the device over the entire workspace. To quantify the kinematic/dynamic performance of the device worst-case performance of torque transmission and effective inertia are considered. Both of these indices are conservative workspace inclusive worst-case performance measures that are intolerant of poor performance over the entire workspace.

Problem Definition:

For optimal dimensioning of the exoskeleton as a rehabilitation robot, two objective functions characterizing the kinematic and dynamic performance of the mechanism are considered. The objective of optimization is to maximize the worst-case torque transmission of the mechanism while simultaneously minimizing the effective mass over the predetermined workspace.

Worst-case torque transmission can be calculated by a workspace search for maximum of minimum torque value at finger joints. Defining τ_{act} and

τ_{end} as actuator and end effector torques respectively and J as the jacobian:

$$\tau_{end}(q_1, q_2, q_3) = \tau_{act} \cdot J^{-1}(q_1, q_2, q_3)$$

Then first objective function can be defined as

$$F_1 = \max_{q_1 \in W_1, q_2 \in W_2, q_3 \in W_3} \tau_{end}(q_1, q_2, q_3)$$

where q_1, q_2, q_3 are the angular positions and W_1, W_2, W_3 are the workspace of MCP, PIP and DIP joints of finger respectively. Since τ_{act} is constant the first objective function is directly proportional to $J^{-1}(q_1, q_2, q_3)$.

$$F_1 = \max_{q_1 \in W_1, q_2 \in W_2, q_3 \in W_3} J^{-1}(q_1, q_2, q_3)$$

Worst-case effective mass can be calculated as the minimum of maximum effective mass on device throughout the workspace. Defining M as mass matrix of the robot and effective inertia as EI:

$$EI(q_1, q_2, q_3) = J^{-1}(q_1, q_2, q_3) \cdot M(q_1, q_2, q_3) \cdot J^{-T}(q_1, q_2, q_3)$$

Then second objective function can be defined as

$$F_2 = \min_{q_1 \in W_1, q_2 \in W_2, q_3 \in W_3} EI(q_1, q_2, q_3)$$

where q_1, q_2, q_3 are the angular positions and W_1, W_2, W_3 are the workspace of MCP, PIP and DIP joints of finger respectively.

The column matrix of objective functions for the device F can written as

$$F = \begin{pmatrix} F_1 \\ F_2 \end{pmatrix}$$

while constraints are imposed in order to prevent any mechanical collision, perform motion in one direction and satisfy four-bar requirements over the whole workspace.

The first constraint of the optimization problem is that while actuated link is rotating in a direction finger knuckles must rotate in the same direction. The direction change in the actuated link must be the only reason for a change in the direction of finger movement. In a formal explanation sign of the angular velocity of actuated linkage and finger joints must be same. Since the angular velocities of finger joints and actuated linkage are related with the Jacobian matrix as:

$$\omega_{fingerjoints} = \omega_{actuated} * J$$

Jacobian must have positive value throughout the whole workspace as:

$$J(q_1, q_2, q_3) \geq 0 \quad \forall \quad q_1 \in W_1, q_2 \in W_2, q_3 \in W_3$$

Thus first constraint is

$$G_1 = -J(q_1, q_2, q_3) \quad \forall \quad q_1 \in W_1, q_2 \in W_2, q_3 \in W_3$$

The second constraint is that the chosen link lengths must satisfy four-bar construction criteria in the whole workspace which is the linkage with the largest length must be smaller than the total length of other linkages.

This requirement can be expressed as the following for a four-bar mechanism with links r_0, r_1, r_2 and r_3:

$$max([r_0, r_1, r_2, r_3]) < r_0 + r_1 + r_2 + r_3 - max([r_0, r_1, r_2, r_3])$$

which is equal to

$$2 \cdot max([r_0, r_1, r_2, r_3]) - (r_0 + r_1 + r_2 + r_3) < 0$$

Then second constraint is

$$G_2 = 2 \cdot max([r_0, r_1, r_2, r_3]) - (r_0 + r_1 + r_2 + r_3) \quad for \quad all \quad four-bar \quad structures$$

The second constraint must hold for the four-bar structures defined in Figure 2.8 which are

$$r0 - r1 - r2 - r3$$

$$r1 - r2 - r4 - r5$$

and

$$r6 - 7 - r8 - r9$$

The third constraint is to prevent any mechanical collision during the motion of finger. There are two possible collisions which requires precaution. Actuated link can collide with the actuator or the base platform of the robot. These two collisions may occur at the limits of the workspace. Therefore a check is needed at both ends of the workspace. From the geometry of the the system the angle of the actuated linkage (define as $r1_{angle}$) is limited to be within a range $[-80° \quad 140°]$ throughout the whole motion of finger. The

angle of the actuated linkage is calculated through inverse kinematics of the system.

Thus third constraint is

$$-80° \leq r1_{angle} \leq 140°$$

equivalently

$$G_3 = \begin{pmatrix} r1_{angle} - 140 \\ -r1_{angle} - 80 \end{pmatrix}$$

The column matrix (5x1) of constraint functions for the device, G, can written as

$$G_{(5x1)} = \begin{pmatrix} G_1 \\ G_2 \\ G_3 \end{pmatrix}$$

The negative null form of the multi-objective optimization problem can be stated as

$$min \quad F(\alpha, \beta, \gamma)$$

$$G(\alpha, \beta) \leq 0$$

$$\alpha_l \leq \alpha \leq \alpha_u$$

where F represents the column matrix of objective functions that depend on the design variables α, parameters β, and workspace positions γ. Symbol G represents the inequality constraint function that also depend on design

Table 2.6: Definition of design variables

D.V.	Var.	Definition	Range
α_1	L1	Length of first link	50-120 (mm)
α_2	L2	Length of second link	50-120 (mm)
α_3	L31	Length of first part of third link	30-60 (mm)
α_4	L32	Length of second part of third link	0-60 (mm)
α_5	L4	Length of fourth link	20-70 (mm)
α_6	γ_3	Angle of third link	0-180 (deg)

variables and parameters. Finally, α_l and α_u correspond to the lower and upper bounds of the design variables, respectively.

The optimization is performed over a wide design space while problem has six design variables indicated in Figure 2.9: link lengths and angles as summarized in Table 2.6. Upper α_u and lower α_l limits on the design parameters are imposed according to statistical data on human finger and ergonomics.
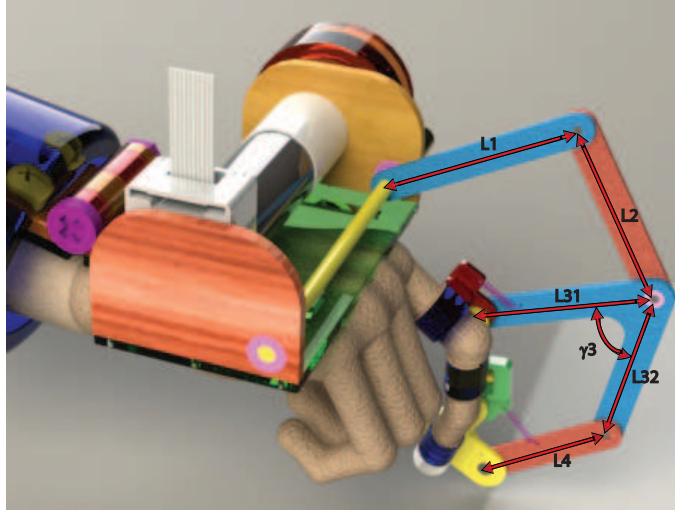
Figure 2.9: Design variables of the optimization problem

Solution Methods

The formulation for the multi-criteria optimization problem for best worst-case performance of the device is described.

The multi-criteria optimization of the finger rehabilitation device is solved using the framework introduced in [68, 82]. This optimization framework is based on Normal Boundary Intersection (NBI) method which is proposed by Das et al. [83] to efficiently obtain the Pareto-front curve characterizing the design trade offs. NBI method does not depend on scales of the functions and yields a Pareto-front curve consisting evenly distributed points. This method is computationally efficient that fast gradient based optimization techniques are used for solving single-criteria subproblems. Computational performance of NBI is further increased by using solution of a subproblem to initialize the next subproblem. This method is more advantageous than weighted sum methods since it also searches for the points on the non-convex regions of the feasible domain.

The single criterion optimum of each objective function are required in order to initiate the problem. Since the objective functions are non-convex and non-smooth, the shadow points are calculated by the culling algorithm. Culling algorithm is an efficient form of brute force method which performs independent searches in workspace and parameter-space reducing the size of parameter-space after every workspace search.

The algorithm works as follows: a global performance index is obtained by calculating the worst-case function value over the workspace for an initial parameter choice. For the workspace configuration where the global performance index is encountered, a parameter-space search is conducted. Then

parameters which have a worse value than the global performance index are eliminated from the parameter-space since they are dominated. The second workspace search is performed for the parameter which has the best function value in the previous parameter-space search and algorithm continues with a culling again. Therefore, the workspace search is remarkably reduced. So it is obvious that culling method is an efficient algorithm for min-max problems since it reduces the workspace volume and consequently search time.

Since the performance of the culling algorithm is highly dependent on the discretization and our problem has a wide design space, high discretization error might attained. Therefore after applying a coarse culling algorithm with high discretization a finer second culling search is performed with lower discretization in a smaller design space. Finally a pattern-search algorithm is used around the result obtained from second fine culling search.
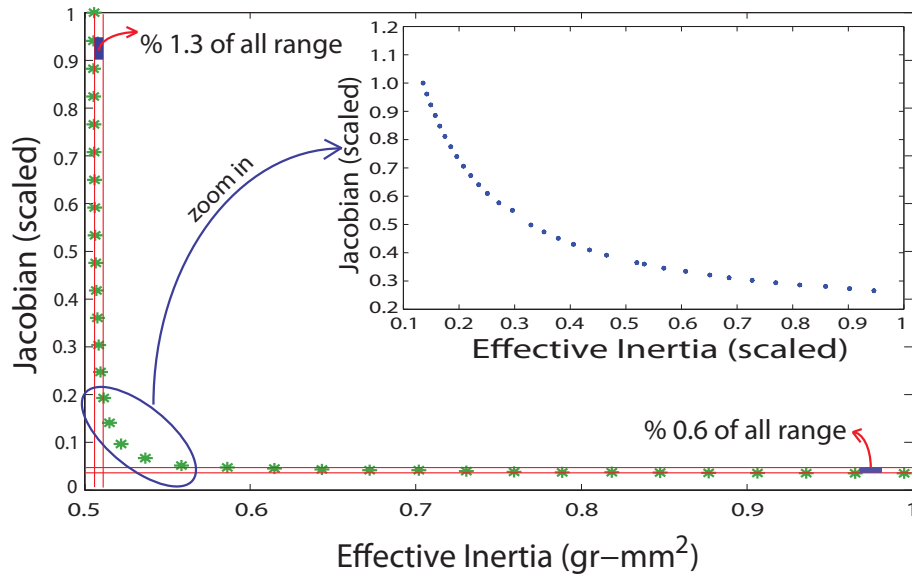
Figure 2.10: Pareto-front plot of the min-min optimization problem

54

Results

The Pareto-front curve characterizing the trade-off between the kinematic efficiency of the mechanism and the effective mass over the workspace of the finger device is calculated and equivalent result on worstcase torque-effective inertia is presented in Figure 2.10. From this plot one can observe that both objectives vary an important amount for different values of design variables for the finger device in a limited range. Trade-off amount is negligible at the limits of the plot. Yet there is a trade-off at the area where we will choose our best solution. Therefore the part which has trade-off is scaled in order to have a chance to make a choice from a wider candidate solution space.
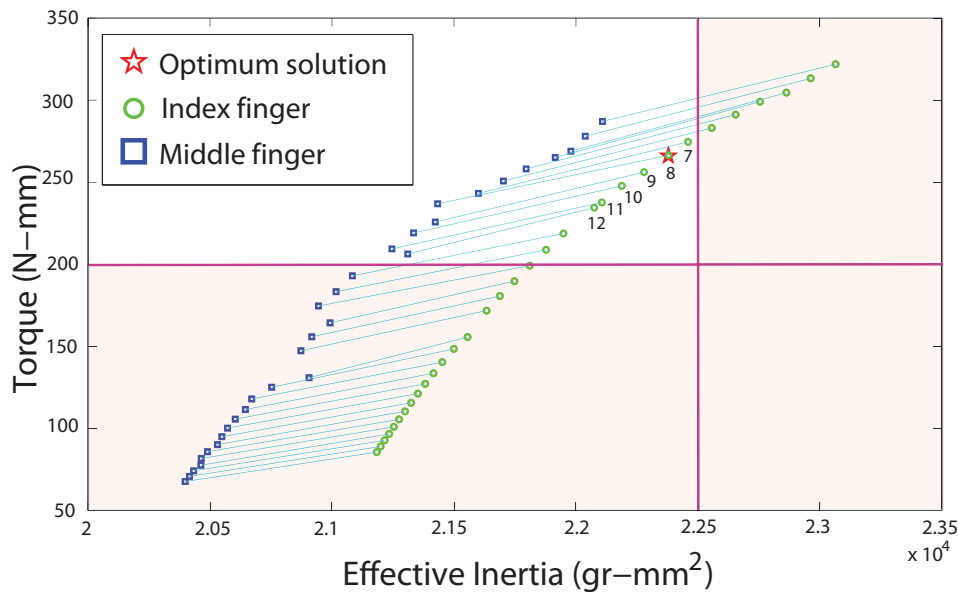
Figure 2.11: Pareto-front plot of index finger mapped for middle finger

All of the points on the Pareto-front curve are nondominated solutions of the multi-criteria optimization problem. A unique "optimal solution" can be

selected from this set considering the primary objective and design thresholds on the performance requirements. To have a better idea about the worst-case torque values of the optimization result, Jacobian is mapped into transmitted torque. Thresholds on the performance requirements are introduced in Figure (2.11)-(2.12)-(2.13) such that minimum torque must be higher than $200Nmm$ which is the requred torque to activate the third knuckle of the finger as explained in Table 2.4 and also an inertia threshold is selected as $2.25x10^4 gr - mm^2$ in order to have a number of feasible solutions limited with mass property. The thresholds are decided such that the compromise solution assigns acceptable values for both of the objectives. It is important to note that the thresholds are introduced after the Pareto-front curve is generated and the trade-off between the competing criteria is carefully studied. Apriori assignment of such thresholds, without first gaining an insight into the trade-off, is prohibitive.
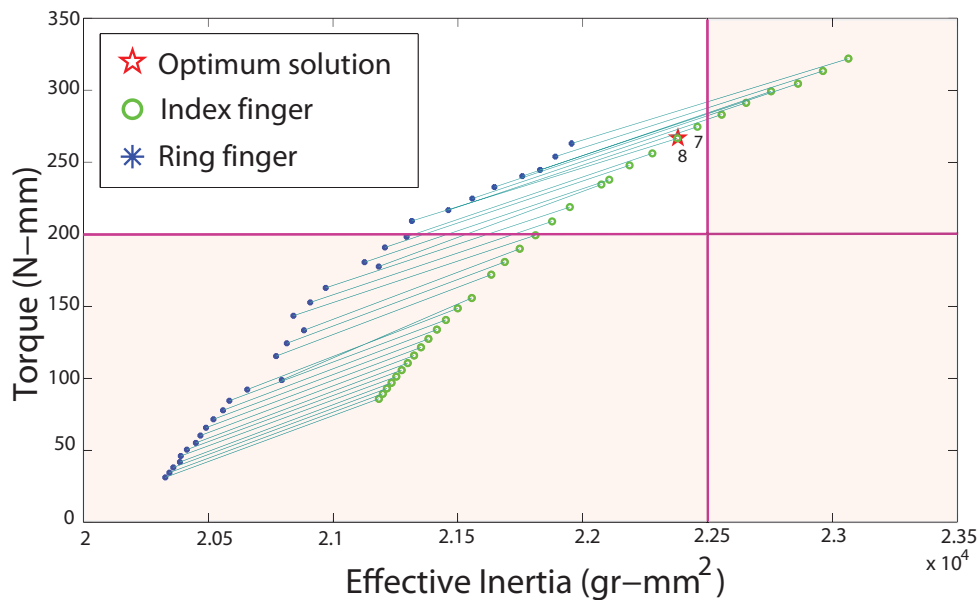
Figure 2.12: Pareto-front plot of index finger mapped for ring finger

56
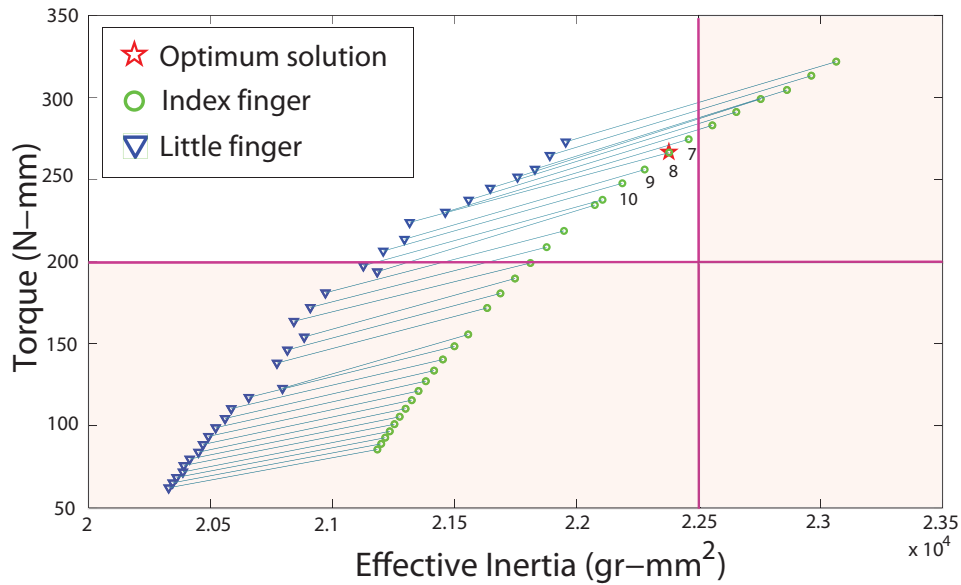
Figure 2.13: Pareto-front plot of index finger mapped for little finger

Another criteria to decide which point on the curve to choose is looking up the performances of the points when finger is used with other fingers. The Pareto curve is formed for index finger since it is the most widely used and injured finger yet the device is designed to use with all fingers and the defined thresholds must be hold with middle, ring and pinky fingers. The Pareto curve formed for index finger is mapped for the other fingers and the defined thresholds are applied. The candidate solutions are determined as the ones which passes the threshold for both fingers. After applying the thresholds to all fingers, the non-eliminated solutions are illustrated as points 7-12 in Figure 2.11 for middle and index finger, 7-8 in Figure 2.12 for ring and index finger and 7-10 in Figure 2.13 for little and index finger. Therefore 7th and 8th points are the ones which satisfy all constraints for all fingers. Considering their manufacturing precision errors 7th and 8th points refer

nearly same values and best solution is chosen as:

$$x^* = \begin{bmatrix} 81 & 50 & 30 & 21 & 20 & 153 \end{bmatrix}^T.$$

Resulting values of worst torque and effective inertia that can be met through whole motion range for ad-hoc and optimum design are given Table 2.7.

Table 2.7: Performance comparison of optimal and ad-hoc designs

	Torque	Effective Inertia
ad-hoc design	42.1283(Nmm)	$5.112x10^4(gr-mm^2)$
optimal design	261.6252(Nmm)	$2.2343x10^4(gr-mm^2)$

Chapter III

3   Implementation of the Systems

After solving the kinematics and performing the optimization work, dimensions of the devices are determined, appropriate mechanical and electronic components are selected. Finite Element Analysis are performed for the critical parts which are exposed to high loads. Also working capability of the systems are ensured by simulations and animations before manufacturing process.

3.1   Stroke Device

Direct drive DC motors are chosen as to actuate the $3 - \underline{R}RP$ mechanism. The power transmission is fulfilled using capstan mechanism with a 1:6 transmission ratio. Direct drive motor with capstan transmission ensures back-drivability of the system. The motor selection is performed such that the maximal continuous torque that can be applied to the patient's wrist is over 2 Nm. The motors are equipped with optical encoders with 500 counts per revolution. With quadrature decoding and considering the forward kinematics of the device, the position resolution of the system is 0.0559 mm for the translation and 0.03 degrees for the rotation DoF of the end-effector.

The moving and base platforms, as well as all the linkages are manufactured from 6061 aluminium. Task based attachments are rapid prototyped using ABS plastic. The overall design has relatively few parts, is robust and easy to manufacture. The robotic interface is 21 x 24 x 24 cm^3 in size and weights about 2700 gr.

Complying with the ergonomic and phycological design suggestions in [84], the end-effectors are designed to be comfortable and modular such that the patients can be attached to and de-attached from the device easily and quickly. To maximize comfort and hygiene, critical surfaces are covered with a silicon and disposable medical bands.

The controllers for the system are programmed in C and implemented in real-time at 1 kHz utilizing a PC running the RTX real-time operating system. However, the controllers can also be ported to an embedded target for home-based use. The forward and inverse kinematics of the $3 - \underline{R}RP$ mechanism are solved using numerical integration [85]. Since, the encoders situated on the actuators are only capable of position measurement, angular velocities are estimated using Euler approximation with adaptive windowing technique [86], in an effort to reduce the numerical noise.

3.1.1 End Effectors

One of the unique features of the wrist/forearm and grasp rehabilitation system is the possibility of enabling different exercises by simply altering its modular end-effectors. In particular, three different types of end-effectors are designed for the device: specified motion imposing end-effectors, the external hand module, and task oriented attachments.

Specified motion imposing end-effectors:

Specified motion imposing end-effectors target concurrent and coordinated motion of hand grasp with wrist rotations (palmar/dorsal flexion and abduction/adduction), similar to the exercises depicted in Figure 2.2. Two examples of such end-effectors are illustrated in Figure 3.1. In particular, the end-effector illustrated in Figure 3.1-a and 3.1-b relies on a slider-crank mechanism to convert rotational motion of the $3 - \underline{R}RP$ end-effector into the linear opening and closing motion of the hand attached to a handle pair. With this mechanism in place, the translational motion of the $3-\underline{R}RP$ can be employed to exercise palmar-dorsal flexion of the wrist, while grasp/release motions are being concurrently imposed to the hand (see Figure 2.2-a and 2.2-b).
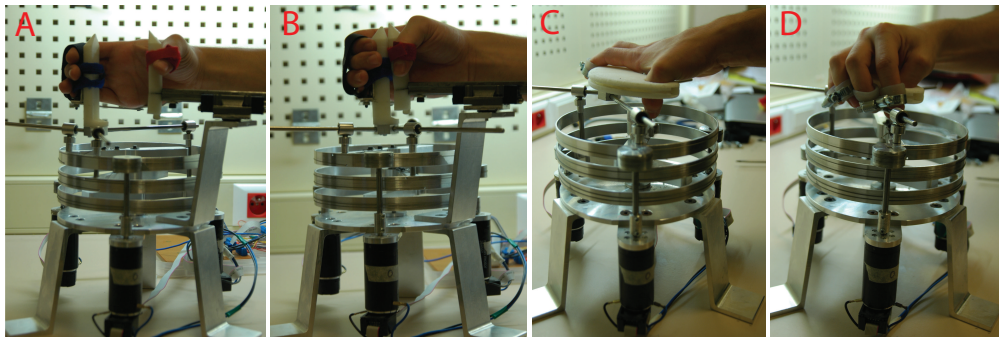
Figure 3.1: Specified motion imposing end effectors

The end-effector pictured in Figure 3.1-c and 3.1-d is based on a cam mechanism and is designed to impose grasping/releasing motions to the hand concurrently with the wrist abduction/adduction movements (see Figure 2.2-c and 2.2-d). When this end-effector is in place, the rotation of the $3 - \underline{R}RP$ end-effector enforces opening and closing of the hand. While using this end-

effector each finger is covered with a silicon ring and is attached to the device by the means of rings constrained to slide on the cam profile. The aperture amount can be adjusted with this design, by simply selecting from several cam surface alternatives.

The external grasping end effector:

The external hand module (Figure 3.2) is an independently actuated end-effector and appends system with one extra DoF. Using this end-effector, the movements depicted in Figure 2.2-a and 2.2-b can be exercised, which includes hand grasp and wrist flexion/extension. Using this end effector, grasp/release of hand can be controlled independent from wrist/forearm motions. Also the described finger exoskeleton can also be attached to the $3 - \underline{R}RP$ device to act as an alternative external module, targeting individual finger movements (for example, to exercise pinch grasps).

Figure 3.2: The external hand module

Task oriented end effectors:

Task oriented attachments are end-effectors used to simulate ADL tasks. Since ADL exercises have been shown to be very effective to help patients gain their independence, a simple coupling mechanism is designed to allow regular objects to be attached to the $3 - \underline{R}RP$ end-effector. With this coupling mechanism, lightweight everyday items, such as pens, cards, jar lids, door handles, knobs, keys, or toothbrushes or their lightweight replicas can be attached to the device to exercise ADL scenarios in a robot-assisted rehabilitation setting. The ADL scenarios are also supported with force feedback and virtual reality simulations, to provide immersion and to increase motivation.

Figure 3.3: Task oriented end effectors working in horizontal plane

The selection of the end effectors are done by considering most common ADL. It is ensured that all of the wrist/forearm motions can be exercised with the pinch types described in Section 2.1.1 through the selected end effectors. The primarily chosen ADL imposing end effectors are illustrated in Figure 3.3 and Figure 3.4.
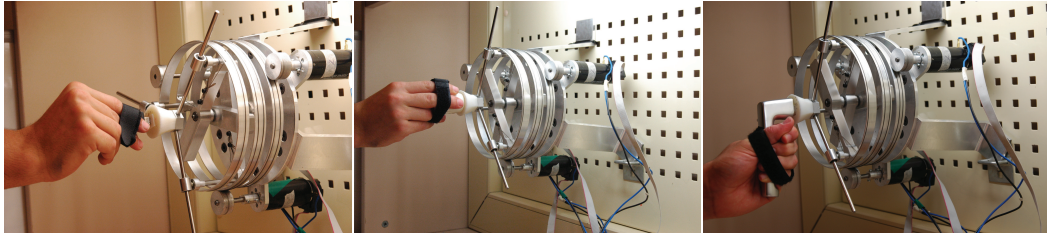
Figure 3.4: Task oriented end effectors working in vertical plane

In this manner selected end effectors are:

Key allows pronation/supination motion of forearm while hand is in key pinch position.

Handle allows pronation/supination motion of forearm while hand is in hook grasp position.

Card allows flexion/extension and abduction/adduction motion of wrist while hand is in lateral and palmar prehension position.

Knob allows pronation/supination motion of forearm, flexion/extension and abduction/adduction motion of wrist while hand is in cylindrical and spherical prehension position.

Pen allows flexion/extension and abduction/adduction motion of wrist while hand is in chuck grip position.

Brush allows flexion/extension and abduction/adduction motion of wrist while hand is in power grasp position.

Also other real-objects or lightweight replicas can be appended to set of these end effectors for different therapy levels.

3.1.2 VR Integration

The rehabilitation therapies feature force feedback and are supported by VR animation scenarios, such as door opening, key turning. While performing these exercises, real objects are used. Figure 3.5 presents screen shots from sample VR animation scenarios. The former one is a hold, rotate, place and drop game. The rules of the game can be summarized as: User should go to a vicinity of the object in order to hold it. Using full motions of mechanism, user should place the shapes in proper holes in proper orientation. The latter one is a right key-right hole game. Same rules in the previous game are valid. Yet they impose different motions to wrist and employ different muscles. Other VR exercises include simple games that provide frequent feedback about the success of the actions, as well as the quality of the performance, to encourage participation and to promote concentration.
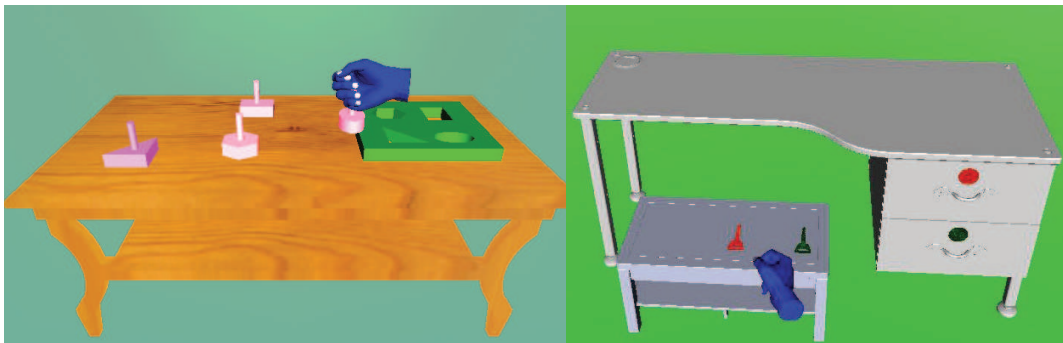

Figure 3.5: Screen shot of the sample VR scenarios

A graphical user interface (GUI) is designed to help the therapist to choose the type of the attached end-effector, the amount and speed of the wrist/hand movement, the amount and direction of the assistance/resistance and the number of repetitions during therapies.

3.1.3 Therapy Modes

The rehabilitation system supports a measurement mode and three distinct therapy modes: passive, assistive, and resistive.

In the measurement mode, the device actuators are disabled and patient movements are recorded. These recordings can be used to determine the RoM of the forearm pronation/supination or the wrist flexion/extension and abduction/adduction with the hand aperture. Furthermore, in the passive mode, these recordings can also be repetitively imposed to the patients as pre-recorded exercises.

In the passive mode, the robotic device is controlled by a disturbance observer based position controller. This controller views human as a disturbance and imposes pre-recorded movements to the patient. Note that, along with a disturbance torque observer, this mode can also be used to measure isometric strength of the joints by detecting the force thresholds of the patient.

Assistive and resistive modes are similar in that an impedance controller is utilized for both modes. The impedance controller is designed to work in the task space, since assigning impedances in joint space is rather counter-intuitive. To faithfully assign desired decoupled impedance values along each separate DoF of the device, model-based dynamics compensation is utilized. In assistive and resistive modes, patients are also motivated with force-feedback VR games presented on the visual display. In these modes, the robot supports/ressists the motion of the patient with the proper amount of force feedback.

3.2   Tendon Device

The final design of the finger rehabilitation robot is presented in Figure 3.6. The size of the finger exoskeleton is minimized to prevent possible self-collisions and collisions with other fingers. The weight of the finger exoskeleton is kept low by using 6061 aluminum to fabricate the links and the grounded bracket, hard plastic to manufacture the capstan transmission. The overall device weighs 185g without the actuator. The weight of the device is distributed over the wrist and forearm using an adjustable splint. Weight of the device can further be distributed over the body by relocating the actuator away from the wrist. Mechanism is attached to the finger using snap fasteners. The finger exoskeleton is actuated by a direct drive DC motor equipped with an optical encoder.
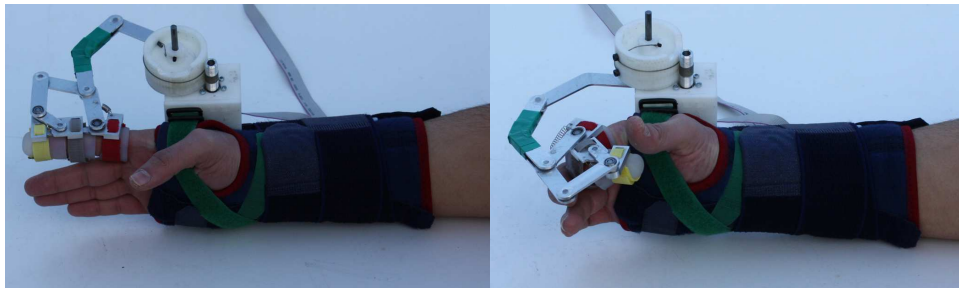
Figure 3.6: Tendon robot in extended and flexed configurations

The finger rehabilitation system is controlled by a PID controller. Sensor measurement are given as input to a PC using an I/O card capable of 16 bit A/D conversion. The control torques for the finger exoskeleton is calculated in real-time and fed back to the device. A graphical user interface (GUI) which displays the motion of the finger at 30Hz during flexion and extension is supplied. The therapist can record the initial and final positions of the finger,
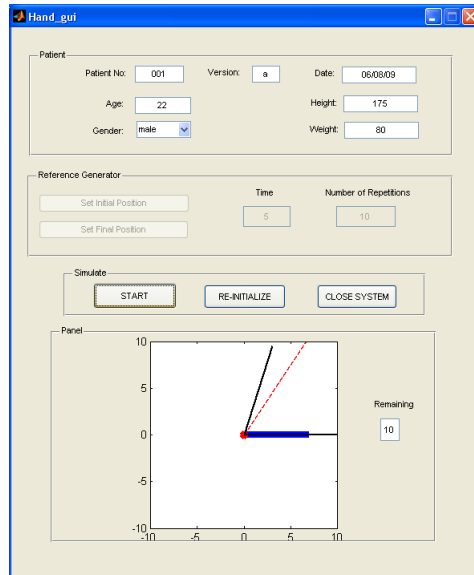
Figure 3.7: Graphical user interface

determine the amount and direction of assistance/resistance, the number of repetitions and the period of exercise via the GUI (see Figure 3.7).

3.2.1   Mounting

As discussed in the Section 2, mounting of the device to the hand is important and have to be done in less than 2 minutes while for accurate measurement a robust mounting must be ensured. Yet mounting the device to hand in an easy, comfortable and robust way is a difficult manner for a finger exoskeleton since there is not much gap between fingers and exoskeleton tied to one finger might discomfort neighboring finger. We have tried different methods to tie the finger of patient to the device. Among the tried methods, strips, ring, bracelet and pipe clip are the ones illustrated in Figure 3.8 which did not give desired comfort.
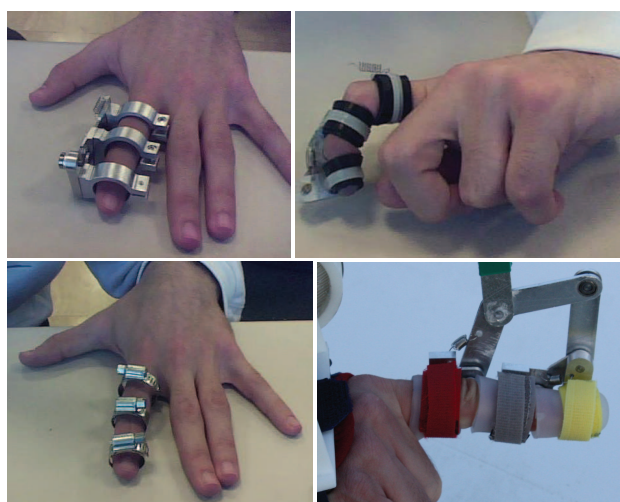
Figure 3.8: Used methods for mounting

Also as a part of their graduation project, 2 Manufacturing Systems undergraduate student conducted a survey in order to see the views of patients, engineers and therapists under supervision of Prof. Gurdal Erdek and Prof. Volkan Patoglu. Furthermore, the optimal mounting structure of the robot is discussed as "Design Decision Making" course project in "Pennsylvania State University" under supervision of Prof. Gul E. Okudan. Different solution methods proposed in these studies are demonstrated in Figure 3.9. The proposed solution methods and survey data afforded assistance to our decision on mounting structure. Some data and results of these studies are given at the Appendix C.
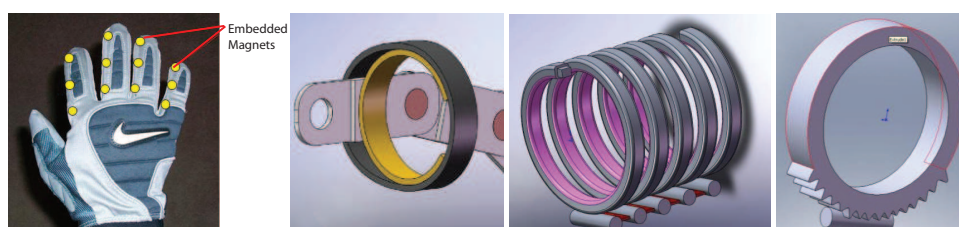
Figure 3.9: Some of proposed methods for mounting
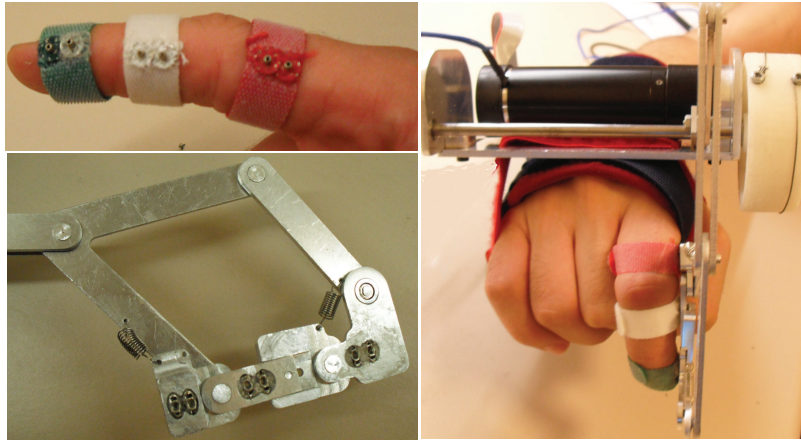
Figure 3.10: Final decision for mounting

After all of the discussions and surveys, considering various choices, importance of the requirements for patient and therapist, it is concluded to have a structure which

- has metal connection for robustness

- velcro type contact for hygiene

- smooth surface for comfort

- multiple rings for ergonomics

The structure used in the decision making method for these conclusions are available in Appendix C. It is determined that by embedding snap fasteners (two for each knuckle in order to ensure robustness) to the mechanism, fastest, most robust and comfortable way of mounting is applied. Details of the proposed structure and a finger mounted by the decided method is shown in Figure 3.10 for clearance.

3.2.2 Adjustability

Ensuring robust mounting was important for exact position measurement. However finger is not the only part to be tied but also wrist must be tied since tension on the tendons are directly depended on position of wrist. Therefore wrist must be tightened and its angle must be adjusted to a desired value. Wrist is tightened to device through straps while its angle is adjusted by a hinge structure as shown in Figure 3.11-a.
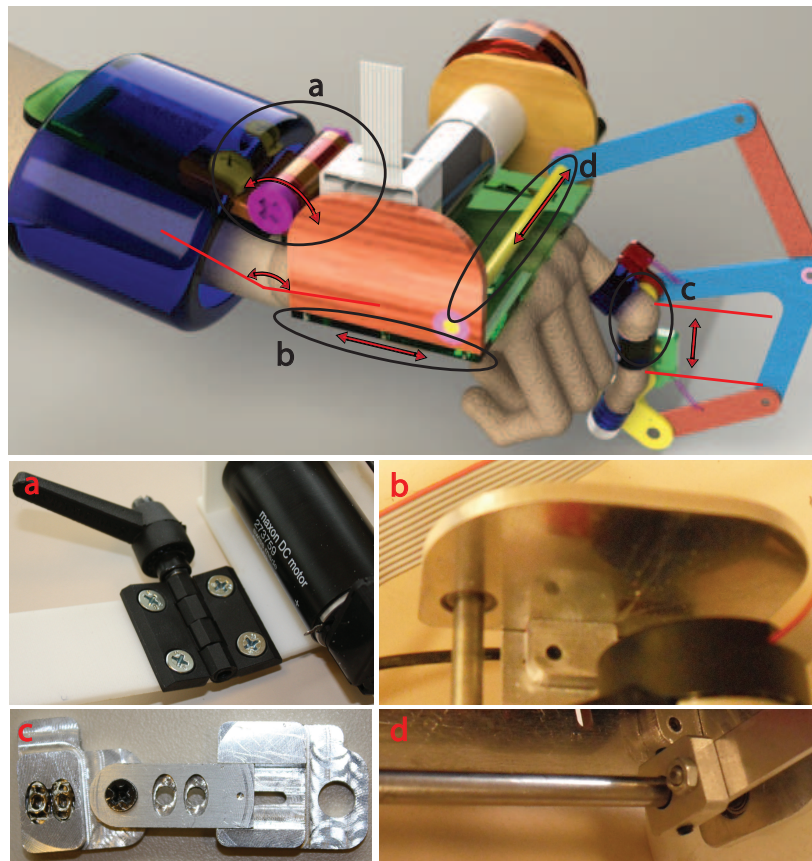
Figure 3.11: Adjustment details of the finger rehabilitation system

Another adjustment of the mechanism is a more crucial one for ergonomics.

Since the finger is a part of the system, adjusting center of rotation of device with finger joint becomes critical. Yet finger length changes according to patients age, sex even nationality. Thus concentricity of center of rotation is ensured by adjustable lengthened links as shown in Figure 3.11-c.

Moreover, the tendon robot can be applied to any finger by tightening the screw on the actuated link at desired position on the rotating shaft as shown in Figure 3.11-d. Since hand sizes of people differ, size adjustment is ensured by sliding the edge parts of the robot on the base as in Figure 3.11-b.

3.2.3 Therapy Modes

Currently, the proposed finger rehabilitation system supports four different modes of tendon repair therapy, namely, passive, active, active-assisted, and active-constrained modes. In the passive mode, finger exoskeleton moves the injured finger on predetermined trajectories while the patient remains passive. This mode is similar to the Duran technique used in conventional tendon therapy, where a therapist enforces coordinated motions to the injured finger within closely controlled joint limits, while the patient stays passive throughout the therapy. The active mode is used when early mobilization needs to be exercised. In this mode, the injured finger is active and the patient follows desired finger trajectories while the device is passive (or in dynamics/friction compensation mode). This mode is similar to conventional tendon therapy when the patient is required to perform active movements of flexion and extension exercises. In the active-assisted mode the finger exoskeleton encourages the patient to stay active during extension (flexion), similar to the role of the rubber band used in the Kleinert method.

In contrast, in the active-constrained mode, the finger exoskeleton applies resistance to keep the patient passive during flexion (extension) of the injured finger while the patient is active during extension (flexion). This mode is also similar to the rubber band exercises used in the Kleinert method.

Chapter IV

4   Controller Synthesis and Implementation

Both of the systems are controlled by RTX real-time operating system. The controllers are programmed in C and implemented in real-time at 1 kHz. Stroke Device is controlled by disturbance observer based position controller and impedance controller while tendon device is controlled by conventional PID controller since it has simpler dynamics and 1 active degrees of freedom.

4.1   Disturbance Observer Based Position Controller

Disturbance observer based control algorithms are used to compensate modeling uncertainties and external disturbance [87, 88]. The error obtained by the difference between model output and actual output is considered as equivalent disturbance for the model. When disturbance observer is applied to a model, dynamics of robot can be considered as a simple inertia which can be obtained without complex computation of dynamic equations.

Dynamics of the stroke robot can be written by a set of highly nonlinear and coupled differential equations as:

$$M(q)\ddot{q} + C(q,\dot{q}) + N(q) + F(\dot{q}) = \tau$$
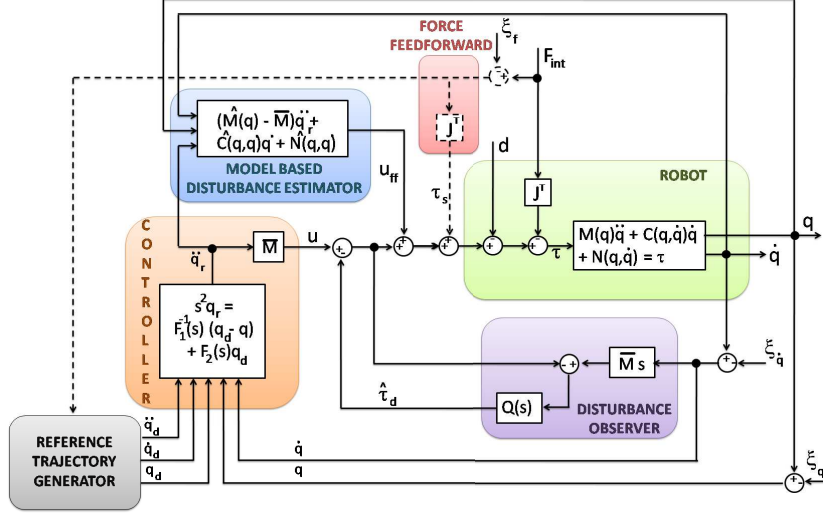
Figure 4.1: Generic model for disturbance observer based position controller

where M(q) is the inertia matrix and $C(q, \dot{q}), N(q), F(\dot{q})$ are, respectively, the coriolis and centrifugal forces, the gravity loading, and the friction force. And τ is the torque applied to the joint of robot manipulator. Also q , $\dot{q}$ and $\ddot{q}$ are the angular position, velocity and acceleration, respectively. For simplicity, the robot dynamics can be rewritten as a fixed inertia term plus an equivalent disturbance torque given by

$$\bar{M}\ddot{q} + \tau_d(q, \dot{q}, \ddot{q}) = \tau$$

where $\bar{M}$ is a diagonal matrix of inertia obtained by taking mean of mass matrix of the system through a complex trajectory. $\tau_d(q, \dot{q}, \ddot{q})$ implies equivalent disturbance including all unmodeled dynamics.

When the equivalent disturbance is obtained via disturbance observer, dynamics of robot can be decoupled by eliminating the equivalent disturbance by adding the estimated disturbance signal to the control input. Therefore,

a simple control strategy can be applied to track a desired trajectory.

In the generic model shown in Figure 4.1 disturbance observer block involves $\bar{M}$ and Q(s). Inverse dynamics of the model is assumed to be $\frac{1}{\bar{M}}s$ while Q(s) is a first order low pass filter since dynamics of the system can be modeled as a first order system. The filter is used for reducing measurement noise effect. For a disturbance signal whose maximum frequency is lower than cut-off frequency of Q(s), the disturbance signal is effectively rejected and the real plant behaves as a nominal plant. Then the robot dynamics can be considered as

$$\bar{M}\ddot{q} = \tau$$

For the controller block of the system joint space error is used since control is directly applied to actuators. Through the calculation $s^2 q_r = F_1^{-1}(s)(q_d - q) + F_2(s)q_d$, angular acceleration is derived and multiplied by $\bar{M}$ to obtain control input.
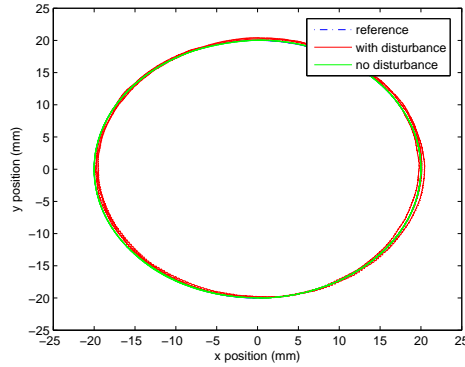
Figure 4.2: Circle tracking through PD controller

A robust position control is done through disturbance observer based controller. A circle is tracked with and without physical continuous disturbance and result is given in Figure 4.2. When the test is done under a physical

continuous disturbance the rms values seen on error are: 0.3563 mm for x, 0.3248 mm for y and 0.3293 degrees for θ. The rms values are much more smaller under no physical disturbance.

4.2   Impedance Controller

Impedance control is a task space control method which was proposed by Hogan as controlling motion by creating a response for the interaction force in the form of impedance [89, 90, 91]. Impedance control associates displacement and force at the contact point of robot with the environment.Since $3 - \underline{R}RP$ robot is an impedance-type device with high back-drivability and low inertia, applying impedance controller to the $3 - \underline{R}RP$ device by canceling nonlinear robot dynamics would be meaningful.
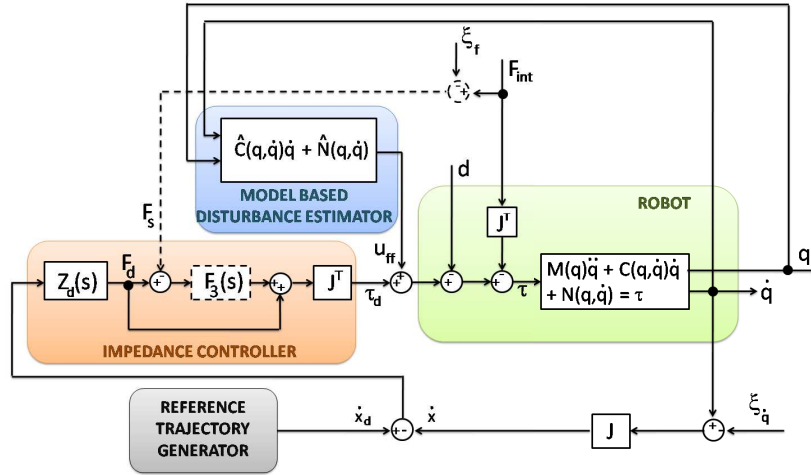
Figure 4.3: Generic block diagram for impedance control

A generic impedance controller is represented in Figure 4.3 by block diagrams. The measured position in joint space is mapped into the task space

77

through the jacobian matrix (J) in order to have knowledge on end effector's actual position. Reaction forces are obtained by multiplying the desired impedance with the error of the end effector's position and velocity. End effector reaction force/torque is passed through Jacobian transpose in order to determine required actuation torques. The obtained torque is fed into the system after eliminating the nominal nonlinear device dynamics through model based disturbance estimator. However, since force sensors are required for defining the force errors, the force controller term $F_3(s)$ is taken to be zero and open loop impedance control is implemented.

Simply, in the control structure we are using a stiffness and damping as:

$$u = K(x_d - x_a) - B(\dot{x}_d - \dot{x}_a)$$

where u is the control input, K is the spring stiffness, B is the damper viscosity, x_d and x_a are desired actual positions while $\dot{x}_d$ and $\dot{x}_a$ are desired and actual velocities of the end effector, respectively.
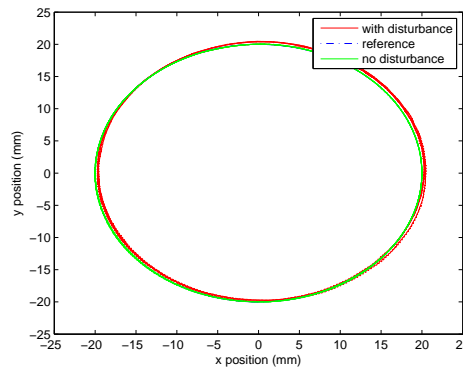
Figure 4.4: Circle tracking with/out load under impedance control

Tracking experiments for the impedance control of the $3 - \underline{R}RP$ robot is performed and results are represented in Figure 4.4. In this experiment,

78

robot is desired to track a circle under no disturbance and with a continuous disturbance. When the test is done under a physical continuous disturbance the rms values seen on error are: 0.2981 mm for x, 0.2912 mm for y and 0.3419 degrees for θ.
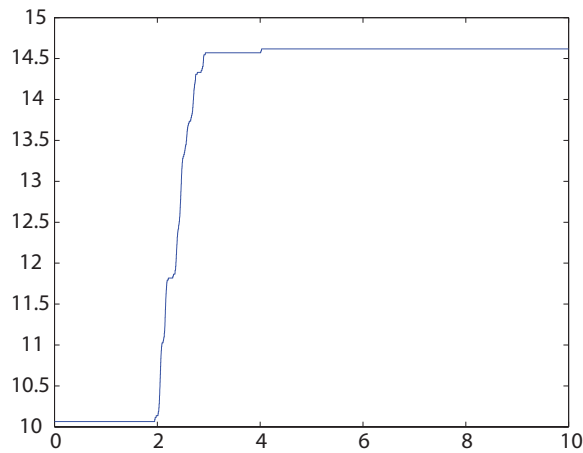
Figure 4.5: Impedance control verification

Also another experiment applied under impedance control is done to verify whether the applied impedance is correct or not. The impedance (to be more specific the stiffness) along the x-direction was commanded as 1000 N/m. Then, a force of 4.905 N (500gr load under the action of gravity with a pulley) was applied along this direction and the motion of the end effector was observed to be 5 mm as expected. Results of this experiment is demonstrated in Figure 4.5. The small position error and delay at tracking is due to unpreventable friction in the pulleys of the experimental setup.

Chapter V

5   Usability Tests and Characterization

In this section, functionality and performance of the devices are examined. Both of the devices are tested to check their usability for rehabilitation purposes. Also stroke device is tested to check whether it can be used as a measurement device for the range measurement of wrist and forearm or not. Furthermore, performance of both of the devices are characterized in simulation and experimentally.

5.1   Stroke Device

5.1.1   Usability Tests

Human subject experiments with healthy volunteers have been conducted to examine the usability of the $3-\underline{R}RP$ system, the effectiveness of the device to deliver various rehabilitation exercises to hand, wrist and forearm, and its applicability as a measurement device.

Experimental Setup

The experimental setup consisted of a desktop computer, a monitor screen, and the $3-\underline{R}RP$ rehabilitation system. Participants sat in front of the monitor and one hand of the participant was attached to the device. The elbow of the participant was supported to ensure a natural and comfortable posture. For the usability tests the cam-based end effector and slider crank-based end effectors are used (see Figure 3.1). Also for the measurement test an exoskeleton type wrist device is attached to the $3-\underline{R}RP$ and position data is recorded by both of the devices for comparison. The setup for the measurement test is illustrated in Figure 5.1.
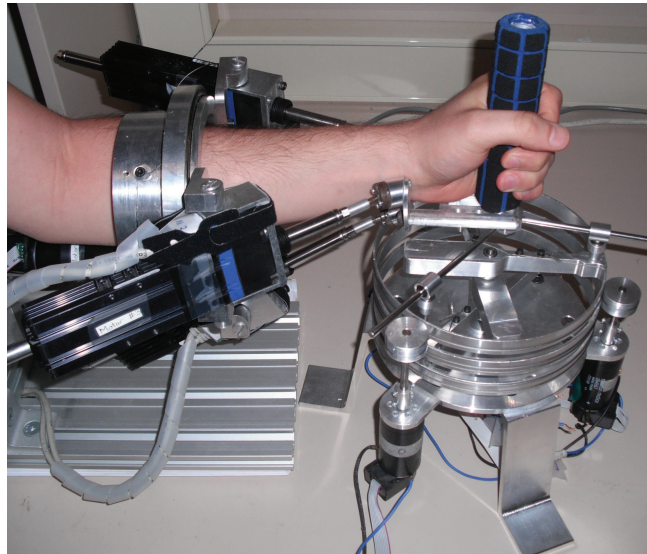
Figure 5.1: Experimental setup for comparison test

Testing the Therapy Modes and the Measurement Mode

Two sample therapeutic tasks, discussed in Section 2, were carried out. In the first task, the slider crank-based end effector was used to impose the movement depicted in Figure 2.2-b to the patient. During the motion, that consisted of concurrent movement of the palmar/dorsal flexion of the wrist with the hand opening, the subject was guided by the device, while the position data was recorded by the device encoders. This motion was repeated several times. The desired aperture of the hand, the flexion/extention of the wrist and the duration of therapy were set as reference values and mapped to the actuator rotations through the inverse kinematics of the device.

For the second task, the cam-based end effector was used to impose the movement depicted in Figure 2.2-d. This motion is a combination of abduction/adduction of the wrist with the hand grasp. Once again, the desired amount of the aperture of the hand and the abduction/adduction of the wrist were mapped into the actuator angles through the inverse kinematics of the device. The equation characterizing the cam profile was also used to determine the hand aperture.

As a part of the usability tests, other types of exercises including ADL with the wrist flexion/extension, abduction/adduction and the forearm pronation/supination were also tested by utilizing different end-effectors and orienting the device in various configurations. In these tests participants are motivated through integrated VR animations and games.

To test the efficacy of the device as a measurement tool, the all forearm/wrist rotations collected through the $3 - \underline{R}RP$ mechanism is compared to a wrist exoskeleton, SUkorpion WR [28]. In this experiment the end effec-

tor of the $3 - \underline{R}RP$ robot is tied to the exoskeleton device and measurements done by both of the devices are separately recorded and compared.

The exoskeleton type device have better measurement accuracy, since its axes are perfectly aligned with the human joint axes and the measurement of individual joint angles is possible with the device. For the comparison, typical wrist and forearm movements were performed when the subject is simultaneously attached to both devices and position data were recorded. It is hypothesized that there might be an acceptably small amount of difference between the measurements of $3 - \underline{R}RP$ and SUkorpion WR. Typical measurement errors made by using $3 - \underline{R}RP$ mechanism are characterized in the next subsection.
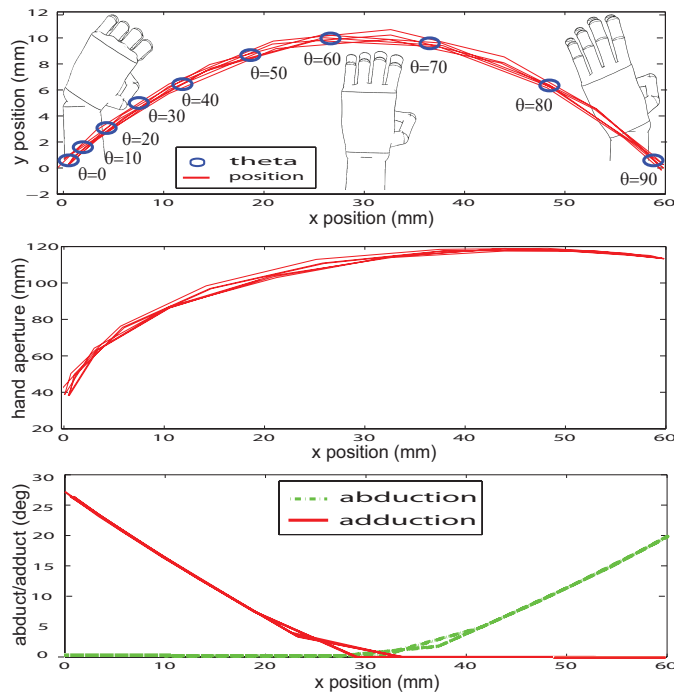
Figure 5.2: Results of the usability tests for slider crank-based end effector
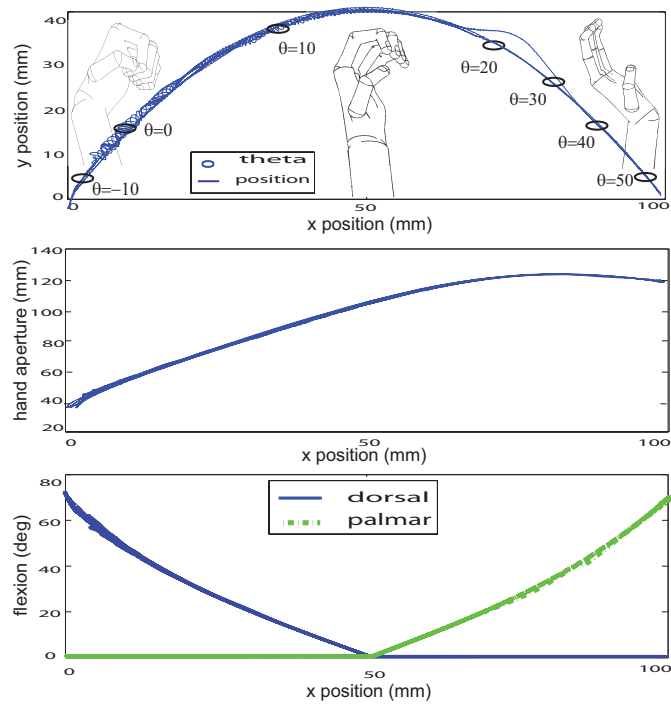
Figure 5.3: Results of the usability tests for cam-based end effector

Results

The plots of the position data collected during the two sample therapeutic tasks are illustrated in Figure 5.2 and Figure 5.3. In particular, Figure 5.2 presents the position, the orientation, the aperture of the hand and the flexion/extension of the wrist for slider crank-based end effector, while Figure 5.3 present the same values and the abduction/adduction of the wrist instead of flexion/extension for the cam-based end effector. While using the slider crank-based end-effector, the concurrent motion of the hand aperture and the palmar/dorsal flexion of the wrist; and while using the cam-based end effector, the concurrent motion of the hand aperture and the abduc-

84

tion/adduction of the wrist can be observed from related figures.

Recorded data has not been presented here pertaining to the other usability test; however, these tests provided evidence that the device can cover whole natural RoM of the human forearm/wrist, as well as the hand aperture. Feasibility of using the device in different orientations to exercise various complex motions have also been demonstrated. In general, the participants were satisfied with the ergonomy of the device and its practical use. Moreover, they expressed that the ADL tasks integrated with force-feedback VR simulations were immersive and motivating.
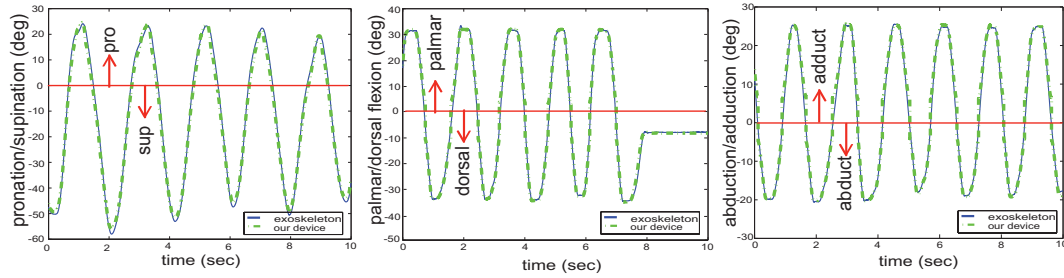
Figure 5.4: Comparison of wrist motion measurements recorded using the rehabilitation system and the SUkorpion exoskeleton

Figure 5.4 presents the plots of the position data collected during the measurement experiments. In particular, the wrist abduction/adduction, extension/flexion and the forearm pronation/supination measurements taken using both the $3 - \underline{R}RP$ mechanism and the SUkorpion WR exoskeleton are plotted on this figure. It can be observed from Figure 5.4 that the measurements with the $3 - \underline{R}RP$ mechanism closely follows the measurements with the exoskeleton. The RMS values of the errors between the data measured by $3 - \underline{R}RP$ device and the exoskeleton are found as:

$$RMS - error_{abd-add} = 1.69^o,$$

85

$$RMS - error_{flex-ext} = 1.64^o,$$

$$RMS - error_{pro-sup} = 2.09^o.$$

The errors are mainly due to the unavoidable misalignment of the task-space based rehabilitation device with the human joints axes. The self adjusting exoskeleton does not suffer from such misalignments. The measurement errors in the range of 2.09^o are acceptably low for quantification of the daily patient progress, and qualifies the device as a practical measurement tool for in-home use. A repeated measures ANOVA (with therapy modes as between-subject factor, session as within subject factor) was carried out to determine significant effects. The results revealed a significant main effect of therapy modes (F(2,23)=218.66, p=0) and no significant effects of devices (F(1,23)=0.06, p=0.8096) or interaction (F(2,23)=0.46, p=0.6399).

Since the $3-\underline{R}RP$ robot covers the whole ROM of the human wrist/forearm and has fine measurement accuracy, it can be used as a measurement tool. Sample measurements taken from three subjects to characterize the RoM of their wrist flexion/extension, abduction/adduction and forearm pronation/supination are tabulated in Table 5.1.

Table 5.1: Measured ROM of forearm and wrist

Joint	S#1	S#2	S#3
Forearm Supination	91°	81°	92°
Forearm Pronation	75°	69°	77°
Wrist Palmar Flexion	73°	75°	78°
Wrist Dorsal Flexion	70°	76°	73°
Wrist Abduction	30°	33°	39°
Wrist Adduction	21°	18°	25°

5.1.2 Characterization

As discussed in Section 2, a hand device have to meet different criteria like safety, range of motion, force/torque requirements and some ergonomic issues. The characterization of the actual device performance is fundamental to establish the validity of the design and discover whether or not there are any shortcomings. To this end, the device has been tested on several such criteria, reinforcing its adequate performance on each of them.

One of the most important criteria for any force-feedback device is its force/torque capability. Peak instantaneous and peak continuous force and torque which the system can provide is directly related DC motor characteristics. The actuators used in the system are Maxon RE35 DC motors which can supply a maximum continuous torque of 0.107 Nm and maximum peak torque of 0.949 Nm. Also the capstan drive with a 1:6 ratio increases the apparent force observed at the end effector. Using the Jacobian transpose end effector maximal values are found around the nominal workspace of the mechanism: Continuous values are $F_x = F_y = 16.05$ N, $\tau_\theta = 1.926$ Nm while instantaneous values are $F_x = F_y = 142.35$ N, $\tau_\theta = 17.082$ Nm.

The stability limit for stiffness rendering is another widely accepted performance measure of force feedback devices especially impedance type devices. Since $3 - \underline{R}RP$ robot is an impedance type device and works in task space, stiffest virtual wall that can be rendered stably became more of an issue. The highest stiffness value is experimentally obtained under impedance controller by zeroing the damping viscosity parameter and increasing stiffness parameter of the controller continuously until system becomes unstable. The instability is observed to occur at a value of k = $3x10^4$ N/m along the

x and k $= 3x10^4$ N/m along the y direction; while the rotational stiffness values are measured as k $= 310$ Nm.

Position bandwidth is also an important criteria for any robot. For a rehabilitation robot in order to have safe interaction with motion of human, it is an adequate performance to have a higher bandwidth than human limits which is known as 10 Hz. To measure the bandwidth of the $3-\underline{R}RP$ robot, its Bode magnitude plot is experimentally determined under closed-loop position control as presented in Figure 5.5. From this Bode plot, the closed-loop position bandwidth of the device is measured as 57.3 Hz.
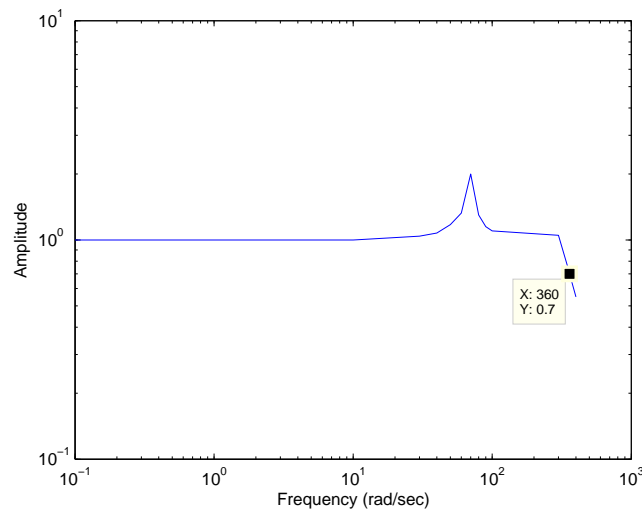
Figure 5.5: Bode magnitude diagram and bandwidth of the system

As commonly known, inertia is the resistance of a robot's (or more general a physical object's) change in its state of motion. It is obvious that the performance of a robot depends on its apparent inertia. For a force feedback, impedance type device, decreasing the apparent inertia is desired since it enhances performance of the device. However, inertia of a robot depends on its position. Thus as a performance measure, average apparent inertia of

88

robot is calculated by averaging the inertia values of robot while it is tracking a complex trajectory. The singular values of the average apparent inertia matrix are obtained for translational and rotational directions of $3 - \underline{R}RP$ robot respectively as: $\sigma_x = \sigma_y = 0.2509 kg$ and $\sigma_\theta = 0.00245 kg - m^2$.

Safety is one of the most crucial requirements of a rehabilitation device and back-drivability can be assigned as a measure of safety. Back-drivability of the $3 - \underline{R}RP$ robot is ensured by using direct drive actuation and capstan transmission with low increase ratio. The experiments to measure the back-driveability of the mechanism concluded that the minimum forces/torques in the end-effector coordinates with which the associated degree of freedom can be moved are as follows: $F_x = 1.6$ N, $F_y = 0.9$ N, $\tau_\theta = 0.25$ Nm.

Resolution gives us the maximum possible error which can not be realized by the system. Encoder used with the motors are HEDL 5540 type which has a resolution of 500 counts per revolution. It is multiplied by 4 due to quadrature rate and divided by gear ratio 6. Finally it is found that the maximum error that can not be realized is $0.03°$ per actuation. Mapping this value to end effector through Jacobian, maximum error is obtained as 0.0559 mm for x-y directions and $0.03°$ for rotational axis.

Although the dynamic performances mentioned so far are of paramount importance for the the mechanism, for a rehabilitation device, the range of motion of the mechanism may well supersede them all. The reason is that, after an injury, the human hand loses its original range of motion (RoM) which can only be regained by proper exercises. If the mechanism does not cover a large portion of this RoM, then it is impossible to prescribe those motions. As a result, the space spanned by the mechanism has to be tested and ensured to conform with typical human kinematics presented in Table

89

2.1. The range of motion of the mechanism is experimentally tested and results are then compared with simulation results as presented in Figure 5.6.
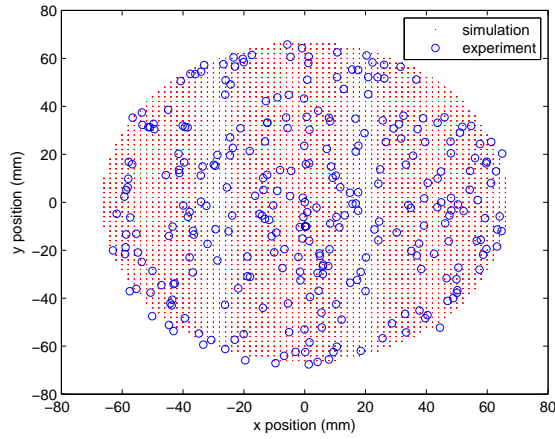
Figure 5.6: Reachable workspace of the system

The sum of the characterization results for the $3 - \underline{R}RP$ robot are tabulated in Table 5.2.

Table 5.2: Stroke device characteristics

Criterion	x	y	θ	robot
Instantaneous Peak Force/Torque	142.35 N	142.35 N	17.082 Nm	-
Continuous Peak Force/Torque	16.05 N	16.05 N	1.926 Nm	-
Virtual Wall Rendering	$3x10^4$ N/m	$3.3x10^4$ N/m	310 Nm	-
Effective Inertia	0.266 kg	0.262 kg	0.00259 kgm^2	-
Back drivability	0.26 N	0.14 N	0.039 Nm	-
Workspace Coverage	-66.5 to 66.5 mm	-66.5 to 66.5 mm	-180 to 180 degrees	-
Resolution	0.0559 mm	0.0559 mm	0.03 degrees	-
Position Bandwidth	-	-	-	57.3 Hz

5.2 Tendon Device

5.2.1 Usability Tests

A human subject experiment was conducted to quantify and compare the effect of the finger exoskeleton on the amount of voluntary contraction of the muscles attached to the flexor tendons during active (patient driven) and passive (therapist or exoskeleton guided) exercises. It is hypothesized that during the exoskeleton driven mode the voluntary contractions of the muscles will stay as low as the therapist guided exercises. It is also expected that due to the dynamics of the device, voluntary contraction levels for active patient motions with the device will be higher than the levels without the device. One of the goals of this experiment is to obtain a quantifiable measure of device interference during active motions, such that need for active dynamics compensation can be justified.

Participants

Four participants (2 males, 2 females, ages 23–28, all right-handed), all graduate students in engineering, participated in the experiment. All subjects reported a high level of physical activity and were free of musculoskeletal, cardiac, pulmonary and metabolic disorders. The participants were given extra credit for an engineering class upon completion of the experiment. All participants signed consent forms approved by the IRB of Sabancı University

to allow human performance data to be obtained and analyzed.

Tasks

The task was selected as repetitive flexion/extension motion of the index finger throughout the range of the MCP joint with a period of six seconds. The participants were given time to exercise the task before recording their data. During the experiment, visual and auditory reference signal were displayed to help participants with the timing of the task. Participants were instructed to perform smooth motions while trying to stay close to the period of the reference signal. Participants were specifically told to stay relaxed and not to perform jerky motions during the trials.

Experiment Setup

The experimental setup consisted of a desktop computer, a monitor screen, a wristband, and the underactuated force feedback finger exoskeleton. Participants sat in front of the monitor screen and index fingers of their dominant hands were firmly attached to the device. The elbows of the participants were supported to obtain a natural and comfortable posture. To ensure a robust and repeatable coupling between the finger and the exoskeleton, a wristband was tight wrapped around the wrist in order to stabilize its movement at a constant angle of $20°$. Then, the base platform of the exoskeleton was tied over the wrist via bandage straps and the transverse location of the finger exoskeleton was adjusted on the driver shaft to fit the natural finger motions.

To maximize comfort and hygiene, each phalanx of index finger was covered with a silicon ring before being attached to the exoskeleton using Vectro straps. The joint axes of the exoskeleton mechanism naturally adapts to the rotation of finger joints thanks to sliders embedded into the linkage design. Figure 5.7 illustrates a participant coupled to the exoskeleton device.
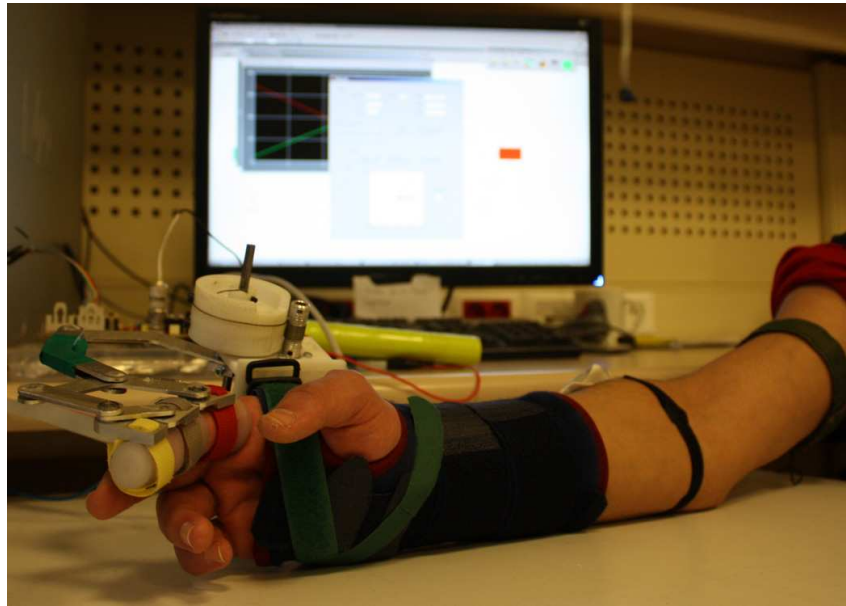
Figure 5.7: A participant attached to the finger exoskeleton device

sEMG Signal Acquisition and Processing

sEMG signals were measured using self-adhesive Ag-AgCl electrodes that are very close to perfectly non-polarizable electrodes. After skin preparation procedure of disinfecting, pairs of electrodes were positioned with an inter-electrode distance of 2 cm over the belly of the extensor digitorum communis and extensor indicis proprius [92]. The grounding electrode was attached over

the bicep. Since wrist extensor muscles (extensor carpi ulnaris, extensor carpi radialis longus, and extensor carpi radialis brevis) are closer to the surface of the skin compared to the muscle group actuating the index finger, the wrist motions were constrained to minimize crosstalk due to sEMG signals generated from these neighboring muscles.

Motion artifacts and low frequency disturbances in the raw EMG signals were suppressed by using a passive high pass filter with a cut off frequency of 20Hz. High frequency noise were attenuated utilizing low pass filter with cut off frequency of 500Hz. In addition to these filters, a fourth order active band pass filter with pass band 20-500Hz was utilized. An instrumentation amplifier with gain 1000 was used to amplify the measured signals. The A/D conversion is executed via Quanser Q8, 16bit ADC card. To prevent aliasing, the sampling rate was selected as 1kHz, which is appropriate for sEMG signals with typical frequency contents ranging form 6Hz to 500Hz.

Experiment Procedure

The experiment consisted of 4 sessions: active without the exoskeleton (A), active with the exoskeleton (F), passive without the exoskeleton (human guided) (H), and passive with the exoskeleton (exoskeleton driven) (E). Each session contained 6 subsessions and each subsession consisted of 10 trials, with each trial lasting 6 seconds. Six subsessions were separated by two to three minute breaks, such that the participants completed a session in less than 30 minutes. Details of the experiment design are schematically represented in Figure 5.8.

The active (A) trials served as the control set for the active with finger
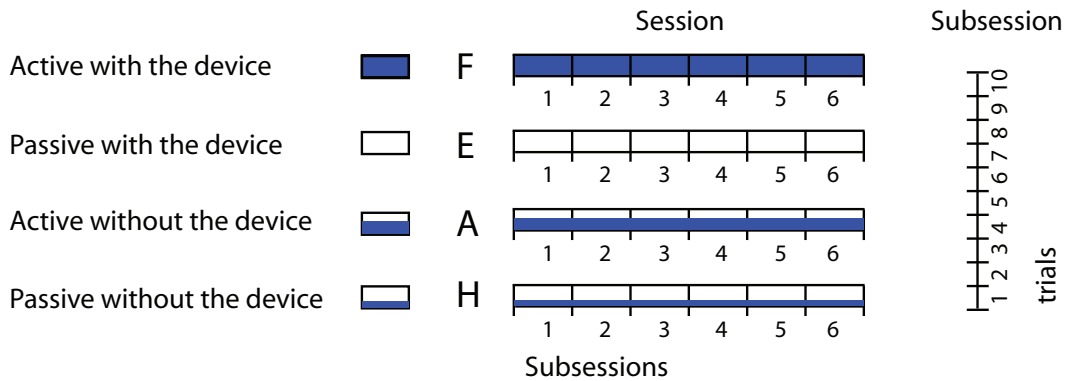
Figure 5.8: Schematic representation of the experiment design

exoskeleton (F) trials, while the human guided passive (H) trials were the control set for the exoskeleton driven passive (E) trials. During the exoskeleton driven (E) trials the actuators of the device provided guidance forces while during the human guided passive (H) trials the participants imposed the motion of the finger using their other hands. Each participant took place in all of the experiment sessions. Order of the sessions was randomly assigned for each subject. Before the experiment, each participant was given a maximum of five minutes to become familiar with the finger exoskeleton and the task.

Task Performance Measures

The task performance measure analyzed to assess the each participant was selected as the average of RMS of the sEMG signal. Since the sEMG signals are superpositions of the electrical potentials generated by motor units, the amplitude of SEMG signals are associated with the motor unit activities [93]. In the literature, the RMS value of an sEMG signal, which reveals its mean

power in time domain, has been proposed as a reliable measure of the force contribution of the muscle or the muscle group [94].

RMS values were calculated during intervals of 60s. During this interval, the muscle goes through both flexion and extension states. Envelopes of the rectified EMG signals have been calculated by post processing the rectified sEMG signals with a 250Hz FIR filter. In order to control for individual differences in task performance, each participant was asked to perform an evaluation task. The purpose of the evaluation session was to measure the resting and maximum voluntary contraction thresholds of each participant so that the experiment data can be normalized. The envelopes were post-processed by subtracting resting potential offsets determined for each subject during the evaluation experiment. To locate the onset and offset time of muscle extensions on the rectified sEMG signals, the signals were convolved with their envelopes. Finally, the percent voluntary contractions were also calculated by normalizing the mean RMS of the EMG signal by the mean RMS value pertaining to maximum voluntary contraction.

Data Analysis

A repeated measures ANOVA was utilized to verify the tested hypotheses. The experiment consisted of two factors, namely the guidance mode and subsessions. The guidance mode was between-subjects, with levels A, F, H, and E. Six subsessions were analyzed as a within-subject factor. Dependent-measures t-tests were adapted as the appropriate multi comparison strategy.

Results and Discussion

Four conditions, namely, active without the exoskeleton (A), active with the exoskeleton (F), passive without the exoskeleton (H), and passive with the exoskeleton (E), were compared to determine the muscle activation levels during various guidance methods. Figure 5.9 presents typical data collected from a participant during all four conditions.
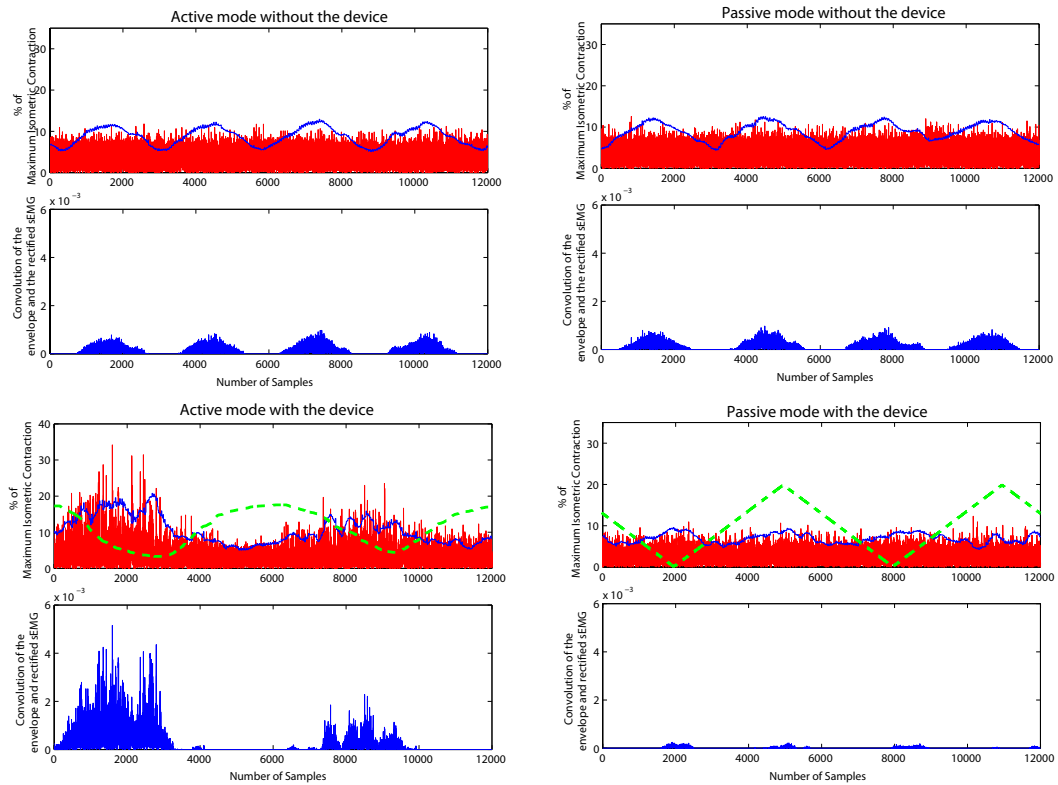
Figure 5.9: Typical data of the participants during all four conditions

A repeated measures ANOVA with between-subject factors (guidance as between-subject factor, session as within-subject factor) was carried out to determine significance of the four guidance modes. The results revealed a

97

significant main effect of guidance and no significant effects of subsession or interaction. A summary of these ANOVA results is listed in Table 5.3.

Table 5.3: Summary of significance measured by ANOVA

Effect	Significance
Guidance	$F(3, 60) = 6.11, \ p < 0.01^*$
Subsession	$F(5, 60) = 1.54, \ p > 0.05$
Interaction	$F(15, 60) = 1.18, \ p > 0.05$

Dependent-measures t-tests were conducted to compare between guidance modes. Muscle activation levels between H and E, E and A, and A and H guidance modes were found not to be statistically significant. However, muscle activation levels of E mode was significantly lower than F mode (F(1,30)=8.01, p $<$ 0.05), H mode was significantly lower than F mode (F(1,30)=5.98, p $<$ 0.05), and A mode was significantly lower than F mode (F(1,30)=5.45, p $<$ 0.05). The box plot of the experimental results is presented in Figure 5.10.
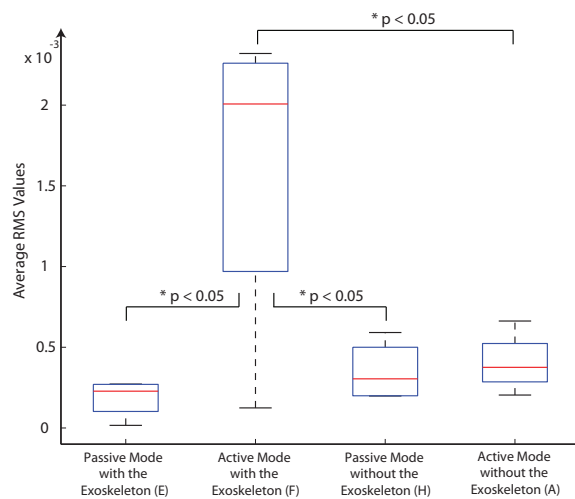
Figure 5.10: Box plot of the experimental results

The statistical results indicate that exoskeleton driven mode (E) is as effective as therapist guided (H) exercises in reducing muscle activation levels. The muscle activation levels of active (A) and passive (H) movements without the device are similar, as noted in the literature [6]. The muscle recruitment in active movement with the device (F) is significantly higher than active movements without the device (A). This result is expected, since the device dynamics always interfere with the motion. However, significant levels of muscle recruitment in F mode suggests that higher backdriveability needs to be targeted during design iterations and active dynamics compensation is required during active modes with the device.

5.2.2 Characterization

Tendon device is characterized in a similar way with the stroke device. Since it has an underactuated structure, and 2 passive degrees of freedom, some of the performance measures are tested within different criteria.

After first prototype implementation of the device, torque capability and weight of the device is observed as problematic. Therefore some optimization study is performed and best actuator and link lengths are selected. The actuators used in the system are Maxon RE30 DC motors which can supply a maximum continuous torque of 0.862 Nm and maximum peak torque of 1.02 Nm. Also the gear system (Planetary gearhead with 1:4.8 and capstan mechanism with 1:6 increase ratio) increases the apparent force observed at the end effector. Using the Jacobian transpose end effector maximal values are found around the nominal workspace of the mechanism: Continuous values, $\tau_{MCP} = 1.0939$ Nm $\tau_{PIP} = 0.993$ Nm, $\tau_{DIP} = 0.483$ Nm while instantaneous

values, $\tau_{MCP} = 12.944$ Nm $\tau_{PIP} = 11.75$ Nm, $\tau_{DIP} = 5.7207$ Nm.

In order to increase the force torque capability of the device, transmission ratio is also optimized by changing the link lengths. The worst case transmission ratio is calculated throughout the workspace and found as: TR_{MCP} = 10.2:1, TR_{PIP} = 6.06:1 and TR_{DIP} = 13.09:1.

Device kinematics steers the link lengths to be extremely large, in order to limit the link lengths effective inertia of the device is also optimized. The singular values of this inertia matrix are determined in a similar way as done for stroke device : $\sigma_{MCP} = 54.088 kg - mm^2$, $\sigma_{PIP} = 86.192 kg - mm^2$ and $\sigma_{DIP} = 22.343 kg - mm^2$.

Since system has an underactuated structure and has springs for joint passivity which force the PIP and DIP joints to nominal position, the minimal forces in these joints are zero. The experiments to measure the backdriveability of the mechanism concluded that the minimum torques in the end-effector coordinates with which the associated degree of freedom can be moved are as follows: $\tau_{MCP} = 1.6$ Nm, $\tau_{PIP} = 0$ Nm, $\tau_{DIP} = 0$ Nm.

Resolution at each joint is calculated by using encoder resolution and its mapping through Jacobian of each joint for the whole workspace. Encoder used with the actuator is Maxon MR type which has a resolution of 512 counts per revolution. It is multiplied by 4 due to quadrature rate and divided by gear ratio 4.8 and capstan ratio of 6. Finally it is found that the maximum error that can not be realized is 0.0061° from encoders. Worst case resolution is obtained as 0.063° degrees at MCP joint, 0.034° degrees at PIP joint and 0.08° for DIP joint.

The workspace spanned by the mechanism has to cover the motion range of finger. Since finger is a kinematic part of the device, workspace of the

device is limited with the motion ranges of each joint. However, excluding the finger, robot has mechanical limits at 94.55° for PIP joint and at 99.05° for DIP joint while it has no limitations for MCP joint.

Grasp capability is a very important criteria for an underactuated finger mechanism. Nevertheless the robot can grasp every object which human can grasp since the grasping part of the device is human finger.

Feasibility of usage of the device for hands with various sizes is another important criteria of the device characteristics. Thanks to the its kinematic details, device has a wide range of adjustability. It can be put on by any finger with any DIP and MCP knuckle lengths while it has a limitation on PIP length. Yet the PIP knuckle length range (28 to 36 mm) covers the anthropomorphic human finger lengths. Additionally wrist angle adjustment also has no limitations. Finally the hand length is adjustable between the range 63-93 mm.

A summary of the characterization results for the tendon robot is given in Table 5.4.

Table 5.4: Tendon device characteristics

Criterion	MCP	PIP	DIP	Robot
Instantaneous Peak Torque	12.944 Nm	11.75 Nm	5.7207 Nm	-
Continuous Peak Torque	1.0939 Nm	0.993 Nm	0.483 Nm	-
Worst Case Transmission Ratio	10.2:1	6.06:1	13.09:1	-
Effective Inertia	54.088 $kg - mm^2$	86.192 $kg - mm^2$	22.343 $kg - mm^2$	-
Back Drivability	0.022 Nm	0 Nm	0 Nm	-
Resolution	0.063°	0.034°	0.08°	-
Workspace Coverage	No limit	94.55°	99.05°	-
Knuckle Length Adjustability	No limit	28-36 mm	No limit	-
Hand Length Adjustability	-	-	-	63-93 mm
Wrist Angle Adjustability	-	-	-	No limit
Grasp Capability	-	-	-	Hand limits

Chapter VI

6   Conclusion & Future Works

Hand is most frequently used and injured part of the body and rehabilitation of hand is very important since loss of hand function causes serious damages in patients social, economical and psychological life. In this manner, we have developed 2 rehabilitation systems for the purpose of regaining the hand function after any injury.

First device is a task-space oriented, impedance type, 3-DoF, portable haptic interface which has been developed to deliver rehabilitation therapies and to administer RoM/strength measurements for the upper extremity, including forearm, wrist and hand. Usability studies have been conducted and the efficacy of the device on performing concurrent, coordinated motions of the hand and the forearm/wrist has been shown. The measurement accuracy of the device has been characterized through a comparison test with a forearm/wrist exoskeleton and it is shown that there is no statistically significance between measurements of $3 - \underline{R}RP$ and an exoskeleton.

Kinematic analysis of the $3 - \underline{R}RP$ mechanism is solved analytically and a single objective workspace optimization is performed in order to achieve best performance from the device. Furthermore device performance is characterized considering requirements of a rehabilitation device.

Second device is a finger exoskeleton which has been developed to deliver tendon therapy exercises. The finger exoskeleton is designed to assist flexion/extension motions of the finger within its full range, in a natural and coordinated manner, while keeping the tendon tension within acceptable limits. Usability studies have been conducted and the efficacy of exoskeleton driven exercises on reducing muscle requitement levels has been shown.

The exoskeleton can simultaneously measure finger movements, interaction forces, and muscle activities. These measurements provide quantitative measures of recovery and can guide physical therapy programs. Moreover, the utilization of the finger exoskeleton in a clinical setting may help determination of the complex map from extrinsic signals such as measure finger movements, interaction forces, and muscle activities to the tendon tensions.

Moreover kinematics of the under-actuated device is analytically solved and optimum link lengths are found which maximizes torque transmission while minimizing effective inertia of the system. Device performance is also characterized.

Future works include human subject studies with unhealthy subjects for both of the devices. If a reliable model of the tendon loading can be developed, then less conservative tendon rehabilitation therapies can be developed for tendon therapy. Novel therapies can potentially reduce the recovery times; hence, the treatment costs. Also implementation of embedded controls, external graphical user interface for home use are planned for both of the devices' future works.

Appendix A

Abduction: The movement of a limb away from the midline of the body.

Acute stroke: A stage of stroke starting at the onset of symptoms that lasts for a few hours thereafter.

Adduction: The movement of a limb toward the midline of the body.

Blood clot: Blood that has been converted from a liquid to a solid state. Also called a thrombus .

Cerebellum: A region of the brain that plays an important role in motor control.

Cerebrovascular accident: The sudden death of some brain cells due to lack of oxygen when the blood flow to the brain is impaired by blockage or rupture of an artery to the brain.

Cerebellum: An impairment in spatial perception and stability.

Early mobilization: Procedure to accelerate the ability of a patient to walk or move about by reducing the time to ambulation.

Edema: The swelling of soft tissues as a result of excess water accumulation.

Emboli: Something that travels through the bloodstream, lodges in a blood vessel and blocks it.

Extension: The process of straitening or the state of being strait.

Flexion: The process of bending or the state of being bent.

Hemiplegia: Paralysis of one side of the body.

Hemorrhage: Bleeding or the abnormal flow of blood.

Mallet Finger Injury: A tear of tendon that straightens the end joint of the finger.

Nausea: A sensation of unease and discomfort in the upper stomach with an urge to vomit.

Paralysis: Loss of movement.

Phantom Limb: The missing limb in amputees.

Pronation: The process of bending or the state of being bent.

Supination: Rotation of the forearm and hand so that the palm is up.

Tendon: The tissue by which a muscle attaches to bone. A tendon is somewhat flexible, but fibrous and tough.

Tendon Sheath: Layer of membrane around a tendon which permits the tendon to move.

Tone: The degree of tension in a muscle at rest

Vascular: Relating to the blood vessels of the body.

Vessel: A tube in the body that carries fluids: blood vessels or lymph vessels.

Voluntary Muscle Contraction: Muscle activation which occurs as a result of conscious effort originating in the brain and controlled by the central nervous system.

Appendix B

$3 - \underline{R}RP$ Forward Kinematics

Configuration level forward kinematics of the $3 - \underline{R}RP$ robot is solved by eliminating the intermediate variables.

From the Figure 2.5 one can observe that:

$$x\overrightarrow{n_1} + y\overrightarrow{n_2} + s_1\overrightarrow{k_1} - l_1\overrightarrow{t_1} = \overrightarrow{0}$$

$$x\overrightarrow{n_1} + y\overrightarrow{n_2} + s_2\overrightarrow{l_1} - l_2\overrightarrow{s_1} = \overrightarrow{0}$$

$$x\overrightarrow{n_1} + y\overrightarrow{n_2} + s_3\overrightarrow{m_1} - l_3\overrightarrow{v_1} = \overrightarrow{0}$$

6 scalar equations can be derived as:

$$x + s_1 cos(\theta + \frac{\pi}{3}) - l_1 cos(q_1) = 0$$

$$y + s_1 sin(\theta + \frac{\pi}{3}) - l_1 sin(q_1) = 0$$

$$x + s_2 cos(\theta + \pi) - l_2 cos(q_2) = 0$$

$$y + s_2 sin(\theta + \pi) - l_2 sin(q_2) = 0$$

$$x + s_3 cos(\theta - \frac{\pi}{3}) - l_3 cos(q_3) = 0$$

$$y + s_3 sin(\theta - \frac{\pi}{3}) - l_3 sin(q_3) = 0$$

For simplicity define:

$$c_{11} = l_1 cos(q_1)$$

$$c_{12} = l_1 sin(q_1)$$

$$c_{21} = l_2 cos(q_2)$$

$$c_{22} = l_2 sin(q_2)$$

$$c_{31} = l_3 cos(q_3)$$

$$c_{32} = l_3 sin(q_3)$$

Then we can write:

$$x + s_1 cos(\theta + \frac{\pi}{3}) = c_{11}$$

$$y + s_1 sin(\theta + \frac{\pi}{3}) = c_{12}$$

$$x + s_2 cos(\theta + \pi) = c_{21}$$

$$y + s_2 sin(\theta + \pi) = c_{22}$$

$$x + s_3 cos(\theta - \frac{\pi}{3}) = c_{31}$$

$$y + s_3 sin(\theta - \frac{\pi}{3}) = c_{32}$$

The intermediate variables can be written as:

$$s_1 = \frac{c_{11} - x}{cos(\theta + \frac{\pi}{3})}$$

$$s_2 = \frac{c_{21} - x}{cos(\theta + \pi)}$$

$$s_3 = \frac{c_{31} - x}{cos(\theta - \frac{\pi}{3})}$$

Then by eliminating the intermediate variables:

$$y + \frac{c_{11} - x}{cos(\theta + \frac{\pi}{3})} sin(\theta + \frac{\pi}{3}) = c_{12}$$

$$y + \frac{c_{21} - x}{cos(\theta + \pi)} sin(\theta + \pi) = c_{22}$$

$$y + \frac{c_{31} - x}{cos(\theta - \frac{\pi}{3})} sin(\theta - \frac{\pi}{3}) = c_{32}$$

which are equal to

$$y + (c_{11} - x)tan(\theta + \frac{\pi}{3}) = c_{12}$$

$$y + (c_{21} - x)tan(\theta + \pi) = c_{22}$$

$$y + (c_{31} - x)tan(\theta - \frac{\pi}{3}) = c_{32}$$

Since

$$tan(a + b) = \frac{tan(a) + tan(b)}{1 - tan(a)tan(b)}$$

and

$$tan(-a) = -tan(a)$$

The equations can be written in the form of:

$$y + (c_{11} - x)\frac{tan(\theta) + tan(\frac{pi}{3})}{1 - tan(\theta)tan(\frac{pi}{3})} = c_{12}$$

$$y + (c_{21} - x)\frac{tan(\theta) + tan(\pi)}{1 - tan(\theta)tan(\pi)} = c_{22}$$

$$y + (c_{31} - x)\frac{tan(\theta) + tan(\frac{-pi}{3})}{1 - tan(\theta)tan(\frac{-pi}{3})} = c_{32}$$

Placing the values of scalars:

$$y + (c_{11} - x)\frac{tan(\theta) + \sqrt{3}}{1 - \sqrt{3}tan(\theta)} = c_{12} \tag{B-1}$$

$$y + (c_{21} - x)\tan(\theta) = c_{22} \tag{B-2}$$

$$y + (c_{31} - x)\frac{tan(\theta) - \sqrt{3}}{1 + \sqrt{3}tan(\theta)} = c_{32} \tag{B-3}$$

The equations B-1, B-2, B-3 can be simplified as:

$$(c_{11} - c_{21} + \sqrt{3}c_{12})tan(\theta) - \sqrt{3}x - \sqrt{3}tan(\theta)y = c_{12} - c_{22} - \sqrt{3}c_{11} \tag{B-4}$$

$$xtan(\theta) = y + c_{21}tan(\theta) - c_{22} \tag{B-5}$$

$$(c_{31} - c_{21} - \sqrt{3}c_{32})tan(\theta) + \sqrt{3}x + \sqrt{3}tan(\theta)y = c_{32} - c_{22} + \sqrt{3}c_{31} \tag{B-6}$$

By adding Equation B-4 to Equation B-6:

$$(c_{11} - c_{21} + \sqrt{3}c_{12} + c_{31} - c_{21} - \sqrt{3}c_{32})tan(\theta) = c_{12} + c_{32} + \sqrt{3}c_{31} - c_{22} - c_{22} - \sqrt{3}c_{31}$$

For simplicity define:

$$K = c_{12} + c_{32} + \sqrt{3}c_{31} - c_{22} - c_{22} - \sqrt{3}c_{31}$$

$$L = c_{11} - c_{21} + \sqrt{3}c_{12} + c_{31} - c_{21} - \sqrt{3}c_{32}$$

Then we solve θ as:

$$tan(\theta) = \frac{K}{L}$$

$$\theta = tan^{-1}(\frac{K}{L})$$

Using the $tan(\theta)$ value in Equations B-4 and B-5.

$$(L - \sqrt{3}K)y - (K + \sqrt{3}L)x = c_{12}(L - \sqrt{3}K) - c_{11}(K + \sqrt{3}L) \qquad \text{(B-7)}$$

$$Ly - Kx = Lc_{22} - Kc_{21} \qquad \text{(B-8)}$$

From Equation B-9 y can be written as:

$$y = \frac{Lc_{22} - Kc_{22} + Kx}{L}$$

Replace to the Equation B-7

$$(-\sqrt{3}K^2 - \sqrt{3}L^2)x = L(L - \sqrt{3}K)c_{12} - L(K + \sqrt{3}L)c_{11} - (L - \sqrt{3}K)(Lc_{22} - Kc_{21})$$

Defining

$$M = L(L - \sqrt{(3)}K)c_{12} - L(K + \sqrt{(3)}L)c_{11} - (L - \sqrt{(3)}K)(Lc_{22} - Kc_{21})$$

we can solve for x as:

$$x = -\frac{M}{\sqrt{(3)}(K^2 + L^2)}$$

Using Equation B-9

$$Ly + K\frac{M}{\sqrt{(3)(K^2 + L^2)}} = Lc_{22} - Kc_{21} \qquad \text{(B-9)}$$

Therefore y can be solved as:

$$y = c_{22} - \frac{K}{L}c_{21} - \frac{KM}{\sqrt{(3)}L(K^2 + L^2)}$$

Forward kinematics of the $3 - \underline{R}RP$ is done.

$3 - \underline{R}RP$ Inverse Kinematics

Configuration level inverse kinematics of $3 - \underline{R}RP$ robot is obtained by using Chase's Theorem.

Chase introduces 4 cases for the solution of a vector loop with

$$\vec{a} + \vec{b} + \vec{c} = \vec{0}$$

Chase asserts solutions for the cases when

Case 1 direction of $\vec{c}$ and magnitude of $\vec{c}$ are unknown

Case 2 magnitude of $\vec{a}$ and magnitude of $\vec{b}$ are unknown

Case 3 direction of $\vec{a}$ and direction of $\vec{b}$ are unknown

Case 4 direction of $\vec{b}$ and magnitude of $\vec{a}$ are unknown

Inverse kinematics of $3-\underline{R}RP$ robot includes 3 independent Case 4 problems with the loops (see Figure 2.7):

112

$$\overrightarrow{ZP} + \overrightarrow{PO} + \overrightarrow{OZ} = \overrightarrow{0}$$

$$\overrightarrow{ZQ} + \overrightarrow{QO} + \overrightarrow{OZ} = \overrightarrow{0}$$

$$\overrightarrow{ZR} + \overrightarrow{RO} + \overrightarrow{OZ} = \overrightarrow{0}$$

For case 4 problems Chase proposes a solution:

$$\vec{a} = [-\vec{c} \cdot \vec{a_u} \mp \sqrt{b^2 - [\vec{c} \cdot (\vec{a_u} x \, \vec{k})]^2}]\vec{a_u}$$

$$\vec{b} = -[\vec{c} \cdot (\vec{a_u} x \, \vec{k})] \cdot (\vec{a_u} x \, \vec{k}) \pm \sqrt{b^2 - [\vec{c} \cdot (\vec{a_u} x \, \vec{k})]^2}\vec{a_u}$$

For the first loop

$$\overrightarrow{ZP} + \overrightarrow{PO} + \overrightarrow{OZ} = \overrightarrow{0}$$

$$\vec{a} \quad corresponds \quad to \quad \overrightarrow{ZP}$$

$$\vec{b} \quad corresponds \quad to \quad \overrightarrow{PO}$$

$$\vec{c} \quad corresponds \quad to \quad \overrightarrow{OZ}$$

Therefore the $\vec{c}$ vector is equal to

$$\vec{c} = \begin{pmatrix} x \\ y \end{pmatrix}$$

and the magnitude of $\vec{c}$ is $c = \sqrt{x^2 + y^2}$.

While the unit vector along $\vec{c}$:

$$\overrightarrow{c_u} = \begin{pmatrix} \frac{x}{\sqrt{x^2+y^2}} \\ \frac{y}{\sqrt{x^2+y^2}} \end{pmatrix}$$

The unit vector along $\overrightarrow{a}$:

$$\overrightarrow{a_u} = \begin{pmatrix} cos(\theta + \frac{\pi}{3}) \\ sin(\theta + \frac{\pi}{3}) \end{pmatrix}$$

Cross product of the unit vector along $\overrightarrow{a}$ and z direction:

$$\overrightarrow{a_u} x \overrightarrow{k} = \begin{pmatrix} sin(\theta + \frac{\pi}{3}) \\ -cos(\theta + \frac{\pi}{3}) \end{pmatrix}$$

For simplicity define:

$$K_1 = \overrightarrow{c} \cdot (\overrightarrow{a_u} x \overrightarrow{k}) = x \sin(\theta + \frac{\pi}{3}) - y \cos(\theta + \frac{\pi}{3})$$

Then

$$\sqrt{b^2 - [\overrightarrow{c} \cdot (\overrightarrow{a_u} x \overrightarrow{k})]} = \sqrt{l_1^2 - K_1^2}$$

Thus we can write $\overrightarrow{c}$ vector as:

$$\overrightarrow{b} = -K_1 \begin{pmatrix} sin(\theta + \frac{\pi}{3}) \\ -cos(\theta + \frac{\pi}{3}) \end{pmatrix} \pm \sqrt{l_1^2 - K_1^2} \begin{pmatrix} cos(\theta + \frac{\pi}{3}) \\ sin(\theta + \frac{\pi}{3}) \end{pmatrix}$$

Again for simplicity define:

$$L_1 = -K_1 sin(\theta + \frac{\pi}{3}) - \sqrt{l_1^2 - K_1^2} cos(\theta + \frac{\pi}{3})$$

114

$$M_1 = K_1 cos(\theta + \frac{\pi}{3}) - \sqrt{l_1^2 - K_1^2} sin(\theta + \frac{\pi}{3})$$

Thus we solve the direction of $\overrightarrow{b}$ as:

$$q_1 = tan^{-1} = \frac{M_1}{L_1}$$

For the second loop

$$\overrightarrow{ZQ} + \overrightarrow{QO} + \overrightarrow{OZ} = \overrightarrow{0}$$

$$\overrightarrow{a} \quad corresponds \quad to \quad \overrightarrow{ZQ}$$

$$\overrightarrow{b} \quad corresponds \quad to \quad \overrightarrow{QO}$$

$$\overrightarrow{c} \quad corresponds \quad to \quad \overrightarrow{OZ}$$

Therefore the $\overrightarrow{c}$ vector is equal to

$$\overrightarrow{c} = \begin{pmatrix} x \\ y \end{pmatrix}$$

and the magnitude of $\overrightarrow{c}$ is $c = \sqrt{x^2 + y^2}$.

While the unit vector along $\overrightarrow{c}$:

$$\overrightarrow{c_u} = \begin{pmatrix} \frac{x}{\sqrt{x^2+y^2}} \\ \frac{y}{\sqrt{x^2+y^2}} \end{pmatrix}$$

115

The unit vector along $\overrightarrow{a}$:

$$\overrightarrow{a_u} = \begin{pmatrix} cos(\theta + \pi) \\ sin(\theta + \pi) \end{pmatrix}$$

Cross product of the unit vector along $\overrightarrow{a}$ and z direction:

$$\overrightarrow{a_u} x \overrightarrow{k} = \begin{pmatrix} sin(\theta + \pi) \\ -cos(\theta + \pi) \end{pmatrix}$$

For simplicity define:

$$K_2 = \overrightarrow{c} \cdot (\overrightarrow{a_u} x \overrightarrow{k}) = x \sin(\theta + \pi) - y \cos(\theta + \pi)$$

Then

$$\sqrt{b^2 - [\overrightarrow{c} \cdot (\overrightarrow{a_u} x \overrightarrow{k})]} = \sqrt{l_2^2 - K_2^2}$$

Thus we can write $\overrightarrow{c}$ vector as:

$$\overrightarrow{b} = -K_2 \begin{pmatrix} sin(\theta + \pi) \\ -cos(\theta + \pi) \end{pmatrix} \pm \sqrt{l_2^2 - K_2^2} \begin{pmatrix} cos(\theta + \pi) \\ sin(\theta + \pi) \end{pmatrix}$$

Again for simplicity define:

$$L_2 = -K_2 sin(\theta + \pi) - \sqrt{l_2^2 - K_2^2} cos(\theta + \pi)$$

$$M_2 = K_2 cos(\theta + \pi) - \sqrt{l_2^2 - K_2^2} sin(\theta + \pi)$$

Thus we solve the direction of $\overrightarrow{b}$ as:

116

$$q_2 = tan^{-1} = \frac{M_2}{L_2}$$

For the third loop

$$\overrightarrow{ZR} + \overrightarrow{RO} + \overrightarrow{OZ} = \vec{0}$$

$$\vec{a} \quad corresponds \quad to \quad \overrightarrow{ZR}$$

$$\vec{b} \quad corresponds \quad to \quad \overrightarrow{RO}$$

$$\vec{c} \quad corresponds \quad to \quad \overrightarrow{OZ}$$

Therefore the $\vec{c}$ vector is equal to

$$\vec{c} = \begin{pmatrix} x \\ y \end{pmatrix}$$

and the magnitude of $\vec{c}$ is $c = \sqrt{x^2 + y^2}$.

While the unit vector along $\vec{c}$:

$$\vec{c_u} = \begin{pmatrix} \frac{x}{\sqrt{x^2+y^2}} \\ \frac{y}{\sqrt{x^2+y^2}} \end{pmatrix}$$

The unit vector along $\vec{a}$:

$$\vec{a_u} = \begin{pmatrix} cos(\theta - \frac{\pi}{3}) \\ sin(\theta - \frac{\pi}{3}) \end{pmatrix}$$

117

Cross product of the unit vector along $\vec{a}$ and z direction:

$$\vec{a_u} x \vec{k} = \begin{pmatrix} sin(\theta - \frac{\pi}{3}) \\ -cos(\theta - \frac{\pi}{3}) \end{pmatrix}$$

For simplicity define:

$$K_3 = \vec{c} \cdot (\vec{a_u} x \vec{k}) = x \sin(\theta - \frac{\pi}{3}) - y \cos(\theta - \frac{\pi}{3})$$

Then

$$\sqrt{b^2 - [\vec{c} \cdot (\vec{a_u} x \vec{k})]} = \sqrt{l_3^2 - K_3^2}$$

Thus we can write $\vec{c}$ vector as:

$$\vec{b} = -K_3 \begin{pmatrix} sin(\theta - \frac{\pi}{3}) \\ -cos(\theta - \frac{\pi}{3}) \end{pmatrix} \pm \sqrt{l_3^2 - K_3^2} \begin{pmatrix} cos(\theta - \frac{\pi}{3}) \\ sin(\theta - \frac{\pi}{3}) \end{pmatrix}$$

Again for simplicity define:

$$L_3 = -K_3 sin(\theta - \frac{\pi}{3}) - \sqrt{l_3^2 - K_3^2}cos(\theta - \frac{\pi}{3})$$

$$M_3 = K_3 cos(\theta - \frac{\pi}{3}) - \sqrt{l_3^2 - K_3^2}sin(\theta - \frac{\pi}{3})$$

Thus we solve the direction of $\vec{b}$ as:

$$q_3 = tan^{-1} = \frac{M_3}{L_3}$$

Inverse kinematics of the $3 - \underline{R}RP$ is done.

Configuration Level Kinematics of the Finger Robot

The following calculation is performed for a generic four-bar mechanism. This method is applied to all loops demonstrated in Figure 2.8. Since the forward and inverse problem has the same formulation and solution method, just one of the problem (forward) is solved here.
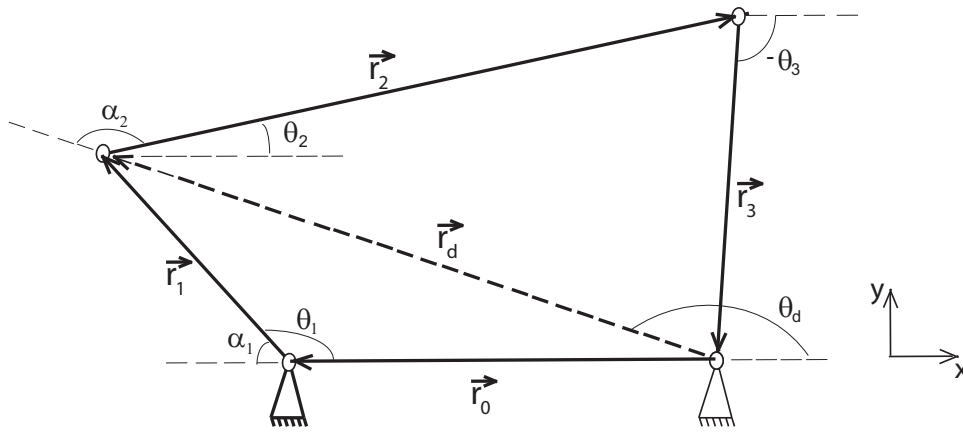
Figure 6.1: Kinematics of a four-bar mechanism

For the four-bar linkage shown in Figure 6.1,diagonal can be written as:

$$\overrightarrow{r_d} = \overrightarrow{r_0} + \overrightarrow{r_1}$$

We are to determine the linkage position for a given angle θ_1 if all the link lengths are known. Taking the dot product of each side of this equation with itself, we have

$$\overrightarrow{r_d} \cdot \overrightarrow{r_d} = (\overrightarrow{r_0} + \overrightarrow{r_1}) \cdot (\overrightarrow{r_0} + \overrightarrow{r_1})$$

which can be written as

$$r_d^2 = r_0^2 + 2r_0 r_1 cos(\alpha_1) + r_1^2$$

where the angle between $\overrightarrow{r_0}$ and $\overrightarrow{r_1}$ is $\alpha_1 = 180 - \theta_1$. Thus above equation becomes equivalent to law of cosines:

$$r_d^2 = r_0^2 - 2r_0 r_1 cos(\theta_1) + r_1^2$$

The direction of the diagonal can be calculated in terms of the x and y components of $\overrightarrow{r_0}$ and $\overrightarrow{r_1}$:

$$sin(\theta_d) = \frac{r_{0y} + r_{1y}}{r_d}$$

and

$$cos(\theta_d) = \frac{r_{0x} + r_{1x}}{r_d}$$

$$tan(\frac{\theta_d}{2}) = \frac{1 - cos(\theta_d)}{sin(\theta_d)}$$

Using the above 3 equations we are able to determine θ_d.

We continue the analysis with the loop closure equation

$$\overrightarrow{r_d} + \overrightarrow{r_2} + \overrightarrow{r_3} = \overrightarrow{0}$$

then

$$-\overrightarrow{r_3} = \overrightarrow{r_2} + \overrightarrow{r_d}$$

Taking the dot product of each side of this equation with itself, we have

$$\vec{r_3} \cdot \vec{r_3} = (\vec{r_d} + \vec{r_2}) \cdot (\vec{r_d} + \vec{r_2})$$

which can be written as

$$r_3^2 = r_d^2 + 2r_2 r_d cos(\alpha_2) + r_2^2$$

so that

$$cos(\alpha_2) = \frac{r_3^2 - r_2^2 - r_d^2}{2r_d r_2} \quad for \quad 0 \le \alpha_2 \le 180$$

Then

$$\theta_2 = \theta_d \mp \alpha_2$$

The sign before α_2 depends on the mode of assembly of the linkage. If the vector loop is clockwise negative sign applies; if counterclockwise, the positive sign applies.

The position of link 3 may be found by using the dot product in a similar manner.

$$\vec{r_3} = -(\vec{r_0} + \vec{r_1} + \vec{r_2})$$

Then,

$$sin(\theta_3) = \frac{r_{3y}}{r_3}$$

and

$$cos(\theta_3) = \frac{r_{3x}}{r_3}$$

and θ_3 can be found from the equation

$$tan(\frac{\theta_3}{2}) = \frac{1 - cos(\theta_3)}{sin(\theta_3)}$$

Appendix C

The method used for selection of the mounting structure of the tendon device is explained in this section.

The procedure used in the studies are shown in Figure 6.2.
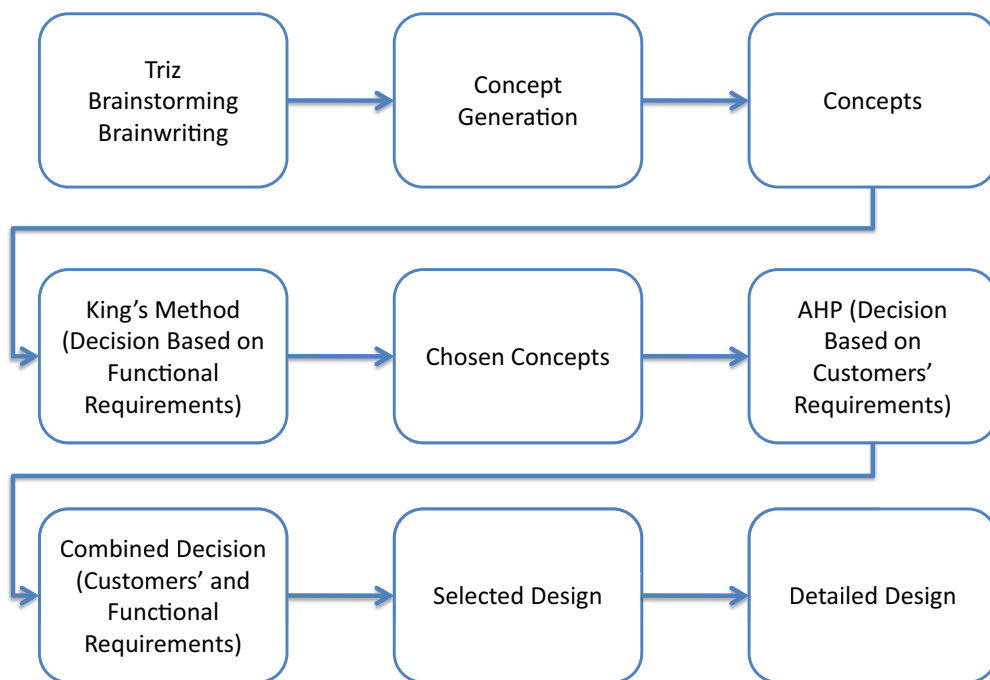
Figure 6.2: Proposed Decision Procedure

To have a clear understanding of the problem, the requirements of the customer have to be analyzed. In this case, there are two kinds of end customers:

1. The Patient who has injured his hand/finger and in need of therapy.

2. The therapist/nurse who is going to control the device and assist the patient.

The data are collected by approaching the two types of customers and asking them what they felt was required of the rings. To analyze the customer requirements, a hierarchal objective list is formulated by asking the two types of customers. To prioritize the Customer Requirements and arrange them in order, The Analytic Hierarchy Process (AHP) is used. Two different hierarchial list of objectives formed for the tendon device are demonstrated as follows with their rankings in parenthesis:

Hierarchical List of Objectives Sample I:

1. Cost (0.11)

   - Maintenance (0.4)

   - Reliability (0.2)

   - Material (0.4)

2. Effective (0.044)

   - Same Quality Treatment as Therapy (0.23)

   - Heals Correctly (0.68)

   - Quick Recovery (0.09)

3. Flexibility (0.071)

   - Adjustability (1.0)

4. Safety (0.505)

- No Further Injury (0.714)

- No Sharp Edges (0.143)

- No Risk of Shocks (0.143)

5. User Friendly (0.269)

  - Ease of Use and Setup (0.096)

  - Quiet (0.012)

  - Lightweight (0.044)

  - Comfortable Material (0.032)

  - Does not Inhibit Movements (0.085)

Hierarchical List of Objectives Sample II:

1. Comfort (0.37)

  - Allergic Reactions (0.58)

  - Quick Release if hurting (0.22)

  - Feel of Device on Finger (0.09)

  - Feel to other fingers (0.09)

  - Weight (0.03)

2. User friendly (0.28)

  - Easy to Fit (0.41)

  - No Special Tools Required (0.38)

  - Easy to Clean (0.17)

- Easy to Store (0.04)

3. Durable (0.17)

   - Easy Maintenance (0.21)

   - Large Number of Cycles of Use (0.25)

   - Reliability (0.54)

4. Aesthetics (0.14)

   - Does Not Look Scary (0.59)

   - Color (0.09)

   - Shape (0.32)

5. Cost (0.04)

   - Maintenance Cost (EG: Back Up Costs) (0.61)

   - Production Costs (EG: Material Cost) (0.39)

The Morphological charts are formed for concept generation which summarizes the functions and chosen options. Again the following two morphological charts are the formed samples as Table 6.1 and 6.2.

Table 6.1: Morphological chart for concepts I

FUNCTIONS	OPTIONS
Hold Finger Without Slippage	Glove - Magnetic Ring - Inflatable Tubes - Velcro Straps - Chain - Latching Rings
Transmitted Motor's Motion	Bolts - Magnets - Sticky Substance Rope/String - Latch - Plug

Table 6.2: Morphological chart for concepts II

FUNCTIONS	OPTIONS
Comfort	Plastic - Coating - Stainless Steel - Rubber
User Friendly	Electromagnets - Vectro - Button Mechanism
Durable	Multiple Rings - Single Ring - Attached Single Ring
Aesthetics	Smooth Surface - Rubber Pad - No Holes

In order to select the best combination of options from morph charts, a new concept selection method (CSM) is used. In the CSM, the modified decision matrix was somewhat used as a screening process for the second selection method. The five configurations that scored the highest were then passed along to the second method, AHP. These configurations are shown in Table 6.3 and 6.4.

Table 6.3: AHP and the modified King's method calculations I

Configuration		MDM Score	AHP Score	Multiplied Score
Chain	Bolts	0.44	0.107	0.047
Glove	**Magnets**	**0.42**	**0.246**	**0.103**
Chain	Latch	0.40	0.129	0.052
Glove	Sticky Substance	0.38	0.267	0.101
Glove	Rope/String	0.38	0.251	0.095

The design consisted of concepts: gloves and magnets. It is determined that the gloves would be made out of a neoprene material and that the magnets would be embedded into this material. Several different size gloves would need to be made in order to account for various patient hand sizes. The neoprene material, which is used to make things such as wet suits and knee braces, would be capable of stretching to account for small variations within each of the glove sizes.

Table 6.4: AHP and the modified King's method calculations II

	Importance	Stainless Steel	Plastic	Coating	Electromagnets	Button	Velcro	Smooth Surface	Rubber Pad	No Holes	Multiple Rings	Single Ring
Comfort	0.37	6	7	7	4	8	8	9	8	6	7	3
User Friendly	0.28	7	7	7	8	8	7	8	7	7	5	9
Durable	0.04	9	4	5	7	5	3	5	5	4	8	4
Aesthetics	0.17	7	3	7	7	6	5	8	6	5	5	5
Cost	0.14	4	6	2	2	2	7	6	5	5	4	7
		6.29	6.06	6.22	5.47	6.7	**6.87**	**7.97**	6.84	5.89	**5.72**	5.62

As solved, the highest total score among the concepts in each category is

selected. The selected concepts by this method are as follows: Stainless steel - Velcro - Smooth surface - Multiple rings.

Finally combining the two optimal solutions for suggested above, we propose the snap fastener method for mounting the device to finger.

References

[1] j. Marty, B. Porcher, and R. Autissier. Hand injuries and occupational accidents: Statistics and prevention. *Ann Chir Main*, 4(2):368–370, 1980.

[2] C. A. Trombly. Occupational therapy for physical dysfunction. *Stroke*, pages 454–471, 1989.

[3] T. Scott and P. Peckham. Upper etremity neuroprostheses using functional electrical stimulation. *Bailliere's Clinical Neurology*, 4:57–75, 1995.

[4] Bureau of labor statistics. `http://www.bls.gov/cps/tables.htm#charemp`.

[5] Occupational safety and health administration. `http://www.bls.gov/iif`.

[6] J. T. Dennerlein. Finger flexor tendon forces are a complex functon of finger joint motions and fingertip forces. *Journal of Hand Therpahy*, 18:120–127, 2005.

[7] J. W. Strickland and S. V. Glogovac. Digital function following flexor tendon repair in zone II: A comparison of immobilization and controlled passive motion techniques. *Journal of Hand Surgery*, 5A:537–543, 1980.

[8] T. Tanaka, P. C. Amadio, C. Zhao, M. E. Zobitz, and K. N. An. Flexor digitorum profundus tendon tension during finger manipulation. *Journal of Hand Theraphy*, 18:330–338, 2005.

[9] G. Van Strien. Postoperative managment of flexor tendon injuries. *Rehabilitation of the Hand*, pages 390–409, 1990.

[10] K. M. Stewart. Concepts in hand rehabilitation. *Tendon Injuries*, pages 353–392, 1992.

[11] C. D. Kerr and J. R. Burczak. Dynamic traction after extensor tendon repair in zones 6, 7 and 8: A retrospective study. *Journal of Hand Surgery*, 14B:21–22, 1989.

[12] R. B. Evans. Clinical application of controlled stress to the healing extensor tendon: a review of 112 cases. *Physical Theraphy*, 69:1041–1049, 1989.

[13] J. Hunter and E. Mackin. *Rehabilitation of the Hand: Surgery and Therapy*. St Louis, Mosby, 1995.

[14] John Chae. Neuromuscular stimulation for upper extremity motor anf functional recovery in acute hemiplegia. *Stroke*, 9(29):975–979, 1998.

[15] G. Yavuzer, R. Selles, N. Sezer, S. Sutbeyaz, B. Bussmann, F. Koseoglu, B. Atay, and H. Stam. Mirror therapy improves hand function in subacute stroke: a randomized controlled trial. *Arch Phys Med Rehabil*, 89(29):393–398, 2008.

[16] J. W. Strickland. Flexor tendon repair. *Hand Clinics*, 1:55–68, 1985.

[17] M. N. Halikis, P. R. Manske, H. Kubota, and M. Aoki. Effect of immobilization, immediate mobilization, and delayed mobilization on the resistance to digital flexion using a tendon injury model. *Journal of Hand Surgery*, 22:464–472, 1997.

[18] H. E. Kleinert, T. Gill, and B. Schlafy. Primary repair of flexor tendons. *The Hand*, pages 199–212, 1988.

[19] K. W. Cullen, P. Tolhurst, and P. R. E. Lang. Flexor tendon repair in zone 2 followed by controlled active mobilisation. *Journal of Hand Surgery*, 14B:392–395, 1989.

[20] D.W. Repperger, B.O. Hill, C. Hasser, M. Roark, and C.A. Phillips. Human tracking studies involving an actively powered, augmented exoskeleton. In *Biomedical Engineering Conference, 1996., Proceedings of the 1996 Fifteenth Southern*, pages 28–31, Mar 1996.

[21] D.G. Caldwell, O. Kocak, and U. Andersen. Multi-armed dexterous manipulator operation using glove/exoskeletoncontrol and sensory feedback. In *Intelligent Robots and Systems 95. 'Human Robot Interaction and Cooperative Robots', Proceedings. 1995 IEEE/RSJ International Conference on*, volume 2, pages 567–572, 1995.

[22] M. Bergamasco, B. Allotta, L. Bosio, L. Ferretti, G. Parrini, G.M. Prisco, F. Salsedo, and G. Sartini. An arm exoskeleton system for teleoperation and virtual environments applications. In *Robotics and Automation, 1994. Proceedings., 1994 IEEE International Conference on*, pages 1449–1454 vol.2, May 1994.

[23] H. Kazerooni. The human power amplifier technology at the university of california, berkeley. In *Robotics and autonomous systems*, volume 19, pages 179–187, 1996.

[24] Guilin Yang, Hui Leong Ho, Weihai Chen, Wei Lin, Song Huat Yeo, and M.S. Kurbanhusen. A haptic device wearable on a human arm.

In *Robotics, Automation and Mechatronics, 2004 IEEE Conference on*, volume 1, pages 243–247 vol.1, Dec. 2004.

[25] A. Gupta, M. O'Malley, V. Patoglu, and C. Burgar. Design, control and performance of ricewrist: A force feedback wrist exoskeleton for rehabilitation and training. *IEEE Transactions on Robotics Research*, 27(2):233–251, February 2008.

[26] J.C. Perry, J. Rosen, and S. Burns. Upper-limb powered exoskeleton design. *Mechatronics, IEEE/ASME Transactions on*, 12(4):408–417, Aug. 2007.

[27] Y. S. Kim, J. Lee, and M. Kim. A force reflected exoskeletontype masterarm for human-robot interaction. *Systems, Man and Cybernetics, Part A: Systems and Humans, IEEE Transactions on*, 35(2):198–212, March 2005.

[28] A. Erdogan, A.C. Satici, and V. Patoglu. Design of a reconfigurable force feedback ankle exoskeleton for physical therapy. In *ASME/IFToMM International Conference on Reconfigurable Mechanisms and Robots*, pages 400–408, 2009.

[29] Li-Qun Zhang, Hyung-Soon Park, and Yupeng Ren. Developing an intelligent robotic arm for stroke rehabilitation. In *Rehabilitation Robotics, 2007. ICORR 2007. IEEE 10th International Conference on*, pages 984–993, June 2007.

[30] T. Nef, M. Mihelj, G. Colombo, and R. Riener. Armin - robot for rehabilitation of the upper extremities. In *Robotics and Automation,*

2006. ICRA 2006. Proceedings 2006 IEEE International Conference on, pages 3152–3157, May 2006.

[31] S. Hesse, G. Schulte-Tigges, M. Konrad, A. Bardeleben, and C. Werner. Robot-assisted arm trainer for the passive and active practive of bilateral forearm and wrist movements in hemiparetic subjects. In *Arch. Phys. Med. Rehabil.*, volume 84, pages 915–920, 2003.

[32] C.D. Takahashi, L. Der-Yeghiaian, V.H. Le, and S.C. Cramer. A robotic device for hand motor therapy after stroke. In *IEEE International Conference on Rehabilitation and Robotics*, pages 17–20, 2005.

[33] A. Frisoli, F. Rocchi, S. Marcheschi, A. Dettori, F. Salsedo, and M. Bergamasco. A new force-feedback arm exoskeleton for haptic interaction in virtual environments. In *IEEE Eurohaptics*, pages 195–201, 2005.

[34] H.I. Krebs, N. Hogan, M.L. Aisen, and B.T. Volpe. Robot-aided neurorehabilitation. *Rehabilitation Engineering, IEEE Transactions on*, 6(1):75–87, Mar 1998.

[35] J.J. Palazzolo, M. Ferraro, H.I. Krebs, D. Lynch, B.T. Volpe, and N. Hogan. Stochastic estimation of arm mechanical impedance during robotic stroke rehabilitation. *IEEE Transactions on Neural Systems and Rehabilitation Engineering*, 15(1):94–103, 2007.

[36] J. Furusho, T. Kikuchi, K. Oda, Y. Ohyama, T. Morita, N. Shichi, Ying Jin, and A. Inoue. A 6-dof rehabilitation support system for upper limbs including wrists "robotherapist" with physical therapy. In *IEEE International Conference on Rehabilitation Robotics*, pages 304–309, 2007.

[37] J. Furusho, C. Li, X. Hu, N. Shichi, T. Kikuchi, A. Inoue, K. Nakayama, Y. Yamaguchu, and U. Ying Ryu. Development of a 6-dof force display system using er actuators with high-safety. In *Virtual Reality Continuum and Its Applications, 2006. VRCIA 20006. ACM International Conference on*, pages 405–408, 2006.

[38] R.C.V. Loureiro and W.S. Harwin. Reach and grasp therapy: Design and control of a 9-dof robotic neuro-rehabilitation system. In *IEEE International Conference on Rehabilitation Robotics*, pages 757–763, 2007.

[39] C. Mrad, H. Kawasaki, J. Takai, Y. Tanaka, and T. Mouri. Development of a multifingered robotic human upper limb as an inverse haptic interface. In *IEEE International Conference on Systems, Man and Cybernetics*, volume 4, 2002.

[40] L Dovat, O Lambercy, Y Ruffieux, D Chapuis, R Gassert, H Bleuler, CL Teo, and E Burdet. A haptic knob for rehabilitation of stroke patients. In *IEEE International Conference on Intelligent Robots and Systems*, pages 977–982, 2006.

[41] O. Lambercy, L. Dovat, V. Johnson, B. Salman, S. Wong, R. Gassert, T. Milner, Teo Chee Leong, and E. Burdet. Development of a robot-assisted rehabilitation therapy to train hand function for activities of daily living. In *Rehabilitation Robotics, 2007. ICORR 2007. IEEE 10th International Conference on*, pages 678–682, June 2007.

[42] Theraband website. `http://www.thera-band.com/store/products.php?ProductID=22`.

[43] Gripmaster website. `http://www.gripmaster.com.au/index1.htm`.

[44] Powerweb website. `http://www.pwrwebintl.com/`.

[45] Vq orthocare website. `http://www.vqorthocare.com/Products/CPM/Hand8091.php`.

[46] Tyromotion website. `http://www.tyromotion.com/`.

[47] R. Carrey. Manual stretch: Effect on finger movement control and force control in stroke subjects with spastc extrinsic finger flexor muscles. *Archives of Physical Medical Rehabilitation*, 71:888–894, 1990.

[48] M. Adams and S. Thompson. Continuous passive motion use in hand therapy. *Hand Clinics*, 12(1):109–127, 1996.

[49] M. Guidice. Effects of continuous passive motion and elevation on hand edema. *American Journal of Occupational Therapy*, 44(10):914–921, 1990.

[50] H. Kawasaki. Multi-fingered haptic interface robot and its application systems. *Solid State Phenomena*, 144:1–8, 2009.

[51] L. Lucas, M. DiCicco, and Y. Matsuoka. An emg-controlled hand exoskeleton for natural pinching. *Journal of Robotics and Mechatronics*, 16(5):482–488, 2004.

[52] P. Stergiopoulos, P. Fuchs, and C. Laurgeau. Design of a 2-finger hand exoskeleton for vr grasping simulation. *EuroHaptics*, 2003.

[53] A. Frisoli, F. Salsedo, M. Bergamasco, and B. Rossi; M. C. Carboncini. A force-feedback exoskeleton for upper-limb rehabilitation in virtual reality. *Applied Bionics and Biomechanics*, 6:115–126, 2009.

[54] M. Mulas, M.Folgheraiter, and G. An Gini. EMG-controlled exoskeleton for hand rehabilitation. In *IEEE International Conference on Rehabilitation Robotics*, pages 371–374, 2005.

[55] T.T. Worsnopp, M.A. Peshkin, J.E. Colgate, and D.G. Kamper. An actuated finger exoskeleton for hand rehabilitation following stroke. In *IEEE International Conference on Rehabilitation Robotics*, pages 896–901, June 2007.

[56] S. V. Adamovich, G. G. Fluet, A. Mathai, Q. Qiu, J. Lewis, and A. S. Merians. Design of a complex virtual reality simulation to train finger motion for persons with hemiparesis: a proof of concept study. *Journal of NeuroEngineering and Rehabilitation*, 6, 2009.

[57] D. Jack, R. Boian, A. S. Merians, M. Tremaine, G. C. Burdea, and S. V. Adamovich. Virtual reality-enhanced stroke rehabilitation. *IEEE Transactions on Neural Systems and Rehabilitation Engineering*, 9:308–318, 2001.

[58] C. A. Avizanno, F. Barbagli, A. Frisoli, and M. Bergamasco. The hand force feedback: Analysis and control of a haptic device for the human hand. In *IEEE International Conference on Systems, Man and Cybernetics*, pages 989–994, 2000.

[59] A. Wege and G. Hommel. Development and control of a hand exoskeleton for rehabilitation of hand injuries. In *International Conference on Intelligent Robots and Systems*, pages 3046–3051, 2005.

[60] U. Mali and M. Munih. HIFE-haptic interface for finger exercise. *IEEE/ASME Transactions on Mechatronics*, 11:93–102, 2006.

[61] Y. Fu, P. Wang, S. Wang, H. Liu, and F. Zhang. Design and development of a portable exoskeleton based cpm machine for rehabilitation of hand injuries. In *IEEE International Conference on Robotics and Biomimetics*, pages 1476–1481, Dec. 2007.

[62] Y. Fu, P. Wang, and S. Wang. Development of a multi-dof exoskeleton based machine for injured fingers. In *IEEE International Conference on Intelligent Robots and Systems*, pages 1946–1951, Sept. 2008.

[63] K. Sawyer and LaVigne J. *Brunnstrom' Movement Therapy in Hemiplegia: A Neurological Approach.* J B Lippincott Co., 2nd edition, 1992.

[64] S. S. Gamage and J. Lasenby. New least squares solutions for estimating the average centre of rotation and the axis of rotation. *Journal of Biomechanics*, 35(1):87–93, 2002.

[65] H. M. Schmidt and U. Lanz. *Surgical Anatomy of the Hand.* Hardcover, 2004.

[66] J. C. Becker and N. V. Thakor. A study of the range of motion of human fingers with application to anthropomorphic designs. *IEEE Transactions on Biomedical Engineering*, 35:110–117, 1988.

[67] T. Mouri, H. Kawasaki, Y. Nishimoto, T. Aoki, Y. Ishigure, and M. Tanahashi. Robot hand imitating disabled person for education/training of rehabilitation. *Journal of Robotics and Mechatronics*, 20(2):280–288, 2008.

[68] R. Unal, G. Kiziltas, and V. Patoglu. A multi-criteria design optimization framework for haptic interfaces. In *Symposium on Haptic Inter-*

faces for Virtual Environment and Teleoperator Systems, pages 231–238, March 2008.

[69] L. Birglen, T. Laliberte, and C. Gosselin. *Underactuated Robotic Hands.* Springer, 2008.

[70] L. Tsai. *Robot Analysis: The mechanics of serial and parallel manipulators.* New York: John Wiley and Sons, Inc., 1999.

[71] G. Hovland I. Tyapin and T. Brogardh. Workspace optimisation of a reconfigurable parallel kinematic manipulator. *ABB Robotics*, 2007.

[72] G. Alici and B. Shirinzadeh. Optimum synthesis of planar parallel manipulators based on kinematic isotropy and force balancing. *Robotica*, 22:97–108, 2004.

[73] Y. Yang and J. F. O'Brien. A case study of planar 3-rpr parallel robot singularity free workspace design. pages 1834–1838, 2007.

[74] M. T. Masouleh and C. Gosselin. Determination of singularity-free zones in the workspace of planar 3-prr parallel mechanisms. *Journal of Mechanical Design*, 129:649–652, 2007.

[75] M. Gallant and R. Boudreau. The synthesis of planar parallel manipulators with prismatic joints for an optimal, singularity-free workspace. *Journal of Robotic Systems*, 19:13–24, 2002.

[76] H. Li, C. M. Gosselin, , and M. J. Richard. Determination of maximal singularity-free zones in the workspace of planar three-degree-of-freedom parallel mechanisms. *Mechanism and Machine Theory*, 41(10):1157–1167, 2006.

[77] R. Cabas, L. M. Cabas, and C. Balaguer. Optimized design of the underactuated robotic hand. In *International Conference on Robotics and Automation*, pages 982–987, May. 2006.

[78] S. M. Nacy, S. S. Hassan, and S. H. Bakhy. Geometric optimization of three-phalanx prosthesis underactuated fingers using particles swarm algorithm. *American Journal of Engineering and Applied Sciences*, 2(2):381–387, 2009.

[79] L. C. Wu, G. Carbone, and M. Ceccarelli. Designing an underactuated mechanism for a 1 active dof finger operation. *Mechanism and Machine Theory*, 44(2):336–348, Feb. 2009.

[80] S. Yao, M. Ceccarelli, G. Carbone, and Z. Lu. An optimal design for a new underactuated finger mechanism. In *The Second European Conference on Mechanism Science*, pages 149–157, 2008.

[81] L. Birglen and C. Gosselin. Optimal design of 2-phalanx underactuated fingers. pages 110–116, 2004.

[82] R. Unal, G. Kiziltas, and V. Patoglu. Multi-criteria design optimization of parallel robots. In *IEEE Conference on Robotics, Automation and Mechatronics*, pages 112–118, Sept. 2008.

[83] I. Das and J. E. Dennis. Normal-boundary intersection: A new method for generating the pareto surface in nonlinear multi-criteria optimization problems. *SIAM Journal on Optimization*, 8(3):631–657, 1998.

[84] L. Masia, H.I. Krebs, P. Cappa, and N. Hogan. Whole-arm rehabilitation following stroke: Hand module. In *IEEE International Conference on Biomedical Robotics and Biomechatronics*, pages 1085–1089, Feb. 2006.

140

[85] T.R. Kane. *DYNAMICS: Theory and Application*. Number 223. McGraw-Hill, 1985.

[86] F. Janabi-Sharifi, V. Hayward, and C.-S.J. Chen. Discrete-time adaptive windowing for velocity estimation. *Control Systems Technology, IEEE Transactions on*, 8(6):1003–1009, Nov 2000.

[87] R. Volpe and P. Khosla. An experimental evaluation and comparison of explicit force control strategies for robotic manipulators. In *IEEE International Conference on Robotics and Automation*, pages 1387–1393, May 1992.

[88] G. Zeng and A. Hemami. The use of surface electromyography in biomechanics. *Robotica*, 15:473–482, 1997.

[89] N. Hogan. Impedance control: An approach to manipulation: Part i - theory. *Journal of Dynamic Systems, Measurement, and Control*, 107(1):1–7, 1985.

[90] N. Hogan. Impedance control: An approach to manipulation: Part ii - implementation. *Journal of Dynamic Systems, Measurement, and Control*, 107(1):8–16, 1985.

[91] N. Hogan. Impedance control: An approach to manipulation: Part iii - application. *Journal of Dynamic Systems, Measurement, and Control*, 107(1):17–24, 1985.

[92] C. J. DeLuca. The use of surface electromyography in biomechanics. *Journal of Applied Biomechanics*, 13:135–163, 1997.

[93] D. Farina, R. Merletti, and M. R. Enoka. The extraction of neural strategies from the surface EMG. *Journal of Applied Physiology*, 96:1486–1495, 2004.

[94] J. Kollmitzer, R. G. Ebenbichler, and A. Kopf. Reliability of surface electromyographic measurements. *Clinical Neurophysiology*, 110:725–734, 1999.